BIODIESEL PRODUCTION IN LIQUID – LIQUID FILM REACTOR ASSISTED BY MEMBRANES

Mario Andrés Noriega Valencia

Tese de Doutorado apresentada ao Programa de Pós-graduação em Engenharia Química, COPPE, da Universidade Federal do Rio de Janeiro, como parte dos requisitos necessários à obtenção do título de Doutor em Engenharia Química.

Orientadores: Alberto Claudio Habert
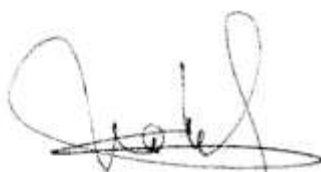　　　　　　　 Paulo César Narváez Rincón

Rio de Janeiro
Novembro de 2016

BIODIESEL PRODUCTION IN LIQUID – LIQUID FILM REACTOR ASSISTED BY MEMBRANES

Mario Andrés Noriega Valencia

TESE SUBMETIDA AO CORPO DOCENTE DO INSTITUTO ALBERTO LUIZ COIMBRA DE PÓS-GRADUAÇÃO E PESQUISA DE ENGENHARIA (COPPE) DA UNIVERSIDADE FEDERAL DO RIO DE JANEIRO COMO PARTE DOS REQUISITOS NECESSÁRIOS PARA A OBTENÇÃO DO GRAU DE DOUTOR EM CIÊNCIAS EM ENGENHARIA QUÍMICA.
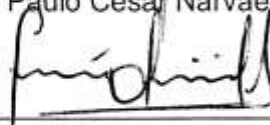
Examinada por:
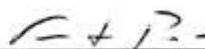
_____
Prof. Alberto Claudio Habert, Ph.D.

_____
Prof. Paulo César Narváez Rincón, Ph.D.

_____
Prof. Iván Dario Gil Chaves, Ph.D.

_____
Prof. Frederico Wanderley Tavares, D.Sc.

_____
Prof. Fernando Luiz Pellegrini Pessoa, D.Sc.

_____
Prof. Frederico de Araujo Kronemberger, D.Sc.

RIO DE JANEIRO, RJ - BRASIL
NOVEMBRO DE 2016

Agradecimentos

PRODUÇÃO DE BIODIESEL NUM REATOR DE FILME LÍQUIDO DESCENDENTE ASSISTIDO POR MEMBRANAS

Mario Andrés Noriega Valencia

Novembro/2016

Orientadores: Alberto Claudio Habert

Paulo César Narváez Rincón

Programa: Engenharia Química

O biodiesel é um importante combustível renovável cuja produção é principalmente limitada por elevados tempos de residência nas seções de reação e separação. Este trabalho estuda a possibilidade de reduzir esse problema, utilizando um reator de filme descendente (RFD) integrado com membranas na forma de fibras ocas. O RFD apresenta elevadas taxas de reação e produtividade, e um efeito positivo sobre a separação de fase. Adicionalmente, a integração de uma membrana permite a remoção simultânea do glicerol. Esta tese apresenta um modelo matemático que descreve o comportamento do reator de filme descendente assistido por membranas e sua validação experimental. O modelo descreve o reator de filme descendente com limitações de transferência de massa e o escoamento através da membrana pela equação de Hagen-Poiseuille, onde a seletividade da membrana é dependente do equilíbrio líquido líquido. Foi realizada uma análise de sensibilidade para compreender o funcionamento do reator integrado com a membrana e identificar as principais variáveis de operação do sistema. O reator proposto apresentou produtividade 12 vezes superior à produtividade média de um reator tradicional de tanque agitado por lotes e a separação de fases com a membrana evita a necessidade de um decantador ou de vários estágios de reação no processo.

Abstract of Thesis presented to COPPE/UFRJ as a partial fulfillment of the requirements for the degree of Doctor of Science (D.Sc.)

BIODIESEL PRODUCTION IN LIQUID – LIQUID FILM REACTOR ASSISTED BY MEMBRANES

Mario Andres Noriega Valencia

November/2016

Advisors: Alberto Claudio Habert
         Paulo César Narváez Rincón

Department: Chemical Engineering

Biodiesel is an important renewable fuel whose production has been limited mainly by high residence times in reaction and separation stages. This work studies the possibility of increasing productivity by implementing a liquid – liquid film reactor (LLFR) integrated with hollow fiber membranes. This reactor takes advantage of both systems: while production of biodiesel using an LLFR is characterized by high reaction rates, productivity and a positive effect on separation stages because interfacial mass transfer area is achieved without mixing, the integration of a membrane permit the simultaneous removal of glycerol, increasing fatty acid methyl esters yield. A mathematical model to predict the behavior of LLFR assisted by membranes (LLFRM) was developed and validated experimentally. The model describes the reactor including mass transfer limitations and flux through the membrane using Hagen-Poiseuille equation, where membrane selectivity is dependent on liquid – liquid equilibrium. A sensitivity analysis was performed to understand the operation of the LLFRM and to identify the main variables of the system. The proposed reactor showed a productivity up to 12 times the average productivity reported for a traditional batch stirred tank reactor (BSTR) and the phase separation with membranes avoid the necessity of multiple reaction steps and decantation stages in the process.

Resumen de la tesis presentada a la COPPE/UFRJ como parte de los requisitos necesarios para la obtención del grado de Doctor en Ciencias (D.Sc.)

PRODUCCIÓN DE BIODIÉSEL EN UN REACTOR DE PELÍCULA DESCENDENTE ASISTIDO POR MEMBRANAS

Mario Andrés Noriega Valencia

Noviembre/2016

Orientadores: Alberto Claudio Habert

Paulo César Narváez Rincón

Programa: Ingeniería Química

El biodiésel es un importante combustible renovable cuya producción se ha limitado principalmente por los altos tiempos de residencia en las etapas de reacción y separación. Este trabajo estudia la posibilidad de reducir este problema mediante el uso de un reactor de película descendente (RPD) integrado con membranas de fibra hueca (RPDM). Este reactor aprovecha las ventajas de los dos sistemas: mientras la producción de biodiésel usando el RPD se caracteriza por altas velocidades de reacción y productividad, y un efecto positivo en la etapa de separación ya que la generación de área interfacial se consigue sin mezclado. La integración de una membrana permite la eliminación simultánea del glicerol. Un modelo matemático para predecir el comportamiento del reactor de película descendente asistido por membranas fue desarrollado y validado experimentalmente. El modelo describe el RPD incluidas limitaciones de transferencia de masa y el flujo a través de la membrana mediante la ecuación de Hagen-Poiseuille, donde la selectividad de la membrana es dependiente del equilibrio líquido - líquido. Se realizó un análisis de sensibilidad para entender el funcionamiento del reactor integrado con membrana y determinar las principales variables del sistema. El RPDM propuesto tuvo una productividad 12 veces superior a la productividad media reportada para un reactor de tanque agitado operado por lotes, mientras que la separación de fases con la membrana elimina la necesidad de múltiples etapas de reacción y la etapa de decantación.

Content

Figure list

Table list

Introduction

The increasing worldwide energy consumption and limited availability of fossil fuels have stimulated the investigation of alternative energy sources. Among the alternative energy sources, biofuels are the most widely used in the transportation sector. Biodiesel and bioethanol have been extensively produced and commercialized because raw materials required for their production are available in many regions around the World. Besides, Their properties are similar to those of diesel and gasoline, which permits their use in current internal combustion engines (BORUGADDA; GOUD, 2012).

Many countries have implemented policies to promote the blending of these biofuels with diesel and gasoline. These policies justify the investment of public resources through subsidies and tax exemptions, based on the prolongation of petroleum availability, the reduction of the negative environmental impact of emissions from fossil fuels and the employment increment in the rural sector (BALAT; BALAT, 2010, VASUDEVAN; BRIGGS, 2008).

At industrial scale biodiesel is mainly produced by transesterification of vegetable oils with methanol using homogeneous basic catalyst, mainly sodium or potassium methoxide. Major constraints in conventional biodiesel production are the high prices of raw materials, the need for multiple reaction steps, reaction limitations associated with the mass transfer and high water consumption in the final biodiesel purification (JURAC; ZLATAR, 2013). Most of the industrial processes use stirred tank reactors in batch (BSTR) or continuous (CSTR) processes (FRASCARI et al., 2008). Kinetic and thermodynamic characteristics of this reaction, where chemical equilibrium is a key factor, imply residence times of about 1 h for the BSTR process (FREEDMAN et al., 1984, NARVÁEZ et al., 2007). The stoichiometric ratio for transesterification is three moles of alcohol per mole of triacylglycerol to obtain three moles of fatty acid ester and one mole of glycerol. In

1

practice, the molar ratio has to be higher than 3:1 to drive the equilibrium to a maximum biodiesel yield. The practical range of methanol to vegetable oil molar ratio has been reported from 3.3:1 to 5.25:1 (BRADSHAW; MEULY, 1944). If a three reaction steps transesterification process is used, the ratio can be reduced to 3.3:1 (FANGRUI; HANNA, 1999).

Biodiesel needs multiple reaction steps due to the constraints of chemical equilibrium and to the need for a product with low triglycerides (TGs), diglycerides (DGs) and monoglycerides (MGs) [1] content. After the first reaction step glycerol formed is removed (by gravity settling) and Ester[2] rich-phase is fed to a second reaction step in which conversion and yield required can be achieved. Thus, the content of bonded glycerol fulfills quality defined in biodiesel product standards. It is possible to produce biodiesel accomplishing standards specifications in a single reaction step using simultaneous reaction and separation processes such as reactive distillation, extraction, and adsorption, processes under supercritical conditions and membrane technology (SHUIT et al., 2012). In these processes, reaction and products removal occur simultaneously, shifting the chemical equilibrium toward the products.

Additionally, low miscibility between raw materials (vegetable oils and methanol) generates mass transfer resistance, mainly when the reaction starts, reducing the overall reaction rate (HOU et al., 2007, NOUREDDINI; ZHU, 1997, ZHENG et al., 2009). In stirred tank reactors, mixing generates the dispersion between phases, which increases the interfacial area and the reaction rate (DEROUSSEL et al., 2001). Higher the mixing speed smaller the size of the drops; thus mass transfer rate increases as well as the residence time in the downstream two-phases separator (KUMAR et al., 2014). As a consequence, there is a reduction in the productivity of the process, especially if emulsions are formed.

Alternatively, in order to reduce residence time and increase process productivity, some intensification strategies as reactive distillation, reactive extraction, oscillatory flow reactors, membrane reactors, cavitation reactors, static mixers, microreactors,

---

[1] Limit concentrations (% w/w) established by the EN 14214 for MG, DG, TG and free G are 0.8, 0.2, 0.2 and 0.02, respectively.
[2] The stage product has content of TG, DG and MG which overcome the limits.

membranes, and liquid - liquid film reactors (LLFR) operated in co-current and counter-current have been researched.

Palm oil biodiesel production in an LLFR has been studied by the Grupo de Investigación en Procesos Químicos y Bioquímicos from Universidad Nacional de Colombia sede Bogotá, operating the reactor both in co-current (NARVÁEZ et al., 2009) and counter-current (CADAVID et al., 2013). This reactor is a device in which interfacial area is created by using a semi-structured packing without dispersing the ester-rich and the alcohol-rich phase into the other. In co-current operation vegetable oil conversion and biodiesel yield were 97.5% and 92.2%, respectively. Residence time in the two-phase separator downstream the reactor was only 5 min. Chemical and phase equilibrium limit yield. Therefore, two reaction stages are necessary to meet the specifications established in biodiesel standards. Process productivity reported in an LLFR operated in co-current was 1.2 m^3 Biodiesel/$m^{-3}h^{-1}$ (CADAVID et al., 2013).

In order to solve the chemical and phases equilibria limitations of an LLFR operated in co-current, CADAVID et al., (2013) studied palm oil biodiesel production in a counter-current reactive extraction column. Results showed palm oil conversion of 97.7% and biodiesel yield of 99.5% in only one reaction stage. The process productivity was 1.8 m^3 Biodiesel/m^3h (CADAVID et al., 2013). However, stability and controllability behavior of the reactor make difficult its industrial implementation.

Membrane reactors combine reaction and separation stages in one unit, with the aim of overcome limitations imposed by the chemical equilibrium, removing one of the products with low energy consumption (ABELS et al., 2013, ARANSIOLA et al., 2014, ATADASHI, I.M. et al., 2011, KISS; BILDEA, 2012, SHUIT et al., 2012). Membranes properties like mechanical strength, chemical and thermal resistances, high surface area per volume unit and high selectivity, have permitted their use in reaction and purification stages for biodiesel production (ATADASHI, I.M. et al., 2011, SHUIT et al., 2012), mainly to remove free and bonded glycerol (ALVES et al., 2013, OTHMAN et al., 2010, WANG et al., 2009) and as a support for heterogeneous catalysts (BAROUTIAN et al., 2011, GUERREIRO et al., 2010, XU et al., 2014).

Therefore, the objective of this study is to evaluate the performance of a liquid-liquid film reactor assisted by membranes (LLFRM), which takes advantage of both technologies achieving high productivity in a single reaction stage, with minimum requirements for separation and purification. The LLFRM is characterized by the LLFR high reaction rate and productivity and the simultaneous removal of products using hollow fiber membranes. This thesis was developed in a doctoral program in co-joint supervision, theoretical and experimental work were developed in the Universidad Nacional de Colombia and the Universidade Federal do Rio de Janeiro. Taking advantage of the experience in LLFR of the Grupo de Investigación en Procesos Químicos y Bioquímicos from Universidad Nacional de Colombia sede Bogotá and the experience in membrane technology of the Laboratorio de Processos de Separação com Membranas e Polimeros from Universidade federal do Rio de Janeiro.

The first chapter of this document presents the main aspects related to the biodiesel production, including some possibilities for process integration, emphasizing on two technologies: LLFR and membrane reactors, presenting their advantages, challenges, and opportunities. The second chapter presents the investigation problem, including hypothesis, objectives, and general methodology. In the third chapter kinetics of vegetable oil methanolysis is presented, which was experimentally developed and adjusted to a mathematical model using a genetic algorithm. The fourth chapter discusses the prediction of liquid-liquid equilibrium LLE in systems composed of biodiesel, alcohol, and glycerol, using UNIFAC. LLE is required for predict permeate and retentate composition, information absolutely necessary to understand LLFRM behavior.

The fifth chapter describes the mathematical model proposed to describe the LLFR including mass transfer limitations including its experimental validation, while the implementation of membranes in the model and the experimental validation is showed in chapter sixth. Finally, chapter seventh presents the mathematical model of the LLFRM and its experimental validation. A sensitivity analysis and an evaluation of the main variables to consider in the integration of the membrane reactor is presented. Finally, conclusions and suggestions for future works are established.

1. Biodiesel production assisted by membranes

1.1 Introduction

Biodiesel is a mixture of fatty acid alkyl esters (FAME) usually obtained by transesterification of vegetable oils or animal fats with methanol. Among the different uses of this intermediate chemical, its use as a biofuel has fostered the industrial production during the last fifteen years. Properties of biodiesel are very similar to the properties of petroleum diesel, permitting the use of the former as a total or partial substitute of the latter in current internal combustion engines. Between the sources of triglycerides employed industrially to produce biodiesel, palm oil, rapeseed oil and soybean oil are the most used, although many other have been investigated as sunflower oil, used cooking oil, jatropha oil, and fats from the meat industry. Selection of the suitable raw material for biodiesel production depends on political, economic and social issues. For this reason, the raw material used varies depending on the geographic location of the crop (BORUGADDA; GOUD, 2012). While in Europe soybean, sunflower and rapeseed oils (SARIN et al., 2007) are the most used, in Colombia palm oil is the most employed. In Brazil and the USA, soybean oil is the mainly used (BERGMANN et al., 2013).

Oil from Jatropha seeds is considered one of the most promising sources for biodiesel production in Asia, Europe and Africa (KARMAKAR et al., 2010) because it can grow in arid and semi-arid areas and survive in poor soils. Its water and fertilizers requirements are low and it is not consumed by livestock. It is also resistant to pests and it has high seed production for periods between 30 and 40 years. In addition, the oil content in the seeds is between 30 and 40% (SARIN et al., 2007). Jatropha grows in tropical and subtropical regions, between 30 degrees north and south latitude and its plantations are rapidly expanding in India, Indonesia and Africa (OPENSHAW, 2000). Given the

similarities between the location and the climatic conditions of these countries with Colombia and Brazil, Jatropha is considered as a potential feedstock for biodiesel production in South America.

Biodiesel is produced industrially by a transesterification reaction. In this reaction a triglyceride (TG) molecule reacts with three molecules of an alcohol preferably, low molecular weight, such as methanol or ethanol in the presence of a basic, acidic or enzymatic catalyst, producing three molecules of fatty acid methyl esters (FAMEs) as product primary and one molecule of glycerol (G) as by-product (Figure 1-1).
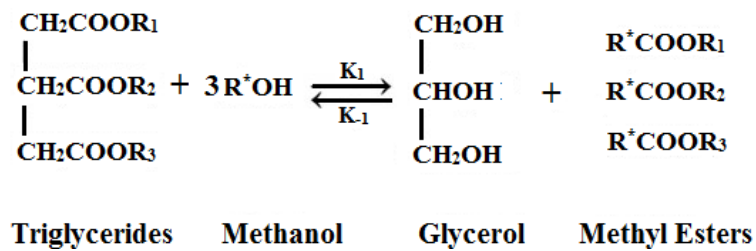
Figure 1-1. Global TG transesterification reaction.

Figure 1-2 shows the methanolysis reaction stages: A TG molecule reacts with methanol (M) to produce DG (step 1), which reacts with another M molecule to produce MG (step 2). Finally, it reacts with another M molecule to produce G (step 3) (FREEDMAN et al., 1984). Each reaction stage produces a FAME molecule. Given the immiscibility of raw materials, the reaction occurs mainly in the ester-rich phase, at the interface between the ester-rich phases and methanol, as well as the small amount of oil dissolved in methanol-rich phase (SHUIT et al., 2012). For this reason, the reaction rate has limitations associated with the mass transfer between the reacting phases (QIU et al., 2010).
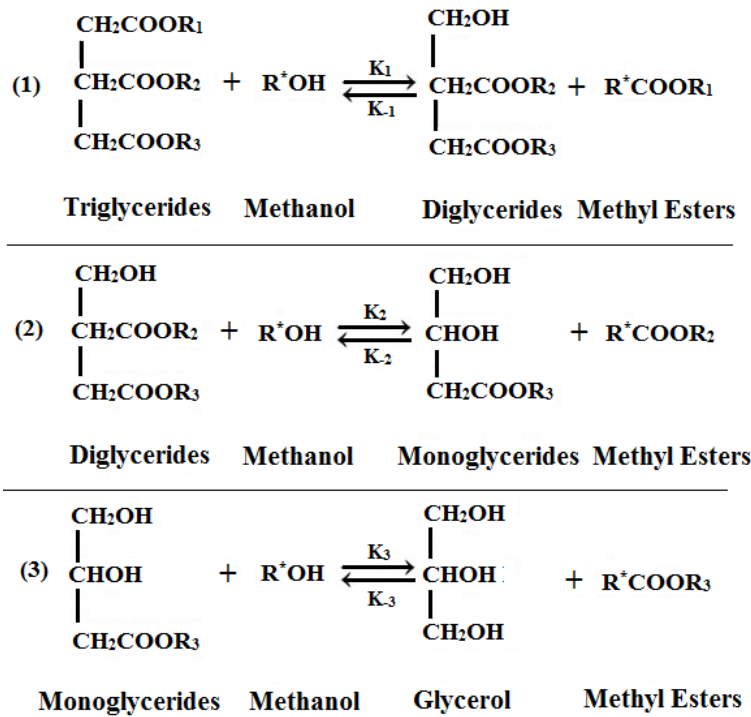
Figure 1-2. TG transesterification in three stages.

Methanolysis kinetic model has been developed using power law models and taking into account the three reversible stages presented in Figure 1-2. Reaction kinetics can be modeled by equations 1-1 to 1-6 (NOUREDDINI; ZHU, 1997).

$$\frac{d[TG]}{dt} = -k_1[TG][M] + k_{-1}[DG][FAME] \tag{1-1}$$

$$\frac{d[DG]}{dt} = k_1[TG][M] - k_{-1}[DG][FAME] - k_2[DG][M] + k_{-2}[MG][FAME] \tag{1-2}$$

$$\frac{d[MG]}{dt} = k_2[DG][M] - k_{-2}[MG][FAME] - k_3[MG][M] + k_{-3}[G][FAME] \tag{1-3}$$

$$\frac{d[FAME]}{dt} = k_1[TG][M] - k_{-1}[DG][FAME] + k_2[DG][M]....... \tag{1-4}$$
$$-k_{-2}[MG][FAME] + k_3[MG][M] - k_{-3}[G][FAME]$$

$$\frac{d[G]}{dt} = k_3[MG][M] - k_{-3}[G][FAME] \tag{1-5}$$

$$\frac{d[M]}{dt} = -\frac{d[FAME]}{dt} \tag{1-6}$$

The main indicators of the biodiesel production are vegetable oil conversion, which quantifies TG consumed in the reaction (equation 1-7), FAME yield, which quantifies TG

7

transformed in FAME (equation 1-8), and productivity, which quantifies plant volume required to produce one m³ of biodiesel in one hour (equation 1-9).

$$Conversion(\%) = \frac{C_{TG}^0 - C_{TG}}{C_{TG}^0} \cdot 100\% \qquad \textbf{(1-7)}$$

$$Yield(\%) = \frac{C_{FAME} - C_{FAME}^0}{3C_{TG}^0} \cdot 100\% \qquad \textbf{(1-8)}$$

$$Productivity = \frac{Biodiesel\_Flow(m^3/h)}{Reactor\_volume(m^3)} \qquad \textbf{(1-9)}$$

The most industrially used catalyst is sodium methoxide. Figure 1-3 shows the methanolysis reaction mechanism with this type of catalyst. Catalytic action is caused by the presence of methoxide ions. This mechanism has three reaction steps (FANGRUI; HANNA, 1999): first, an attack on the carbon atom of the carbonyl group of the triglyceride molecule occurs by the anion of the alcohol (methoxide ion) to form a tetrahedral intermediate. In the second step, the tetrahedral intermediate reacts with the alcohol to regenerate the anion of the alcohol (methoxide ion). Finally, DG and FAME are produced, as a result of a rearrangement of the tetrahedral intermediate.
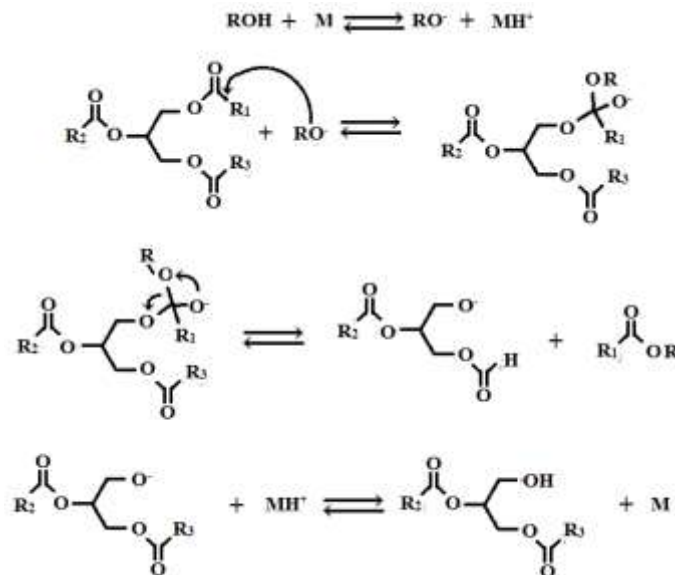
Figure 1-3. Reaction mechanism for the alcoholysis of a triglyceride using alkaline catalysis (Adapted with permission from LOTERO et al., (2005). Copyright 2005ACS).

LLE description in biodiesel systems was first studied by BASSO et al., (2012) who evaluated the LLE in a system of crambe oil biodiesel, ethanol, and glycerol. They compared the experimental data with the Non-Random Two-Liquid (NRTL) and Universal quasichemical Functional group Activity Coefficients (UNIFAC) descriptions, finding deviations up to 1% and 4%, respectively. CHIU et al., (2005) predicted the distribution coefficients of methanol between biodiesel and glycerin phases using the VLE activity coefficients and Wilson model. DI FELICE et al., (2008) correlated the Wilson activity coefficient based on thermodynamic data available in the literature including mixtures of two (biodiesel and glycerol), three (biodiesel, glycerol, and methanol), and four (biodiesel, glycerol, methanol, and water) components. ANDREATTA et al., (2008) used group contribution with association equation of state (GCA-EOS) and the A-UNIFAC model to represent the phase equilibria of the ternary system methyl oleate—methanol—glycerol, at temperatures between 313 and 393 K. A good agreement with the experimental data was obtained particularly with the GCA-EoS model. UNIFAC and UNIFAC- Dortmund models were applied with satisfactory results to the prediction the same system (NEGI et al., 2006). BARREAU et al., (2010) used the Group Contribution Statistical Associating Fluid Theory (SAFT) to predict the liquid-liquid-vapor equilibrium of the ternary system methyl oleate, glycerol, and methanol. Some authors (FOLLEGATTI-ROMERO et al., 2012, OLIVEIRA et al., 2009, 2010) showed that the Cubic-Plus-Association Equation of State (CPA EoS) can successfully predict their experimental data with global average deviations up to 6%. HAKIM et al., (2014) correlated LLE experimental data from canola and sunflower biodiesel, glycerol and methanol with the NRTL and the Wilson−NRF Gibbs free energy models, Recently, DO CARMO et al., (2014) evaluated the LLE in systems composed of biodiesel, glycerol and alcohol using UNIFAC – Dortmund, UNIFAC, UNIQUAC, NRTL, ASOG and other thermodynamic models. The best model to describe the LLE was the UNIFAC – Dortmund model. Currently are available a high number of experimental LLE in the literature, but the current activity models do not represent all these experimental data with an accurate fit, a lot of works present accurate fit using only one kind of biodiesel.

Figure 1-4 shows schematically mass transfer limitations in the biodiesel production. The alcohol diffuses into the ester-rich phase, while TG diffuses into the alcohol-rich phase, creating two reaction zones (D^I and D^{II}), where D^I is the reaction zone in the alcohol-rich

phase and D^{II} is the reaction zone in the ester-rich phase, these zones are defined by the concentration profile in each phase.
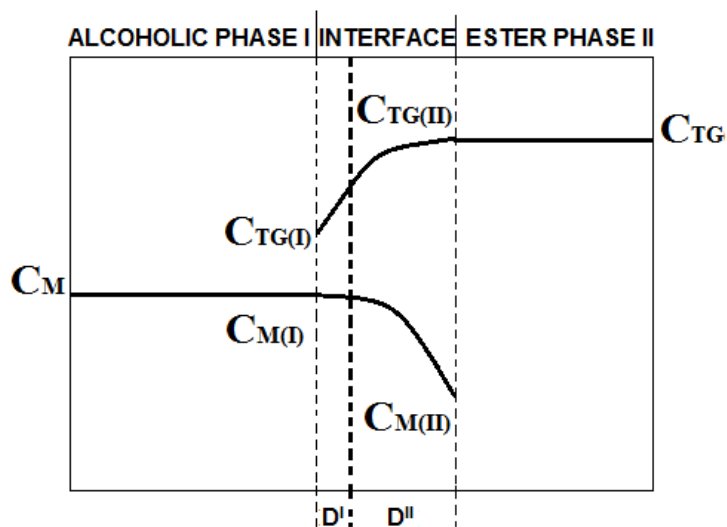
Figure 1-4. Mass transfer resistances.

Figure 1-5 shows mass transfer behavior according to the three reaction stages in TG alcoholysis. The first stage TG and M are transported to the reaction zones (D^I and D^{II}). In the second step, these components react to produce, DG, MG, G, and FAME. Finally, in the third stage, the compounds formed are distributed between the ester and alcohol-rich phase. Distribution of these components in the phases is determined by the phase equilibrium. At low Reynolds numbers, the limiting reaction step is the component transport while at high Reynolds numbers the limiting step is the reaction rate (STAMENKOVIC et al., 2007, ZHENG et al., 2009).

Figure 1-5. Mass transfer limitations according to the reaction stages in the biodiesel production.

Most biodiesel producers use a transesterification multistep reaction process, catalyzed by bases (SALEH, 2011), in order to overcome chemical equilibrium limitations. Figure 1-6 shows the biodiesel process using this type of catalysis.
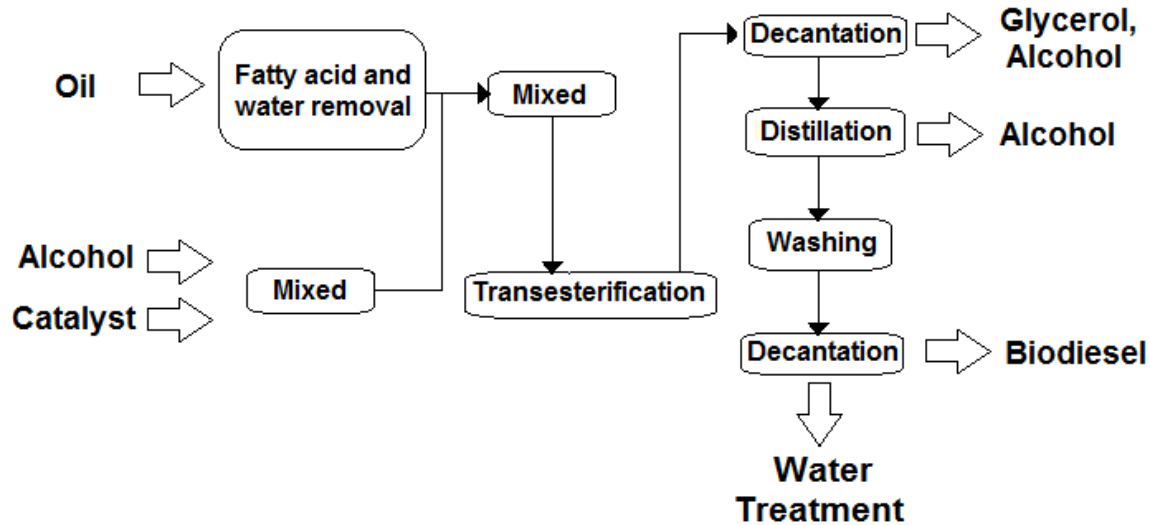
Figure 1-6. Biodiesel process with alkaline catalysis.

Initially, water and Free Fatty Acids (FFAs) are removed from the oil. The first methanolysis stage is developed. Then, glycerol is removed by decantation and the ester-rich phase recovered is fed to a second methanolysis stage. Finally, glycerol produced in the second reaction stage is removed by decantation. Biodiesel is neutralized with an acid solution in methanol and washed with water to remove soap, glycerol, etc. Finally, methanol and water are distilled from biodiesel, and this mixture is distilled to separate water and recover methanol with the purity required for transesterification.

Acid catalysts are useful in the pre-treatment of raw materials with a high content of FFAs. However, acid catalysts show low reaction rates in transesterification (VAN GERPEN, 2005). Meanwhile, enzymes show good catalytic activity in the presence of FFAs, its industrial use is limited due to the cost of enzymes and because it is not possible to produce biodiesel at the conversion and yield required to meet specifications defined in international standards (VAN GERPEN, 2005, HUANG et al., 2008).

The main operation variables in oil methanolysis are:

1. Temperature: temperature reduces mass transfer resistance increasing methanolysis reaction rate. Activation energy towards product formation is higher than activation energy

of reverse reaction, so, an increase in temperature promotes the reaction rate (NARVÁEZ et al., 2007, NOUREDDINI; ZHU, 1997). Methanolysis presents two regions in the concentration profile: the first region is presented at the reaction beginning, where mass transfer controls the process; the second region is faster and kinetics controls the process (NOUREDDINI; ZHU, 1997). Temperature increment increases solubility and consequently reduces mass transfer limitations.

2. Water and Free Fatty Acid content: Alkaline catalysts are sensitive to the presence of water and FFAs. These compounds promote soap formation by neutralization and saponification, which increases the required amount of catalyst and reduces biodiesel yield (CAO et al., 2006, KUSDIANA; SAKA, 2004).The presence of water and free fatty acids has a negative effect on the production of FAME. Raw materials with an acid value over 1mg KOH/g or water, react with NaOH (Catalyst) producing soaps and gels, which reduces catalytic activity, increases viscosity and difficults glycerol separation (FREEDMAN et al., 1984). In order to overcome this limitation methanolysis can be developed in two stages: the first catalyzed by acids transform FFAs to FAMEs, the second catalyzed by bases transform TGs to FAMEs (GHADGE; RAHEMAN, 2005).

3. Catalyst content: Catalyst addition up to 1% based on oil weight increases the reaction rate. However, additions above this concentration do not increase the reaction rate but promote soaps and gels generation (NARVÁEZ et al., 2007). 1% w/w NaOH is as effective as 0.5% w/w Sodium Methoxide because less water is formed during the reaction between sodium hydroxide and methanol. When the molar ratio is 3:1 the activity of sodium methoxide is significantly higher than that of hydroxide (FREEDMAN et al., 1984).

4. Alcohol to oil molar ratio: The stoichiometric ratio for transesterification requires three moles of alcohol for one mole of triacylglycerol to obtain three moles of fatty acid ester and one mole of glycerol. In practice, the ratio needs to be higher than 3:1 to drive the equilibrium to a maximum ester yield. The practical range of molar ratio methanol to vegetable oil was proposed from 3.3 to 5.25:1 (BRADSHAW; MEULY, 1944). If three reaction step transesterification process is used, the ratio is reduced to 3.3:1 (FANGRUI; HANNA, 1999). Alcohol to oil molar ratio over 6:1 does not improve the reaction rate but increases the separation cost.

5. Mixing Regime: Low miscibility between vegetable oil and methanol generates mass transfer resistances, mainly when the reaction starts, reducing the overall reaction rate (STAMENKOVIC et al., 2007, ZHENG et al., 2009). In stirred tank reactors, mixing generates the dispersion between phases, which increases the interfacial area and increases the reaction rate (DEROUSSEL et al., 2001). Higher the mixing speed, smaller the size of the drops, increasing mass transfer rate as well as the residence time in the downstream two-phases separator (KUMAR et al., 2014). The reaction period limited by mass transfer decreases with the rise in stirring speed to a constant value of 1 to 2 minutes when the Reynolds number is above 10,000 (NOUREDDINI; ZHU, 1997).

1.2 Process intensification in biodiesel production

Table 1-1 presents the main intensification technologies in biodiesel production. A microreactor improves mass and heat transfer efficiency using high ratios of surface area to volume and short diffusion distances (KOBAYASHI et al., 2006, SUN et al., 2008, WEN et al., 2009). Reaction temperature is similar to the conventional transesterification process and its residence time is lowest compared with others technologies presented in Table 1-1. Transesterification at supercritical conditions uses methanol in a supercritical state (temperature and pressure above the critical point), to form a homogeneous mixture with the oil. Supercritical biodiesel production has some advantages over other processes: it is not necessary the use of a catalyst, it does not require stirring device and the process is not affected by the presence of FFA and water in the raw materials. Most investigations on supercritical processes reported 90-98% conversion with short residence times (2 min). However, the initial equipment costs are high due to the safety conditions necessary to work at high pressures and temperatures (MAAIRA et al., 2011). Some authors have concluded that processes with supercritical fluids can reduce operational costs by implementing an energy integration strategy (GLISIC; SKALA, 2009, VAN KASTEREN; NISWORO, 2007).

Table 1-1. Process intensification in biodiesel production.

Technology	Molar ratio	Time (min)	Temperature (°C)	Conversion (%)	References
Micro reactor	6:1	5.89	60	99.4	(SUN et al., 2008)
	9:1	0.46	56	99.5	(WEN et al., 2009)
Supercritical condition	9	2	200	99.4	(MAAIRA et al., 2011)
Static mixer	6	30-360	50-60	99	(THOMPSON; HE, 2007)
Oscillatory reactor	1.5	30	50	99	(HARVEY et al., 2003)
Reactive Distillation	4:1	3	65	95.1	(HE, 2006)
	6:1	6	65	94.54	(DE LIMA DA SILVA et al., 2010)
	8:1	6	65	98.18	(DE LIMA DA SILVA et al., 2010)
Centrifugal separator	5-6	1-40	60-75	96-99	(KRAAI et al., 2009)
Ultrasonic reactor	6	240	40	96	(YU et al., 2010)
Co-current LLFR	6	4	60	99	(NARVÁEZ, P. C. et al., 2009)
Counter-current LLFR	6	4	60	99	(CADAVID et al., 2013)

Static mixers are motionless elements that create effective radial mixing of two immiscible liquids using its flow and collisions with the static structure (THOMPSON; HE, 2007). Static mixers can easily be integrated with any technology because they are accessories placed in the inner walls of the pipes to create a more intimate contact between the reactants. Some advantages of static mixers are low space requirements and low costs of maintenance and operation. However, mixing velocity is low because it requires laminar flow, so, the reactor has high residence time (QIU et al., 2010).

Centrifugal separators remove one of the products simultaneously with the progress of the reaction. This device has a rotor rotating rapidly in a static cylinder, generating high shear stress, intensive mixing, and high mass transfer velocity. Rapid phase separation is attained by a high centrifugal force (KRAAI et al., 2009). However, the residence time in this technology is around 10 seconds, not sufficient to reach equilibrium conversion (QIU et al., 2010). Implementation on an industrial scale was proposed using two centrifugal separators in series: the first stage performs biodiesel production and the second stage develops the removal of glycerol and catalyst traces (KRAAI et al., 2009).

Reactive distillation offers the possibility of product removal while the reaction occurs, increasing conversion and yield. In this process, chemical reaction and separation are carried out simultaneously in the same distillation equipment. This process reduces capital costs because the cost of pumping, instrumentation, and piping diminishes as well as energy consumption by the integration of two stages into one. However, maintenance and control are difficult because multiple steady states are possible and local equipment operation may become unstable (DE LIMA DA SILVA et al., 2010).

Ultrasonic reactors use sound energy or energy associated with the flow to form dots where cavitation occurs, so, mass transfer phenomena become more intense. Some advantages of ultrasonic cavitation process are: 1) reaction time reduction, 2) low alcohol to oil molar ratio, 3) low energy consumption, 4) reduction of catalyst concentration, and 5) increase of conversion and selectivity. In contrast, the process has disadvantages such as the need for high reaction temperatures and low power ultrasound to control soaps formation (YU et al., 2010).

Liquid - liquid film reactor (LLFR) is a column packed which generates interfacial area without dispersing one phase in the other, reducing the separation time, increasing the process productivity. This process could be developed in co-current or counter-current, both producing high conversion and yield (CADAVID et al., 2013, NARVÁEZ et al., 2009). This is one of integration technologies proposed in this work, reason why section 1.3 will describe in detail its operation, strengths, and limitations.

Membranes in biodiesel production are physical barriers permitting selective transport of some mixture components. The driving force is the pressure difference between both sides of the membrane (AMIN et al., 2010). Membrane technology is part of process intensification trend in chemical engineering because it can remove reaction products retaining the reaction mixture, which improves process productivity reducing the size of reaction and separation equipment as well as the energy consumption. Given the potential of this technology and the complex considerations that must be taken into account for its implementation, a review of the issues involved in the use of membranes is required to identify the main developments and advances in this technology. Section 1.4 will show a complete review of membranes in biodiesel production.

1.3 Biodiesel production in liquid – liquid film reactor

LLFR is a mechanical device which permits mass transfer between two immiscible liquid phases. One of the liquids (retained phase) wet fibers set extended linearly along the reactor axis creating a film over the packing, while the second liquid (continuous phase) flows over the first film creating a second film over the packing (NARVÁEZ et al., 2009). Figure 1-7 shows schematically the film distribution of both phases over the packing.
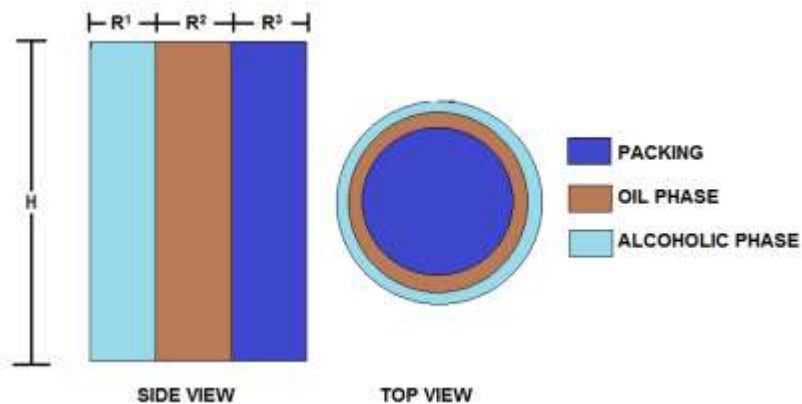
Figure 1-7. Film distribution over the packing.

Films generation increases the interfacial area between both phases without dispersing one phase into the other, which reduces mass transfer limitations in the reaction stage and residence time in the downstream decanter. Figure 1-8 shows the co-current LLFR scheme for biodiesel production.

The oil and methanol are fed at the column top (input 1 and 2 respectively). Downstream, they flow into the packed section starting the reaction. Finally, reaction products distributed in ester-rich and alcohol-rich phases (methanol and catalyst are present in both phases) leave the reactor and the ester and alcohol-rich phase are separated by decantation (output 3 and 4).
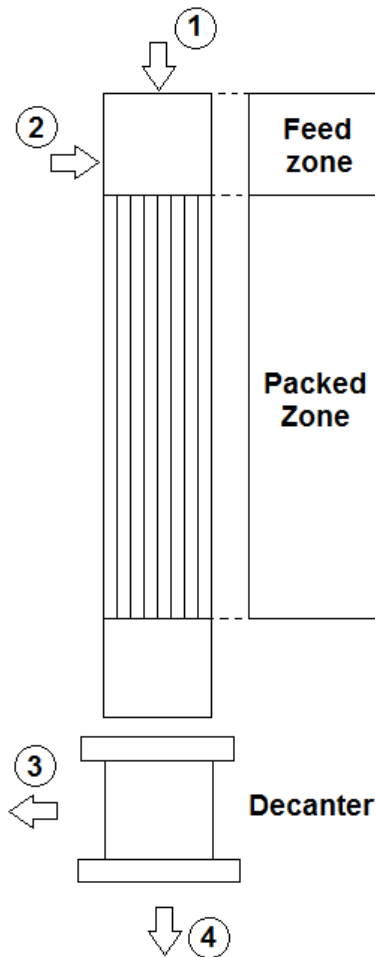
Figure 1-8. LLFR co-current scheme.

LLFR behaves like a PFR reactor (plug flow reactor). If the reactor residence time increases, final conversion and yield increase up to 97.5% and 92.2%, respectively. However, in order to achieve the required product quality the implementation of two reaction stages including decantation between them is necessary (NARVÁEZ et al., 2009).

LLFR can be operated in counter-current scheme achieving 99.9% yield (Table 1-2). The increase in yield compared to co-current flow pattern is a consequence of the continuous glycerol removal (CADAVID et al., 2013). Figure 1-9 shows schematically the operation of the LLFR in counter-current flow pattern. The methanol with catalyst is fed to a nozzle placed at the top of the reactor (input 1) while the oil is fed at the bottom of the reactor (input 4). The ester-rich phase is obtained at the top of the reactor (output 2) and the glycerol-rich phase at the bottom (output 3). The flow pattern into the reactor is a

consequence of density difference between the phases: Although methanol has less density than oil, once glycerol is produced the density of the glycerol-rich phases increases and flows down, while the ester-rich phase has low density and flows up (CADAVID et al., 2013).
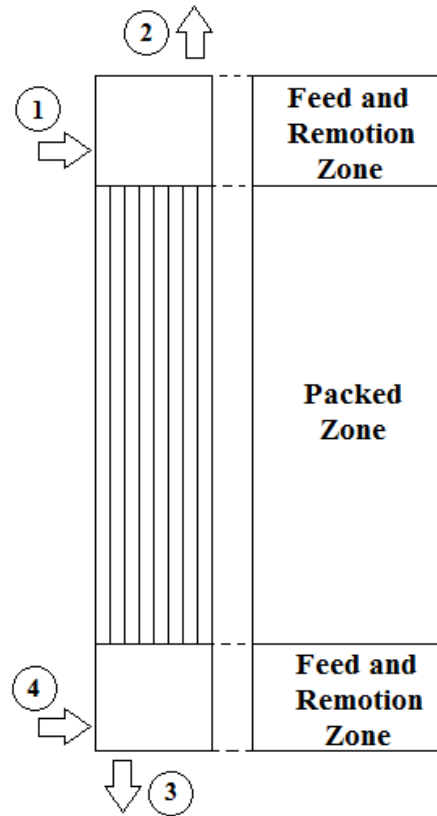
Figure 1-9. LLFR counter-current scheme.

Table 1-2 shows a comparison between LLFR performance and the traditional technology using stirred tank reactors (STR) (CADAVID et al., 2013). Although the counter-current LLFR technology has the highest yield and productivity, the values for the co-current LLFR are at least four times those for the traditional technology. Besides, the LLFR has a positive effect on separation stages, because interfacial mass transfer area is achieved without mixing, which shorter residence time in decantation stage in comparison to STR technology. Despite, the counter-current LLFR requires only one reaction stage to achieve the conversion and yield required industrially, it presents stability and controllability problems (CADAVID et al., 2013).

Table 1-2. Comparison between LLFR and STR for biodiesel production (CADAVID et al., 2013).

Variable	Counter-current	Co-current	STR
Number of reaction stages	1	2	2
Conversion (%)	99.7	99.4	99.9
Yield (%)	99.9	97.2	98.3
Productivity ($m^3/ m^{-3}h^{-1}$)	1.8	1.2	0.3

1.4 Biodiesel production assisted by membranes

Microfiltration (MF) and ultrafiltration (UF) are membrane technologies used for the separation of liquid phase mixtures. The separation occurs by size difference in particles or drops. Components that permeate through the membrane are those whose droplet size is smaller than the membrane pore diameter (permeate). The material retained (retentate) remains in the liquid phase. The process is illustrated in Figure 1-10. Membrane operation is characterized by two fundamental parameters: flux and selectivity. Flux is a measure of the mass able to permeate the membrane and selectivity is a measure of the separation quality.
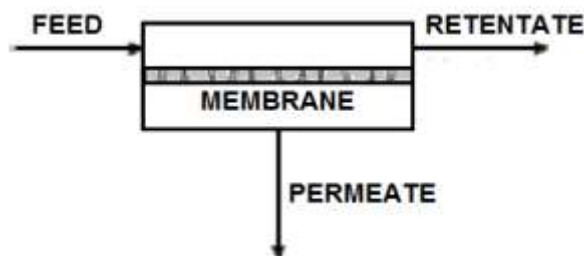
Figure 1-10. Microfiltration and Ultrafiltration process.

Membrane technologies in biodiesel production have two different applications: glycerol removal in purification stages and retention or separation of TGs, DGs, and MGs in the reaction stage. Regardless its application, membranes evaluated can be ceramic or polymeric. The objective is the same in both cases: to prevent the passage of small drops (glycerol or oil) with a physical barrier (membrane). Following, some results about membranes implementation in biodiesel production are shown. In the first section membrane materials implemented (section 1.4.1) are presented. In the second section membrane transport mechanism is described (section 1.4.2). In the third section, main

applications in glycerol removal for biodiesel purification (section 1.4.3) are shown. In the fourth section TG, DG, and MG separation from reactive mixture (section 1.4.4) is presented, and finally, the fifth section presents applications using reactive membranes (section 1.4.5).

1.4.1 Membranes according to the construction material in biodiesel production

Membranes assessed in biodiesel production are inorganic (ceramic) or organic (polymer). Although polymeric membranes are cheaper and easy to synthesize, ceramic membranes are more suitable for systems involving organic solvents, because they have excellent thermal, mechanical and chemical stability, which increases its lifetime (BARREDO-DAMAS et al., 2010, DUBÉ et al., 2007). Table 1-3 shows the main materials reported in the literature for biodiesel production assisted by membranes.

Table 1-3. Membrane materials for biodiesel production.

		Characteristics		Reference
		Material	**Application**	
Ceramic	Al2O3/ TiO2	α-Al_2O_3/TiO_2	MF, UF	(ATADASHI et al., 2012, BAROUTIAN et al., 2011, GOMES et al., 2010, SHI et al., 2010, SHUIT et al., 2012)
	Filtanium TM	TiO_2	UF	(CAO et al., 2008a, 2008b)
	Carbo-Cor	Carbon	MF	(CAO et al., 2007, CHENG et al., 2009, DUBÉ et al., 2007)
	TAMI	ZrO_2 / $Zr(SO_4)_2$	MF, UF	(CHENG et al., 2009, SHI et al., 2010)
	Zeolites	SiO_2, Al_2O_3, MgO, CaO	MF. UF	(ATADASHI, I.M. et al., 2011, INOUE et al., 2007)
Polymeric	PS	Polysulfide		(HE et al., 2006)
	PES	Polyethersulfone	MF, UF, UF	(SALEH, 2011)
	PVDF	Polyvinylidene fluoride	UF	(SALEH, 2011)
	PVA	Polyvinyl Alcohol	MF, UF	(GUERREIRO et al., 2006, 2010)
	PA	Polyamide	UF	(OTHMAN et al., 2010)
	PI	Polyamide	UF	(OTHMAN et al., 2010, SHI et al., 2010, SUBRAMANIAN et al., 2003)
	PAN	Polyacrylonitrile	MF, UF	(HE et al., 2006, SALEH, 2011)
	PP	Polypropylene	MF	(COELHOSO et al., 2000, DINDORE et al., 2005, VENERAL et al., 2013)
Hybrids	$(Zr(SO_4)_2)$ / (SPVA)	$(Zr(SO_4)_2)$/(SPVA)	MF	(SHI et al., 2010, SHUIT et al., 2012)
	TS-1/PDMS	(TS-1) con (PDMS)	MF	(SHUIT et al., 2012, WU et al., 1998)

1.4.2 Membranes transport mechanism in biodiesel production

Figure 1-11 shows the transport mechanism for TG, DG, and MG in the reaction mixture. When TG are present in methanol at low concentration, there is a dispersion of the ester-rich phase (oil droplets) in the alcoholic phase. As a consequence, the alcoholic phase flows through the membrane while oil droplets, bigger than the pore size of the membrane, are retained (CHENG et al., 2009).
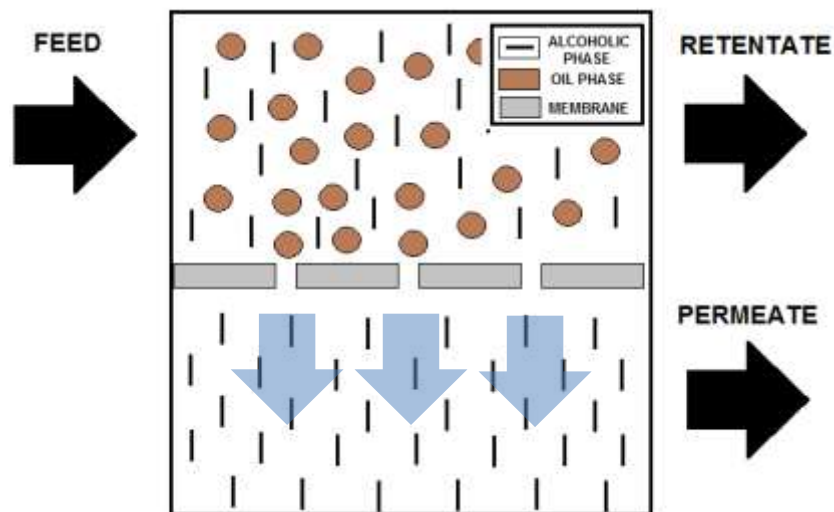
Figure 1-11. Transport mechanism in the biodiesel reaction.

On the other hand, glycerol traces in biodiesel after phase separation (Figure 1-12) are retained by the membrane. Ester-rich phase obtained from decantation stage contains glycerol droplets and soap. Glycerol droplets are retained and only pure biodiesel permeate through the membrane (WANG et al., 2009). Biodiesel is obtained in the permeate accomplishing the quality specifications defined in product standards (SALEH, 2011). A comparison between Figures 1-11 and 1-12 shows both applications have the same transport mechanism.
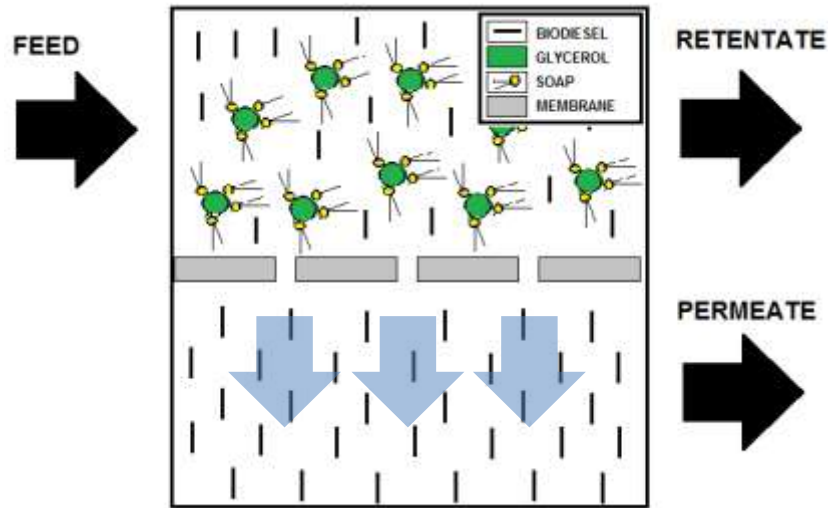
Figure 1-12. Transport mechanism in the biodiesel purification.

Figure 1-13 shows selectivity results for membranes used in biodiesel reaction. CAO et al., (2007) and CHENG et al., (2009), argued retention of TG is reached at methanol to oil molar ratio higher than 6:1. The membrane retains TG and MG at different conversions. However, when the conversion is greater than 25% DGs permeates through the membrane (CAO et al., 2007). ARAUJO et al., (2011) reported glycerol is retained by the membrane independent of the conversion at ratios of methanol to oil lower than 5:1. However, for higher ratios (9:1) glycerol retention is only possible if conversion is higher than 50%. Retention increases with the conversion, confirming glycerol retention by the membrane is only possible at low concentrations of methanol. MUÑOZ et al., (2014) tested the permeation for different binary blends of TG, FAME, G, and M with ceramic membranes, FAME-TG and FAME-M blends did not show any significant difference between permeate and retentate, indicating that separation is only feasible when glycerol is present.
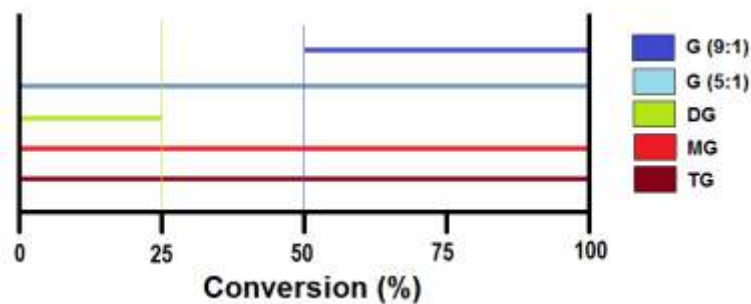
Figure 1-13. Membrane retention for different reactor conversion.

1.4.3 Glycerol removal in biodiesel purification

Traditionally, biodiesel purification is developed by washing it with water. However, this stage is intensive in water consumption and waste generation. In order to solve these drawbacks, membrane technology has been investigated to purify and refine biodiesel separating glycerol traces according to the mechanism described in section 1.4.2 (GOMES et al., 2011). Following, some results about this topic are presented.

- Ceramic membranes

WANG et al., (2009) developed a separation process for biodiesel purification using ceramic membranes. In their work, biodiesel produced from refined palm oil was processed with microfiltration (MF) in order to remove soaps and free glycerol. Membranes with a pore size of 0.6, 0.2 and 0.1 µm were used. The membrane pore size of 0.1 µm was the most appropriate for remove soaps, glycerol, and metals. At this pore size, the effect of pressure drop across the membrane (transmembrane pressure TMP) was studied in the range from 0.05 to 0.20 MPa and at temperatures of 30, 40, 50, 60, 70 °C. The membrane operated at 0.15 MPa and 60 °C showed a stable flux permeate (300 L/m^2h flux). The membrane with pore size of 0.1µm reduced the free glycerol content in permeate to 0.0108 %wt. accomplishing the quality requirement (0.02 %wt. ASTM 6751, EN 14214 and NTC 5444). The membrane was washed with methanol at the end of the operation in order to remove soap and free glycerol accumulated on its surface and pores. The micelle size formed by glycerol and soap was 2.21 µm, (significantly bigger than the biodiesel molecular size). Water consumption was reduced, because it was only required for the neutralization step.

GOMES et al., (2010) used tubular ceramic membranes made of α-Al_2O_3/TiO_2 with pore diameters of 0.2, 0.4 and 0.8 µm. These membranes efficiently separated biodiesel and glycerol. The authors emphasized the importance of TMP during biodiesel purification. Membranes 0.2 µm pore diameter of at TMP of 2.0 bar operated better with a stable permeate flux of 78.4 kg $m^{-2}h^{-1}$ and glycerol retention of 99.4%. Smaller the pore size and lower the methanol concentration in the feed, higher the FAME selectivity and lower the glycerol concentration in the final biodiesel. Subsequently, they evaluated a tubular ceramic membrane (α-Al_2O_3/TiO_2 - pore diameter 0.2 µm) for glycerol removal from soybean biodiesel, adding small amounts of acid water (GOMES et al., 2011). This

addition promotes glycerol removal. They evaluated the glycerol removal using a tubular ceramic α-Al_2O_3/TiO_2 with pore diameters of 0.05, 0.1 and 0.2 μm, with an addition of acidified water (10, 20 and 30% of water with 0.5% HCl), TMP from 1.2 to 3 bar at 50 °C. They established that 0.05 μm membranes operating at 1 bar TMP with the addition of 10% water acidulated increases glycerol retention. Water addition higher than 10% increases the fouling effect in the membrane (GOMES et al., 2013). Finally, they evaluated the influence of oil quality on the biodiesel and glycerol separation by ultrafiltration. The highest free fatty acid content in the crude canola oil, not only favored the formation of a dispersed phase containing glycerol, which was retained by the membrane, but also resulted in the lowest flux decline rates. The ultrafiltration was efficient in removing glycerol, since the highest glycerol content in the permeate was 0.013 wt.% (GOMES et al., 2015).

SALEH et al., (2011) studied glycerol removal from biodiesel using UF and MF ceramic membranes of 0.05 μm and 0.2 μm, respectively, at 0, 5 and 25 °C. Biodiesel quality defined in the standards was achieved using UF membranes during three hours at 25 °C, with concentration factor up to 1.6. ATADASHI et al., (2012) studied glycerol removal from biodiesel using a ceramic membrane Al_2O_3/TiO_2 with a pore size of 0.02 μm. They evaluated the removal at different TMP (100, 200 and 300 kPa), temperatures (30, 50, and 40 °C) and flow rates (60, 105 and 150 L/min). The best operation condition was 200 kPa, 40 °C, and 150L/min, obtaining a flux of 9.08 kg.m^{-2}.h^{-1}) and biodiesel without glycerol. The addition of small amounts of acidulated water to biodiesel maximized the glycerol removal.

▪ Polymeric membranes

SALEH et al., (2010) tested a hydrophilic modified polyacrylonitrile membrane with pore size of 0.1 μm at 25 °C, 552 kPa and water addition from 0.06 to 0.2 %wt. The objective adding water was to increase the glycerol droplet size. Methanol has a negative effect on glycerol separation because the alcohol reduces the dispersed phase formation and increases glycerol solubility in biodiesel. They reported permeate fluxes of 11 and 9 L/m^2h for water additions of 0.1 and 0.2 %wt., respectively, and glycerol concentrations in the permeate of 0.017 and 0.013 %wt., respectively. SALEH, (2011), tested three polymer membranes in the UF range (10-100 nm): polyethersulfone (PES), polyvinylidene fluoride (PVDF) and polyacrylonitrile (PAN). These materials showed high glycerol retention. They developed three tests during 3h at 25 °C. The free glycerol contents in permeate were

0.019% wt., 0.02% wt., 0.017% wt., for PES (1 nm), PVDF (30 kDa), and PAN membrane, respectively.

ATADASHI, I. M. et al., (2011) observed biodiesel recovery in the permeate. Due to the interaction of the hydrophobic membrane with biodiesel (non-polar phase). They reported glycerol content less than 0.02 %wt. The TMP is the variable with the greatest effect on glycerol separation from biodiesel. The use of membranes technology to refine biodiesel can reduce water consumption up to 75%, reducing oil losses up to 44%, improving process yield and environmental performance. CHOI et al., (2005) reported that MF polymeric membranes presented more separation failures than UF.

OTHMAN et al., (2010) tested eight polymeric membranes in nanofiltration. They tested the permeability with products of the transesterification reaction, including TG, DG, MG, glycerol, FAME and methanol, after a neutralization reaction with phosphoric acid (H_3PO_4). Permeability tests were conducted at pH 12.4 and 40 °C. The effect of the TMP in the range from 0 to 3000 kPa in permeate flux was evaluated. At the end of the tests deterioration of all the membranes was observed. The authors found that the effect of pressure on the permeate flux is linear and positive. Temperature also has a positive effect on permeate flux due to the combination of three factors: viscosity reduction, diffusion coefficient increase and increment of the free spaces between polymer chains, which facilitates sorption and diffusion of permeate through the membrane (MACHADO et al., 1999, 2000).

Recently, TORRES et al., (2017) tested hydrophobic polymeric membranes. The poly(vinylidene fluoride) membrane reached a glycerol rejection up to 67% (30 °C and 5 bar) from a biodiesel sample with 0.5 %wt. of water added. Under the same operating conditions, the poly(sulfone) membrane showed a lower separation performance, with glycerol rejection of 48%. High stability and low fouling of the membrane were observed.

▪ Analysis

Table 1-4 shows the main variables on glycerol removal from biodiesel. Membrane material (ceramic and polymeric) do not show an influence on the variables because both scenarios operate under the same separation mechanism, where glycerol micelles are

retained by the membrane. Selectivity increases when methanol concentration, pore size or TMP diminish.

Table 1-4. Main variables on the glycerol removal from biodiesel in purification stage. (NR: No reported, NE: No effect).

	Membrane	Selectivity	Flux	Drop size	Reference
Methanol	Ceramic	Decrease	Increase	Decrease	(SALEH, 2011)
	Polymeric	Decrease	Increase	Decrease	(SALEH, 2011)
Pore size	Ceramic	Decrease	Increase	N.E	(GOMES et al., 2010, SALEH, 2011, WANG et al., 2009)
	Polymeric	Decrease	Increase	N.E	(ATADASHI et al., 2012, SALEH, 2011)
Temperature	Ceramic	N.R	Increase	Decrease	(ATADASHI et al., 2012, SALEH, 2011, WANG et al., 2009)
	Polymeric	N.R	Increase	Decrease	(OTHMAN et al., 2010, SALEH, 2011)
Transmembrane pressure	Ceramic	N.E	Increase	N.E	(ATADASHI et al., 2012, GOMES et al., 2010, WANG et al., 2009)
	Polymeric	N.E	Increase	N.E	(ATADASHI et al., 2012, OTHMAN et al., 2010, SALEH, 2011)
Flow rate	Ceramic	Increase	N.R	N.R	(ATADASHI et al., 2012)
	Polymeric	Increase	N.R	N.R	(SALEH, 2011)

1.4.4 TG, DG and MG separation from the reactive mixture

Membrane integration in the transesterification reaction, selectively remove products (FAME and G) as well as M, improving the productivity and yield. The transport mechanism was presented in the section 1.4.2. Following, the main operating variables and its effect on the permeate flux and selectivity are presented.

- Ceramic Membranes

In order to obtain FAME free from TG, DG, and MG, some membrane processes have been researched. For example, DUBÉ et al., (2007) evaluated a carbon membrane (0.05 µm). This membrane permitted the flow of M, G and FAME retaining TG, DG, and MG. The authors argued that the membrane was able to stop small glyceride drops present as an emulsion. Carbon membranes have high resistance to acidic and basic environments. CAO et al., (2006) studied the effect of membrane pore size and methanol fraction on the performance of a membrane reactor for biodiesel production. It was found that the pore size did not affect the permeate quality. However, at low methanol concentration permeate flow through the membrane was not observed. Carbon membranes with pore size of 0.05, 0.2, 0.5, and 1.4 µm and methanol to oil ratios of 11: 1, 16: 1, 23: 1 and 46: 1 were tested. Separation occurs because the average size of the oil droplets is in the range of 12-400 µm, which is bigger than the membrane pore size.

CAO et al., (2008a) studied the effect of oil composition on the membrane reactor. They found that biodiesel quality is affected by the oil composition. CAO et al., (2008b) studied the effect of methanol recirculation in the production of biodiesel in a ceramic membrane reactor. The authors reported the membrane reactor can retain TG, DG, and MG while removes biodiesel, methanol, and glycerol. When the reactants are mixed, oil drops are formed. These drops are not able to pass through the pores of the membrane, so unreacted vegetable oil is retained and product removal is achieved. However, high concentrations of biodiesel increase diglycerides solubility and it pass through the membrane. A reduction in residence time and catalyst concentration could prevent the presence of DG in permeate.

CHENG et al., (2009) studied UF of TG from biodiesel using the phase diagram Oil/FAME/M. Ceramic membranes (0,14 µm) were tested, showing that ester-rich phase was rejected, while the alcohol-rich phase permeates through the membrane. Different temperatures (20°C, 40°C and 60°C), TMP (0 to 1000 mmHg), flow rates (300 ml/min, 400 ml/min and 500 ml/min) and Oil/FAME/M mass fractions (20/30/50, 20/40/40, 20/65/15 y 20/75/5) were evaluated. They did not identify flow rates or TMP effects on the selectivity, but TMP increment increased the flux, while flow rate reduction diminished the flux. Temperature and feed composition affect the selectivity because change the LLE location.

TG presence in the permeate increases with the temperature. TG was not found at 20/30/50 mass fraction, 600mmHg of TMP and 20 °C. However, the separation was not observed if the mixture is homogeneous, regardless the TMP, flow rate or temperature.

Currently, it is not clear the transport mechanism through the membrane in the biodiesel production. The most logical explanation is the LLE influence on the selectivity (CHENG et al., 2009), but this explanation was not confirmed yet. CHENG et al., (2010) evaluated the biodiesel from canola oil system in batch reactor assisted by membranes. They found the reaction mixture should be heterogeneous (located in the immiscibility region) to ensure TG, DG, MG separation from the products. High catalyst concentration is not necessary. CHENG et al., (2012) studied biodiesel production using a membrane reactor coupled with a pre-reactor. A mathematical model was developed to describe the pre-reactor and the membrane reactor. The model includes transesterification kinetics and liquid-liquid equilibrium. The reactors are located in series and show a synergic effect. Methanol to oil ratio must be higher than 6:1 to guarantee immiscibility of the reaction mixture and membrane separation. BAROUTIAN et al., (2011) used an alkaline catalyst in a heterogeneous membrane packed-bed reactor. The authors used a ceramic membrane reactor tubular module (TiO_2/Al_2O_3), which was filled with potassium hydroxide supported on activated carbon KOH/AC. The catalyst activity decreases to 89.3% of its original value after three uses. During the transesterification, reactor membrane blocked the passage of TG, DG, and MG, while the products pass (FAME, G, and M). The highest conversion was 94% at 70 °C and 0.21 cm/s. Ceramic membrane showed excellent chemical and physical stability; as a matter of fact, it operated for one year without changes.

XU et al., (2013) tested a catalytic membrane ($KF/Al_2O_3/CM$) for biodiesel production from palm oil and methanol, achieving a FAME yield of 90%. The results revealed that the alumina content has an important influence on the thickness and stability of the γ-Al_2O_3/CM layers. The membranes of KF/γ-Al_2O_3/CM show high activity in the transesterification and they can be reused.

- Polymeric membranes

SUBRAMANIAN et al., (2003) studied TG and oleic acid retention in a hydrophobic polymeric membrane (NTGS-2200) with silicone active layer and polyamide support. Experiments were performed with a flat dense membrane in a nitrogen atmosphere. The

effect of pressure, temperature and stirring speed at intervals of 2 to 5 MPa, 20 to 50 °C and 400 rpm, respectively, on membrane performance, were studied. The results showed pressure has a significant effect on permeation rate. The authors stated that the observed behavior of the system suggests the predominant transport mechanism is oil solution-diffusion through the nonporous membrane. The effect of temperature on permeate suggests a convective flow. SARKAR et al., (2010) prepared a dense membrane of polyvinyl alcohol (PVA) with polyethersulfone (PES) for the esterification of oleic acid with methanol using sulfuric acid as catalyst. Esterification process conversion was optimized changing reactive molar ratio, catalyst concentration, and temperature. At molar ratio of oleic acid: methanol from 1 to 27 and after 6 h of reaction, the conversion was 99.9% using 0.3% H_2SO_4 at 65 °C. Product acid value was 0.2 mg KOH/g (less than the specification for biodiesel of 0.5 mg KOH/g). Membrane performance was evaluated by estimating the permeate flux and the degree of separation of binary mixtures of methanol and water. Water concentration increasing from 1 to 3 %wt. leads to an increase in the flux from 1.6 to 5.4 g/m^2h, because of the PVA hydrophilic affinity, cause swelling, increasing the permeate flux and decreasing methanol selectivity. It was also noted that there is competition in the mechanisms of sorption and permeation (solution-diffusion) between methanol and water, because both substances are polar, which is reflected in its moderate separation factor. The membrane performance was evaluated and used for three months, keeping constant the results obtained at the beginning of the test.

CHONG et al., (2012) used a tubular membrane reactor combined with ultrafiltration to produce biodiesel from canola oil via alkali-catalyzed methanolysis, they recycle the retentate continuously. Their experimental results showed that the permeate compositions from the membrane reactor were closely related to chemical phase equilibrium of the system, which was depending on the M to TG molar ratio. TG free permeate can only be obtained if the continuous phase of M was free from TG and the TG rich micelles were retained by the membrane. Then, they used a mathematical model which combines the chemical and phase equilibrium, the model gives a good fit to the experimental data for the conditions tested (OH et al., 2015). Recently, BELLO et al., (2016) showed that poly(ether sulfone) hollow fiber membranes (PES-HFM) have enough chemical and mechanical resistance to be used in the biodiesel production and separation. FILHO et al., (2016) coupled heterogeneously catalyzed transesterification and glycerol extraction using a

membrane contactor and water or ethanol as the extraction phase, they achieved glycerol removal from the reactor and its flux was proportional to the glycerol composition. Nevertheless, they reported a maximal conversion of 35%.

▪ Analysis

Table 1-5 shows the main variables in TG, DG, and MG retention. Membrane flux in ceramic and polymer membranes for the removal of FAME, G and M is favored by high concentrations of methanol, big pore sizes, high TMP and low flow rate. Selectivity increases with high methanol concentrations, small pore sizes, high TMP and high flow rate. Membrane material (ceramic and polymeric) does not have an influence on the variables because in both scenarios the separation mechanism is the same, where oil micelles are retained by the membrane.

Table 1-5. Main variables on the TG, DG and MG retention from biodiesel in reaction stage. (NR: No reported, NE: No effect).

	Membrane	Selectivity	Flux	Drop size	Reference
Methanol	Ceramic	Increase	Increase	Increase	(CAO et al., 2008b, CHENG et al., 2009, 2010)
	Polymeric	Increase	Increase	Increase	(ATADASHI, I. M. et al., 2011)
Pore size	Ceramic	Decrease	Increase	N.E	(CAO et al., 2007)
	Polymeric	Decrease	Increase	N.E	(ATADASHI, I. M. et al., 2011)
Temperature	Ceramic	Decrease	Increase	Decrease	(CHENG et al., 2009, 2010)
	Polymeric	N.R	Increase	Decrease	(ATADASHI, I. M. et al., 2011)
Transmembrane pressure	Ceramic	N.E	Increase	N.E	(ATADASHI, I. M. et al., 2011, CHENG et al., 2009)
	Polymeric	N.E	Increase	N.E	(ATADASHI, I. M. et al., 2011)
Flow rate	Ceramic	Increase	Decrease	N.R	(CAO et al., 2008b, CHENG et al., 2009)
	Polymeric	Increase	Decrease	N.R	(ATADASHI, I. M. et al., 2011)

1.4.5 Reactive membranes in biodiesel production

Reactive membranes are membranes catalytically active and selective, in consequence, reaction and separation occur inside the membrane (SHI et al., 2013). This technology has been investigated in biodiesel production because its implementation can reduce the catalyst and separation cost. Table 1-6 presents reactive membranes evaluated for biodiesel production. Most of the works used fatty acid and methanol as raw material and functionalized membranes with acid characteristic. Thus, membranes assessed are appropriated for esterification, not for transesterification. However, GUERREIRO et al., (2006, 2010) obtained biodiesel from TG by transesterification using reactive PVA membranes. However, PVA pellets were used to cover the catalyst, then, selectivity characteristics were not present. ZHU et al., (2010) mixed PVA with polystyrene sulfonic acid (PSSA) to functionalize the membrane. The final conversion was 92% with reaction times up to eight hours. The modified PVA membrane shows higher catalytic activity with higher amounts of sulphonic acid due to increased SO_3H groups in the polymer matrix (CASTANHEIRO et al., 2006). SHUIT et al., (2012) crosslinked PAN membranes with 5-sulfosalicylic acid (SA). Recently, EL-ZANATI et al., (2016) studied the esterification reactions of ethyl hexanoic acid and acetic acid with ethanol using a catalytic membrane reactor. Maximum conversion obtained were 97.7% and 96%, respectively. Other authors (SHI; LI; ZHOU; QIN; et al., 2016) studied biodiesel production with a catalytic membrane composed by phosphotungstic acid (PWA)/poly(vinyl alcohol) (PVA). A maximal conversion of 40% was reported. However, they report catalytic stability of the PWA/PVA nanofiber only during 10 days. SHI; LI; ZHOU; ZHANG; et al., (2016) prepared a series of alkalized polysulfones membranes as heterogeneous catalyst for the transesterification of soybean oil with methanol. The membrane still kept a conversion of 93.2% after five runs. Finally, a Monolithic KF/hydrotalcite/honeycomb ceramic catalyst was prepared and employed for transesterification in a membrane reactor. The highest biodiesel yield reported was 91.7% (XU et al., 2015).

Table 1-6. Reactive membranes in the biodiesel production.

Reactive mixture	Membrane Material	Conclusion	Reference
Acetic acid and ethanol	PES/SPES	PES/SPES membrane synthesis	(SHAH; RITCHIE, 2005)
FFA and methanol	PSSA/PVA	Membrane thickness does not affect the conversion.	(ZHU et al., 2010)
FFA and methanol	Zr(SO$_4$)$_2$/SPVA	High conversion, yield, and stability, better performance of Zr(SO$_4$)$_2$/SPVA than Zr(SO$_4$)$_2$/PVA.	(SHI et al., 2011)
FFA and methanol	PES/SPES	High methanol quantity and temperature, promote the reaction.	(SHI et al., 2011)
Oleic acid and methanol	PES/SPES	High porosity and membrane thickness promote the conversion.	(SHI et al., 2013)
FFA, methanol, ethanol, propanol and butanol.	PES/Res	Butanol shows the higher conversion.	(ZHANG et al., 2012)
Soybean oil and methanol	PVA	Membrane used as pellets.	(GUERREIRO et al., 2006)
Soybean oil and methanol	PVA with hydrotalcite	Membrane used as pellets. The activity is higher than the hydrotalcite without PVA.	(GUERREIRO et al., 2010)

2. Research problem

2.1 Problem description

Biodiesel is mainly produced by transesterification of vegetable oils and methanol using homogeneous basic catalyst, mainly sodium or potassium methoxide. Most of the industrial processes use BSTR or CSTR. This process has the following limitations:

- Low miscibility between methanol and oil that promotes mass transfer resistance, reducing the reaction rate. This limitation is overtake dispersing the alcohol-rich phase in the ester-rich phase by mechanical stirring. The synergistic effect of mixing and formation of soaps and gels, increases separation times in the two-phase separators downstream reactor.

- Technical specifications required for biodiesel commercialization demand low levels of glycerol, monoglycerides, diglycerides and triglyceride (less than 0.25%). However, given the limitations of chemical and physical equilibrium, it is necessary the use of methanol excess and multistage reaction processes, which reduces the process productivity and profitability.

- The use of homogeneous catalysts is not suitable for low-cost raw materials with high fatty acid levels and high water concentration because promoted the soaps and gels formation that reduce reaction yields and difficult the glycerol separation.

Liquid – Liquid film reactors operated in co-current and counter-current, reduce previously exposed limitations (CADAVID et al., 2013, NARVÁEZ et al., 2009). However, co-current LLFR needs at least two reaction stages to obtain the conversion and yield required in the

industry and the counter-current LLFR presents difficulties with stability and operational control. The aim of this work is overcome LLFR limitations, integrating into an LLFR a membrane to perform the selective removal of glycerol. This removal will reduce product concentration inside the reactor overtaking the equilibrium limitations. This behavior will increase the reactor conversion and yield, without presenting difficulties in the operation stability and control. These factors will increase the process productivity and profitability.

2.2 Hypothesis

It is possible to increase the liquid – liquid film reactor productivity integrating membranes within the reactor. Membranes permit selective removal of reaction products, which shifts the equilibrium towards the biodiesel formation, promoting an increase in conversion, yield, and productivity. Also, it helps to reach the required quality standards (mostly ester concentration) in a single reaction step.

2.3 General objective

To evaluate theoretically and experimentally the performance of a liquid – liquid film reactor assisted by membranes in biodiesel production.

2.4 Specific objectives

1. To determine experimentally the kinetic model parameters for vegetable oils methanolysis.

2. To determine membrane permeability and selectivity for the main components involved in biodiesel production (triglycerides, methyl esters, glycerol, and methanol).

3. To develop a mathematical model for the falling film reactor assisted by membranes.

4. To simulate the liquid – liquid film reactor assisted by membranes using the proposed mathematical model, the obtained kinetic parameters and membrane parameters.

5. To design the intensified reactor (liquid – liquid film reactor assisted by membranes) and to evaluate experimentally their performance in the biodiesel production.

2.5 Methodology

This thesis was developed in a doctoral program in co-supervision scheme, obeying the rules of the two institutions involved: Universidad Nacional de Colombia and Universidade Federal do Rio de Janeiro.

The evaluation of the LLFRM implies the integration of the concepts involved in LLFR and UF through the membrane. Both systems were studied separately and integrated. In order to understand the reactor behavior, the first stage of this study was the determination of the kinetic model to be used. The kinetic model provides information about the effect of temperature, methanol content and catalyst concentration in the reaction. Permeate composition is a function of the LLE. In order to understand the membrane behavior, the second stage was the prediction of the liquid – liquid equilibrium in systems composed of biodiesel, glycerol, and alcohol. The third step was the development of a mathematical model for the LLFR, including its experimental validation. A mathematical model provides information about the hydrodynamic behavior of the system as well as the effect of the flow rate and the quantity of package on reactor performance.

The fourth step of the methodology is the investigation of phase separation using UF membranes. This study describes the membrane behavior and develops a mathematical model experimentally validated. Finally, the mathematical model of the reactor and the membrane were integrated to describe the LLFRM. The predictions of the integrated model experimentally validated were used to choose the main variables for the systems. The best operation conditions were experimentally tested. A mathematical model of the

LLFRM includes the developed models: kinetic model, LLE prediction, LLFR model and UF membrane model.

1) Determination of the kinetic model

Experimental methodology and results for the kinetic model that describes vegetable oil transesterification are presented in chapter 3, including the standardization of the gas chromatography method to determine FAME, MG, DG, and TG, fundamental for this investigation. Tests were performed to study the transesterification of Jatropha and soybean oil. These data plus the previously obtained for palm oil methanolysis were used to adjust a second order kinetic model including the effect of catalyst concentration.

2) Determination of LLE

Numerical methodology to determine the parameters of a modified UNIFAC model to predict the liquid - liquid equilibria is described in chapter 4. In order to find the group interaction parameters (GIP) for the model, a complete database with LLE for systems biodiesel, glycerol and methanol reported in the literature was built. A genetic algorithm was used to find the GIP. The objective function was the difference between the experimental tie lines in the database and the model predictions.

3) Mathematical description and experimental validation of the LLFR

A mathematical model for biodiesel production using an LLFR operated in co-current flow pattern was developed. The model includes mass transfer limitations and describes hydrodynamics inside the reactor. The model was validated with experimental data obtained in a bench level reaction system, studying the effect of the packing surface area to reaction volume ratio packing fraction (444 to 5333 m-1 5 to 60%), VO vegetable oil (VO) flow rate (5 to 40 g min-1) and reactor length (0.25 to 1 m) on conversion and FAME yield, at constant temperature (55°C), catalyst concentration (1% w/w based on VO weight) and molar ratio methanol to oil (6:1). Details about the mathematical model and its experimental validation are described in chapter 5 and annex A.

4) Determination of membrane behavior

Experimental determination of permeability and permeate composition were performed using pure components, binary mixtures, and ternary mixtures involved in the biodiesel production (FAME, G, and M). Experimental validation included an evaluation of Pressure difference through the membrane (ΔP, 0 to -0.6 bar), flow rate (5 to 40 g min^{-1}), feed bulk composition and biodiesel volumetric fraction (0 to 0.6) effects on flux and permeate

composition, corresponding to conventional conditions in biodiesel production. The membrane was tested in the LLFR equipment to reproduce reactor hydrodynamic characteristics. The experimental permeate and retentate compositions were compared to the UNIFAC LLE predictions. Complete methodology is presented in chapter 6.

5) Mathematical description and experimental validation of the LLFRM

A mathematical model for the LLFRM was developed and experimentally validated. This model integrates the LLFR model LLFR (chapter 5) and the UF membrane model (chapter 6). Besides, it uses the kinetic parameters (chapter 3) and the LLE prediction with UNIFAC (chapter 4). The integrated mathematical model was used to describe the LLFRM behavior and to choose the experimental condition for the model validation. Details about the implemented methodology are provided in chapter 7.

3. Kinetics of vegetable oil methanolysis[3]

3.1 Introduction

The first step for a reactor design is the determination of reaction kinetics. The mathematical model for LLFR and LLFRM requires the determination of the kinetic constants. Biodiesel is largely produced from rapeseed, palm and soybean oils. The main raw material for Brazil is soybean oil and for Colombia is palm oil. However, Jatropha oil is considered one of the most promising sources for producing biodiesel in Asia, Europe and Africa (KARMAKAR et al., 2010). This chapter presents the methanolysis kinetic model for three vegetable oil, jatropha, palm and soybean, corresponding to a second order model that includes the effect of temperature and catalyst concentration on reaction rate. This model describes adequately vegetable oil methanolysis, as validated by the Fisher–Snedecor test of unbiased variances. Kinetic model parameters of Jatropha, palm and soybean oils were compared.

3.2 Materials and methods

3.2.1 Mathematical model of the reaction kinetics of vegetable methanolysis

As it was previously mentioned, TG methanolysis consists of three stepwise reversible reactions: partial methanolysis of TG to form DG, partial methanolysis of DG to form MG and partial methanolysis of MG to form glycerol (G). A molecule of FAME is released during each of the three reactions (NARVÁEZ et al., 2007, NOUREDDINI; ZHU, 1997). The kinetic model of vegetable oil methanolysis can be described by the six differential

---

[3] Results of this chapter were presented in (NORIEGA et al., 2014) and (NARVÁEZ et al., 2015).

equations (3-1) to (3-6). The model has a set of eighteen parameters: six reaction rates, k_i, six activation energies, E_i, and six constants related to the effect of the catalyst concentration on reaction rate, k_{icat}.

$$\frac{d[TG]}{dt} = [M]\left(-k_1 e^{\frac{E_1}{RT}}\left(\frac{C_{cat}}{k_{1cat}+C_{cat}}\right)[TG]\right) + [FAME]\left(k_{-1} e^{\frac{E_{-1}}{RT}}\left(\frac{C_{cat}}{k_{-1cat}+C_{cat}}\right)[DG]\right)$$

(3-1)

$$\frac{d[DG]}{dt} = [M]\left(k_1 e^{\frac{E_1}{RT}}\left(\frac{C_{cat}}{k_{1cat}+C_{cat}}\right)[TG] - k_2 e^{\frac{E_2}{RT}}\left(\frac{C_{cat}}{k_{2cat}+C_{cat}}\right)[DG]\right) - [FAME]\left(k_{-1} e^{\frac{E_{-1}}{RT}}\left(\frac{C_{cat}}{k_{-1cat}+C_{cat}}\right)[DG] - k_{-2} e^{\frac{E_{-2}}{RT}}\left(\frac{C_{cat}}{k_{-2cat}+C_{cat}}\right)[MG]\right)$$

(3-2)

$$\frac{d[MG]}{dt} = [M]\left(k_2 e^{\frac{E_2}{RT}}\left(\frac{C_{cat}}{k_{2cat}+C_{cat}}\right)[DG] - k_3 e^{\frac{E_3}{RT}}\left(\frac{C_{cat}}{k_{3cat}+C_{cat}}\right)[MG]\right) - [FAME]\left(k_{-2} e^{\frac{E_{-2}}{RT}}\left(\frac{C_{cat}}{k_{-2cat}+C_{cat}}\right)[MG] - k_{-3} e^{\frac{E_{-3}}{RT}}\left(\frac{C_{cat}}{k_{-3cat}+C_{cat}}\right)[G]\right)$$

(3-3)

$$\frac{d[FAME]}{dt} = [M]\left(k_1 e^{\frac{E_1}{RT}}\left(\frac{C_{cat}}{k_{1cat}+C_{cat}}\right)[TG] + k_2 e^{\frac{E_2}{RT}}\left(\frac{C_{cat}}{k_{2cat}+C_{cat}}\right)[DG] + k_3 e^{\frac{E_3}{RT}}\left(\frac{C_{cat}}{k_{3cat}+C_{cat}}\right)[MG]\right)$$

$$\ldots\ldots - [FAME]\left(k_{-1} e^{\frac{E_{-1}}{RT}}\left(\frac{C_{cat}}{k_{-1cat}+C_{cat}}\right)[DG] + k_{-2} e^{\frac{E_{-2}}{RT}}\left(\frac{C_{cat}}{k_{-2cat}+C_{cat}}\right)[MG] + k_{-3} e^{\frac{E_{-3}}{RT}}\left(\frac{C_{cat}}{k_{-3cat}+C_{cat}}\right)[G]\right)$$

(3-4)

$$\frac{d[G]}{dt} = [M]\left(k_3 e^{\frac{E_3}{RT}}\left(\frac{C_{cat}}{k_{3cat}+C_{cat}}\right)[MG]\right) - [FAME]\left(k_{-3} e^{\frac{E_{-3}}{RT}}\left(\frac{C_{cat}}{k_{-3cat}+C_{cat}}\right)[G]\right)$$

(3-5)

$$\frac{d[M]}{dt} = -\frac{d[FAME]}{dt}$$

(3-6)

In these equations, T is the reaction temperature and R is the universal gas constant. This model includes the temperature effect on the rate constants through the Arrhenius model and the catalyst effect using equation (3-7).

$$A = A^o \cdot \left(\frac{C_{cat}}{k_{cat}+C_{cat}}\right)$$

(3-7)

In equation (3-7) A^o is the standard reaction frequency factor, k_{cat} is a parameter that quantifies the catalyst effect on the reaction and C_{cat} is the catalyst concentration. This equation was proposed because experimental results in vegetable oil methanolysis showed that, when C_{cat} is low, a slight increase in concentration promotes a significant increase in the rate constants. However, when C_{cat} is higher than 1 %wt., an increase in concentration does not generate a proportional increase in the rate constants.

3.2.2 Materials

Jatropha oil was obtained by mechanical extraction of Jatropha curcas seeds using an Inducam LBC1 extractor (Inducam, Colombia). Refined, bleached and deodorized edible grade soybean oil was obtained from SIGRA S.A. (Bogotá, D.C. Colombia). Jatropha and Soybean oil fatty acid profile and some specifications are shown in Table 3-1. Analytical

grade methanol and sodium hydroxide were obtained from Merck (Darmstadt, Germany). Soybean oil was obtained from Sigra S. A. (Bogotá, Colombia) Reference standards, including methyl palmitate, methyl oleate, DL-α palmitin, dipalmitin, tripalmitin, glyceryltrioleate and the silylating agent N,O-bis(trimethylsilyl) trifluoroacetamide (BSTFA) of >99% purity, were purchased from Sigma-Aldrich Chemical Company (St Louis, MO). Tricaprine was obtained from Fluka (Buchs, Switzerland) and used as the internal standard. Pyridine, isopropanol, and toluene of ACS grade were obtained from Mallinckrodt Baker Inc. (Phillipsburg, NJ, USA).

Table 3-1. Oil specifications.

Variable	Unit	Jatropha	Soybean
Palmitic Acid (C16:0)	%wt.	12.11	24.66
Stearic Acid (C18:0)	%wt.	6.02	3.76
Oleic Acid (C18:1)	%wt.	35.75	33.30
Linoleic Acid (C18:2)	%wt.	44.93	31.96
Linolenic Acid (C18:3)	%wt.	0.34	3.86
Others acids	%wt.	0.85	2.46
Acid Value	mg KOH g^{-1}	1.159	0.22
Water content	%wt.	0.07	0.04

3.2.3 Reaction conditions for jatropha oil methanolysis

To study the effect of temperature and catalyst concentration, a multilevel factorial experiment was designed for two variables with three levels for the temperature, and four levels of the catalyst concentration. Keeping in mind the boiling point of methanol at atmospheric pressure where the trials took place, reactions at 40, 50 and 60 °C were studied. For the catalyst concentration the levels were 0.2, 0.4, 0.6 and 1.0 %wt. based on the mass of Jatropha oil. The rotational speed of the impeller, 600rpm, was defined based on previous tests performed to establish a limit value, so that the initial phase controlled by the diffusion was avoided (KUMAR et al., 2014). For all these tests, the methanol to oil molar ratio was constant and equal to 6:1. In order to study the effect of molar ratio, and according to the results of the kinetic study, reactions were conducted at four additional molar ratios: 3:1, 4.5:1, 9:1 and 12:1. For these, the temperature was 60 °C, the catalyst concentration was 0.6 %wt. and the rotational speed was 600 rpm.

3.2.4 Reaction condition for the soybean oil methanolysis

Kinetics of soybean oil methanolysis was developed using NaOH as catalyst at a concentration of 1 wt.% based on soybean oil mass. Taking into account the boiling point of methanol at the atmospheric pressure where the investigation took place, reactions at 40, 55 and 60 °C were performed. Methanol to oil molar ratio and the rotational speed of the impeller were kept constant at 6:1 and 600rpm, respectively. The experiments were performed following the methodology presented in previous works (NARVÁEZ et al., 2007).

3.2.5 Equipment

Methanolysis reactions were performed in a 100 ml glass round bottom reactor equipped with a reflux condenser, a thermometer, and a sampling port. To maintain a constant temperature, the reactor was immersed in a mineral oil bath equipped with an IKA ETS D-4 temperature controller, capable of maintaining the temperature within ± 0.1 °C (IKA Works Inc. Wilmington, NC, USA). Agitation was provided by a magnetically stirred IKS RET basic system (IKA Works Inc, Wilmington, NC, USA).

3.2.6 Procedure

The reactor was initially charged with 50 g of Jatropha or soybean oil. It was submerged in a mineral oil bath at the reaction temperature. Once the vegetable oil reached the reaction temperature, a known amount of sodium hydroxide dissolved in methanol was added according to the catalyst concentration and molar ratio of each test. This solution was heated separately to the reaction temperature. After the addition, the solution was mechanically agitated and reaction time started to be recorded.

3.2.7 Analysis

Samples were collected at specific time intervals. Eleven samples were collected at 0, 1, 2, 3, 5, 10, 15, 30, 60, 90 and 120 minutes, respectively. Samples of 20 mg were derivatized as soon as they were extracted from the reactor by adding BSTFA (N,O-Bis(trimethylsilyl)trifluoroacetamide) as the silylant agent and pyridine as the catalyst at

room temperature. The derivatization time was 60 minutes. After derivatization, the samples were stored at -2 °C until they were analyzed using gas chromatography (GC). The derivatized samples were analyzed for content of FAME, MG, DG and TG content using a GC Agilent 6820 (Agilent Technologies Co. Ltd., Shanghai, China) equipped with a flame ionization detector, fused silica (0.3 m x 0.53 mm) pre-column and SUPELCO SGE HT-5 fused silica capillary column (12 mm x 0.53 mm x 0.15 µm) (SGE International Pty. Ltd., Victoria, Australia). Samples of 1µL were manually injected. After 1 minute of stabilization at 140 °C. The oven temperature was programmed to increase from 140 °C to 380 °C at 20 °C/minutes and remain at 380 °C for 10 minutes. The injector and detector temperatures were 350 °C and 390 °C, respectively. Each run lasted 23 minutes. The carrier gas was nitrogen with a flow of 8 mL/min and a 50:1 split ratio. The acquisition and processing of data were achieved with the program Cerity (Agilent Technologies Co. Ltd., Shanghai, China). The concentrations of glycerol and methanol were determined by material balance.

3.2.8 Identification of the model parameters

Model parameters were determined from experimental data through the minimization of the difference between the experimental and calculated values. The differential equation system was solved using sixth order Runge-Kutta method. A dual population evolutionary algorithm (DPEA) (VIENNET et al., 1996) was used to identify unknown model parameters. The Fisher–Snedecor test of unbiased variances for the identification, validation, and replication of experimental data was used to validate the model (WALTER; PRONZATO, 1997) according to the inequalities (3-8) and (3-9).

- Validation/Identification:

$$\frac{1}{F_\alpha(gl_{Ij}, gl_{Vj})} \leq \frac{V_{Vj}}{V_{Ij}} \leq F_\alpha(gl_{Vj}, gl_{Ij}) \qquad \textbf{(3-8)}$$

- Replication/Identification:

$$\frac{1}{F_\alpha(gl_{Ij}, gl_{Rj})} \leq \frac{V_{Rj}}{V_{Ij}} \leq F_\alpha(gl_{Rj}, gl_{Ij}) \qquad \textbf{(3-9)}$$

In these equations, F_α stands for the value of the Fisher probability distribution function with a significance level α, gl_{Ij} for the degrees of freedom for identification, gl_{Vj} for the degrees of freedom for validation, gl_{Rj} for the degrees of freedom for replication, V_{Ij} for the unbiased variance of identification, V_{Vj} for the unbiased variance of validation and V_{Rj} for the unbiased variance of replication. In this model were used 13 experimental conditions, 7 in identification, 3 in validation and 3 in replication.

3.3 Results and discussion

Although experimental data were obtained for Jatropha and soybean oil methanolysis, results and discussion are going to be focused on the former, because the behavior of both oils is similar.

Figure 3-1 shows the concentration profile of the raw materials and products during Jatropha oil methanolysis. In the first 10 minutes, the consumption rate of methanol and Jatropha oil is high. As the reaction advances and approaches to chemical equilibrium, the reaction rate decreases. After 20 minutes, concentrations of all of the compounds in the reaction mixture were constant. The highest DG and MG concentrations were observed during the first 5 minutes of the reaction and were approximately 0.5 mol/L and 0.1 mol/L, respectively. As equilibrium was reached, these concentrations decreased and stabilized to values less than 0.05 mol/L. All the experiments presented in this work achieve 100% of conversion in the first 5 minutes of the reaction, and for this reason, the conversion was not a good comparison criterion. On the other hand, final FAME yield was different in almost all the conditions tested, reason why it is going to be employed as principal comparison criteria in the results analysis.
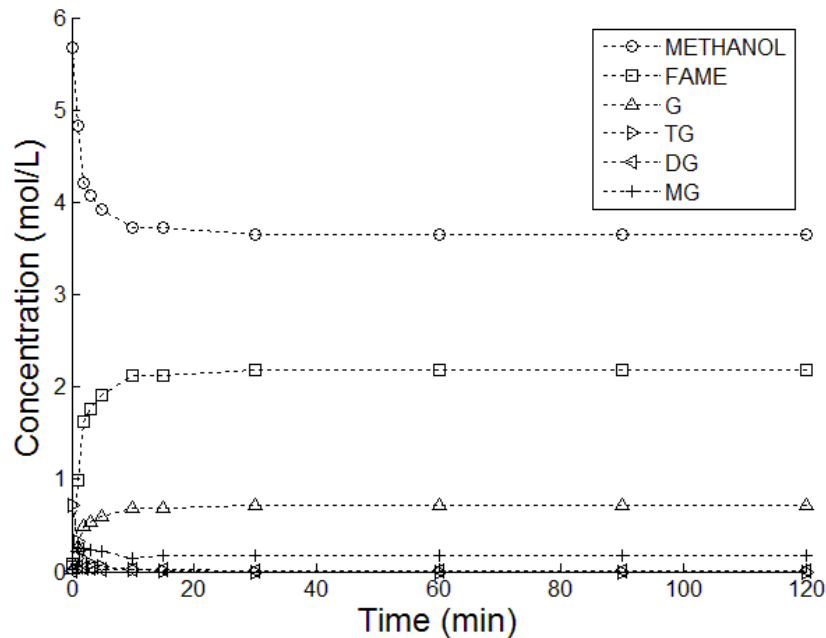
Figure 3-1. Experimental concentration profiles of the raw materials and products during Jatropha oil methanolysis at 50 °C, 0.6 %wt. NaOH and a 6:1 methanol to oil molar ratio.

3.3.1 Effect of catalyst concentration and temperature on FAME yield

The reaction rate was very slow at 0.2 %wt. of catalyst concentration at the three temperatures tested, meaning the minimal quantity of catalyst required is between 0.2 %wt. and 0.4 %wt. of NaOH. The behavior at 0.2 %wt. was not consider for other analysis. Figure 3-2 shows the effect of catalyst concentration and temperature on FAME yield on Jatropha oil methanolysis. This figure shows increasing temperature and catalyst concentration improves reaction rate. The effect is strongest in the first 10 minutes of reaction. The highest final FAME yield was achieved at 60 °C at all the catalyst concentration tested. The difference between the reaction behavior at different catalyst concentration decreases with the increase of temperature; at 60 °C reaction behavior with all the catalyst concentrations are almost equal. It means that an increase in the reaction temperature permits to use a lower quantity of catalyst. In this sense, the best operational conditions were 0.6 %wt. NaOH, 60 °C and 6:1 methanol to oil molar ratio, since this condition allows the reaction to achieve chemical equilibrium faster, obtaining the best

conversion and yield, with the minimal quantity of catalyst. A similar behavior was observed for soybean oil (evaluated in this work) and palm oil, as reported by NARVÁEZ et al., (2007).
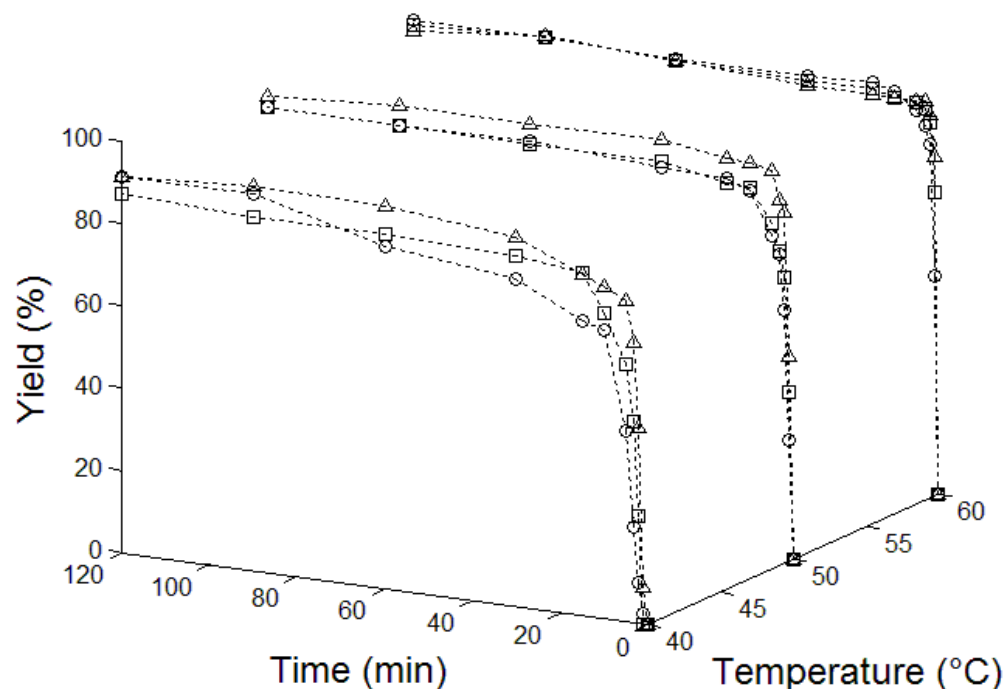
Figure 3-2. Effect of catalyst concentration on FAME yield during Jatropha oil methanolysis with 6:1 methanol to oil molar ratio and catalyst concentration of 0.4 %wt. NaOH (*circles*), 0.6 %wt. NaOH (*squares*) and 1.0 %wt. NaOH (*triangles*).

3.3.2 Effect of methanol to oil molar ratio on conversion and FAME yield

The effect of methanol to oil molar ratio on FAME yield is presented in the Figure 3-3. The increase of methanol ratio between 3:1 and 6:1 accelerates the initial reaction rate and makes possible to achieve faster the chemical equilibrium and at a higher yield. Nevertheless, the behavior presented at 6:1, 9:1 and 12:1 molar ratios is the same, meaning that increments of methanol to oil molar ratio over 6:1 do not improve the yield. A similar trend was observed for soybean oil methanolysis. NARVÁEZ et al., (2007) reported similar observations for palm oil methanolysis.
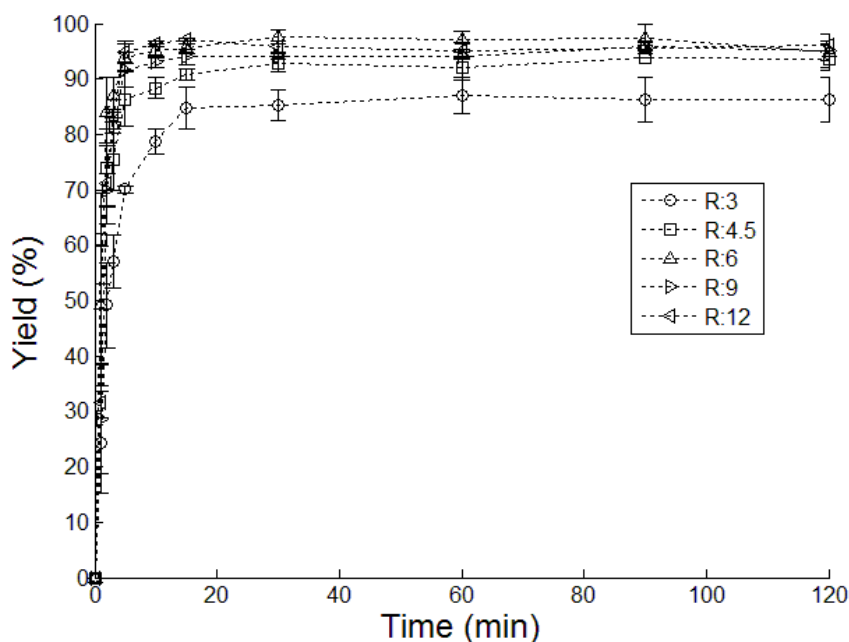
Figure 3-3. Effect of methanol ratio on FAME yield in the Jatropha oil methanolysis at 60 °C and 0.6 %wt. NaOH.

3.3.3 Kinetic model

Table 3-2 reports the parameters of the kinetic model adjusted to the experimental data obtained for Jatropha and soybean oil methanolysis using the dual population evolutionary algorithm (DPEA). In the same table, parameters for palm oil methanolysis adjusted according to the experimental data obtained by NARVÁEZ et al., (2007) are also reported. A similar behavior was observed for all the kinetic constants. The rate constants of all the forward reactions were higher than those of the backward reactions. Thus, vegetable oil methanolysis reaction is shifted towards product formation. However, the activation energy of the reverse reaction was higher than that of the forward reaction for DG+M↔MG+FAME. This behavior indicates that higher temperatures favor the formation of DG from TG and MG. The increase in the catalyst concentration strongly affected all of the forward reactions, but the strongest effect was observed in the reaction MG+M→G+FAME. This analysis indicated that the reaction MG+M→G+FAME is the controlling step of Jatropha and palm oil methanolysis.

Table 3-2. Parameters of the kinetic model for Jatropha oil, Palm oil and Soybean oil methanolysis.

Group	Parameter	Jatropha oil methanolysis	Palm oil methanolysis	Soybean oil methanolysis
Parameters related to the effect of the catalyst $\left(\% {}^{wcat}\!/_{woil}\right)$	k_{1cat}	1.8	3.98	N.A[*]
	k_{2cat}	1.49	2.53	N.A[*]
	k_{3cat}	24.36	25.28	N.A[*]
	k_{-1cat}	0.32	0	N.A[*]
	k_{-2cat}	0.22	0.05	N.A[*]
	k_{-3cat}	0	0.35	N.A[*]
Kinetic constants of the model $\left(\dfrac{L}{gmol \cdot \min}\right)$	k_1	6.71	2.32	3.28
	k_{-1}	0.18	0.92	2.38
	k_2	7.42	7.97	19.71
	k_{-2}	0	0.09	25.98
	k_3	8.17	7	0.61
	k_{-3}	0.05	0.03	0.013
Activation energy $\left(\dfrac{kcal}{gmol}\right)$	E_1	14.7	11.03	13.15[**]
	E_{-1}	13.32	10.81	9.93[**]
	E_2	11.03	9.6	19.86[**]
	E_{-2}	13.72	11.05	14.64[**]
	E_3	15.57	9.35	6.421[**]
	E_{-3}	9.51	10.48	9.59[**]

*Not correlated.
** Adapted from (NOUREDDINI; ZHU, 1997).

3.3.4 Model validation

Figure 3-4 shows the experimental points and concentration curves calculated using the model and the parameters adjusted for the methanolysis of Jatropha oil performed at 50 °C using 0.6 %wt. NaOH as the catalyst. There is an acceptable fit between the experimental and the model predictions. A similar behavior was observed between the other experimental and calculated data.
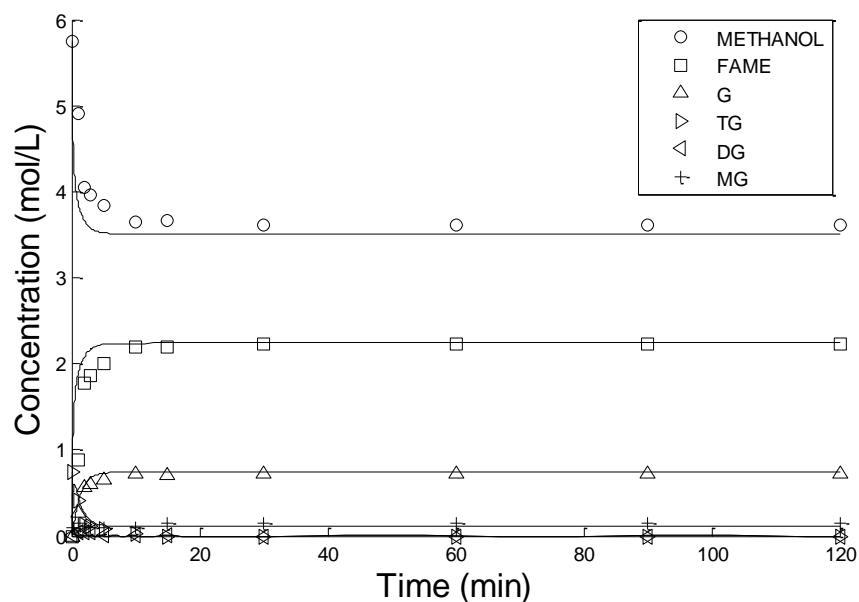
Figure 3-4. Comparison between model correlation and experimental results during Jatropha oil methanolysis at 50 °C, 0.6 %wt. NaOH and 6:1 methanol to oil molar ratio. (*line*) Model prediction, (*symbols*) experimental data.

Figure 3-5 shows experimental data and predictions for reaction progress in the soybean oil methanolysis, calculated using the model and the parameters adjusted for the reaction performed at 55 °C using 1 %wt. NaOH as catalyst. It was observed good fit between experimental data and model predictions. A similar behavior was also found for experimental and calculated data at other reaction conditions. During the first 5 minutes, the consumption rate of methanol and soybean oil reached the highest value. As the reaction advances and approaches to the chemical equilibrium, the reaction rate decreased. After 15 minutes, concentrations of all the compounds in the reaction mixture were constant.
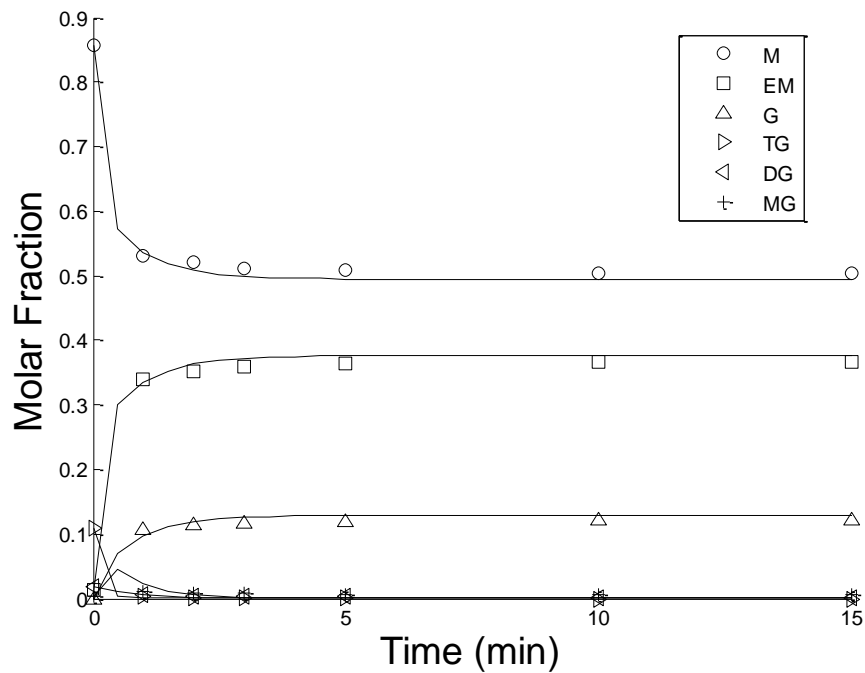
Figure 3-5. Comparison between the kinetics model correlation and experimental results during soybean oil methanolysis at 55 °C, 1.0 %wt. NaOH and 6:1 methanol to oil molar ratio. (*line*) Model prediction, (*symbols*) experimental data.

Figure 3-6 shows the Fisher–Snedecor test of unbiased variances for the experimental data for M, FAME, G, TG, DG, and MG, using freedoms degrees equal to 66 and 141. The entire values were normalized to the minimal value of the tendency (0.5330). The Validation/Identification test proved the quality of the model. According to the data in figure 3-6, the model accurately describes all of the concentration profiles. The Replication/Identification test probes the quality of the experimental procedure. According to the data in figure 3-6, all of the values for the ratio V_1/V_2 are within the Fisher–Snedecor test interval. This information permit to conclude the model using the adjusted parameters adequately predicted the experimental data, with a 95% confidence.
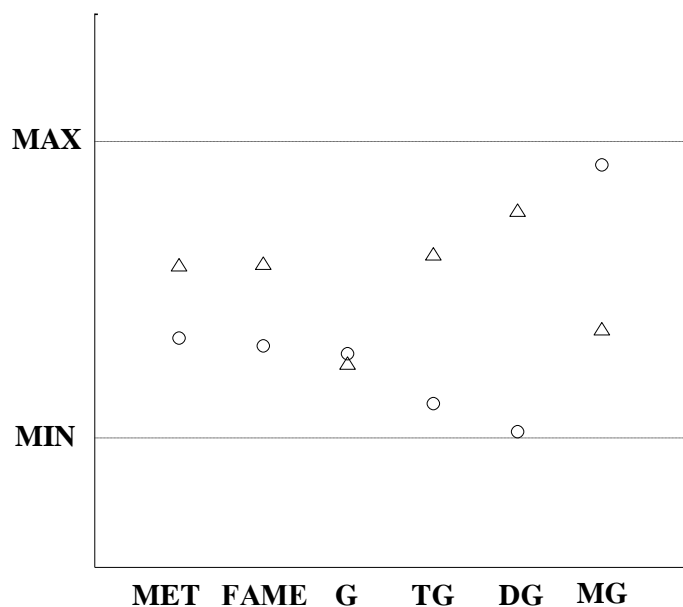
Figure 3-6. Fisher–Snedecor test of unbiased variances for the Validation**/** Identification *(circles)* and Replication**/**Identification *(triangles)* of the kinetic model for Jatropha oil methanolysis.

3.4 Conclusions

The increase in the temperature on vegetable oil methanolysis increases the reaction rate and the final FAME yield. This effect is stronger during its first ten minutes of reaction. The reaction rate is very slow at catalyst concentration of 0.2 %wt. Nevertheless, an increase in the catalyst concentration from 0.2 %wt. to 0.6 %wt. enhanced the reaction rate. The second order kinetic model proposed in this work describes adequately Jatropha and soybean oil methanolysis, as validated by the results of the Fischer-Snedecor test of unbiased variances. Based on activation energies, an increase in reaction temperature favors the production of DG from TG and MG. Reaction MG+M→G+FAME is the controlling step of Jatropha oil methanolysis. The same behavior was observed for Palm oil methanolysis.

3.5 List of symbols and abbreviations

r_i Reaction rate $\left(\dfrac{gmol}{L \cdot \min} \right)$

k_i Kinetic constant $\left(\dfrac{L}{gmol \cdot \min} \right)$

k_{icat} Kinetic constant related to the catalyst concentration

A_i Frequency factor $\left(\dfrac{L}{gmol \cdot \min} \right)$

E_i Activation energy $\left(\dfrac{kcal}{gmol} \right)$

C_{cat} catalyst concentration $\left(\% \; {wcat}/{woil} \right)$

T Temperature $\left(K \right)$

R Gas constant $\left(\dfrac{gmol}{kcal \cdot K} \right)$

$\left[TG \right]$ Triacylglycerol Concentration $\left(\dfrac{gmol}{L} \right)$

$\left[DG \right]$ Diacylglycerol Concentration $\left(\dfrac{gmol}{L} \right)$

$\left[MG \right]$ Monoacylglycerol Concentration $\left(\dfrac{gmol}{L} \right)$

$\left[FAME \right]$ Fatty Acid Methyl Ester Concentration $\left(\dfrac{gmol}{L} \right)$

$\left[G \right]$ Glycerol Concentration $\left(\dfrac{gmol}{L} \right)$

$\left[M \right]$ Methanol Concentration $\left(\dfrac{gmol}{L} \right)$

4. Liquid-liquid equilibrium in the biodiesel production using a UNIFAC correlated parameters[4]

4.1 Introduction

One of the main concerns of vegetable oil methanolysis is the immiscibility between the reactants (methanol or ethanol and vegetable oils), which generates mass transfer limitations at the beginning of the process. In a similar form, reaction products are not miscible (biodiesel and glycerol), characteristically used for a first separation stage in most of the industrial processes. Thus, an adequate description of the LLE of the system of biodiesel, glycerol, and alcohol is fundamental to the modeling, simulation, design, optimization and cost reduction of the biodiesel production, especially when membranes are coupled to the production system.

This chapter presents a correlated set of group interaction parameters (GIP) for the UNIFAC model that adequately describe the LLE of biodiesel systems. To correlate and to verify the GIP, a database including 84 LLE experimental results reported in the literature was built. The database includes biodiesel produced using 23 different vegetable oils and 2 different alcohols (methanol and ethanol), at temperatures between 293.15 K and 353.15 K. The GIP were correlated using an evolutionary algorithm. Model descriptions using the proposed set of GIP were compared with the description of other GIP reported in the literature.

---

[4] Results of this chapter were presented in (NORIEGA et al., 2016)

4.2 Materials and methods

4.2.1 LLE database in the systems of biodiesel-glycerol and methanol or ethanol

Experimental data from 33 references were used to develop the database summarized in Table 4.1. The first 25 references in the database were used to correlate the new set of GIP and the remaining references were used to verify the results. Temperature range of the LLE data is between 293.15 K and 353.15 K. Database includes biodiesel produced using 23 different vegetable oils and two different alcohols, methanol, and ethanol, as raw materials. The number of tie lines for each reference was reported in Table 4.1 and the database has a total of 445 LLE tie lines. All data correspond to the LLE of systems conformed by biodiesel, an alcohol (methanol or ethanol) and glycerol. Every reference included in the database reported the fatty acid profile of the employed biodiesel. This information is fundamental for LLE calculation because biodiesel must be modeled as an average molecule, and to define it, the fatty acid profile is necessary (see section 4.2.3). For this reason, other references that describe this kind of LLE but do not report oil or biodiesel compositions were not used in this work.

Table 4-1. LLE Database of the systems of biodiesel-glycerol and methanol or ethanol.

	System	Temperature (K)	Tie lines	Reference
		Data used in the correlation process		
1	Cottonseed oil biodiesel + Glycerol + Ethanol	293.15	6	(MESQUITA, FRANCISCA M R et al., 2012)
		313.15	6	
		333.15	6	
2	Crambe oil biodiesel + Glycerol + Ethanol	298.15	6	(BASSO et al., 2012)
		318.15	6	
		338.15	6	
3	Sunflower oil biodiesel + Glycerol + Methanol	293.15	5	(ROSTAMI et al., 2012)
		303.15	5	
		313.15	5	
4	Canola oil biodiesel + Glycerol + Methanol	293.15	5	(ROSTAMI et al., 2012)
		303.15	6	
		313.15	5	
5	Soybean oil biodiesel + Glycerol + Ethanol	300.15	5	(LIU et al., 2008)
		323.15	5	
		343.15	7	

	System	Temperature (K)	Tie lines	Paper Reference
6	Jatropha biodiesel + Glycerol + Methanol	303.15 318.15 333.15	6 6 5	(JULIANA R.F. SILVA A, MARCIO A. MAZUTTI B, FERNANDO A.P. VOLL C; MARCOS L. CORAZZA D, MARCELO LANZA E, WAGNER L. PRIAMO F, 2013)
7	Soybean oil biodiesel + Glycerol + Methanol	303,15;318,15;333.15; 298.15;333.15; 293.15; 323.15	7;6;6 4;5; 5;5	(MAZUTTI et al., 2013) (MACHADO et al., 2012) (MESQUITA et al., 2011)
8	Sunflower oil biodiesel + Glycerol + Ethanol	293.15 313.15	6 6	(MESQUITA et al., 2011)
9	Coconut oil biodiesel + Glycerol + Ethanol	293,15 323,15	6 5	(MESQUITA, FRANCISCA MARIA R et al., 2012)
10	Ethyl Linoleate + Glycerol + Ethanol	323.15 353.15	7 7	(FOLLEGATTI-ROMERO et al., 2012)
11	Ethyl Oleate + Glycerol + Ethanol	323.15 353.15	7 6	(FOLLEGATTI-ROMERO et al., 2012)
12	Ethyl Palmitate + Glycerol + Ethanol	323.15 353.15	7 6	(FOLLEGATTI-ROMERO et al., 2012)
13	Ethyl Laureate + Glycerol + Ethanol	323.15 353.15	5 6	(FOLLEGATTI-ROMERO et al., 2012)
14	Macauba pulp oil biodiesel + Glycerol + Ethanol	298.15	6	(BASSO et al., 2013)
15	Jatropha oil biodiesel + Glycerol + Methanol	298.15 308.15 318.15 328.15	3 3 5 5	(ZHOU et al., 2006)
16	Canola oil biodiesel + Glycerol +Ethanol	303.15	5	(OLIVEIRA et al., 2011)
17	Methyl Oleate + Glycerol + Methanol	298.15 308.15 318.15	7 7 7	(LEE et al., 2010)
18	Castor oil biodiesel + Glycerol + Methanol	298.15 333.15	6 7	(MACHADO et al., 2011)
19	Soybean oil biodiesel + Glycerol + Methanol	 303.15 318.15 333.15	3 3 3	(BENETI et al., 2014)
20	Corn oil + Glycerol + Methanol	293.15 303.15 313.15	5 5 5	(ROSTAMI et al., 2012)
21	Frying oil biodiesel + Glycerol + Methanol	293.15 303.15 313.15	5 5 5	(ROSTAMI et al., 2012)
22	Palm oil biodiesel + Glycerol + Ethanol	298.15 323.15	7 7	(ROCHA; FOLLEGATTI-ROMERO, 2014)
23	Castor oil biodiesel + Glycerol +Methanol	298.15	7	(FRANC et al., 2009)

Data used in the verification process

	System	Temperature (K)	Tie lines	Paper Reference

24	Soybean oil biodiesel + Glycerol +Ethanol	298.15	3	(BENETI et al., 2014)
25	Waste fish oil biodiesel + Glycerol +Methanol	298.15	6	(MAGHAMI et al., 2016)
		313.15	6	
		328.15	6	
26	Brazil nut oil biodiesel + Glycerol + Methanol	298.15	6	(GONÇALVES et al., 2014)
		303.15	5	
		323.15	5	
27	Canola oil biodiesel + Glycerol + Methanol	303.15	4	(HAKIM et al., 2014)
		313.15	4	
		323.15	4	
28	Sunflower oil biodiesel + Glycerol + Methanol	303.15	4	(HAKIM et al., 2014)
		313.15	4	
		323.15	4	
29	Castor oil biodiesel + Glycerol + Methanol	303.15	5	(THERM et al., 2013)
		318.15	5	
		333.15	5	
30	Castor oil biodiesel + Glycerol + Ethanol	303.15	5	(THERM et al., 2013)
		318.15	5	
		333.15	5	
31	Soybean oil biodiesel + Glycerol +Ethanol	298.15	6	(FRANÇA et al., 2013)

4.2.2 Liquid – liquid equilibrium calculation

Differences in molecular weight for systems containing biodiesel, glycerol and alcohol are large, so using mass fractions instead of molar fractions for calculations of LLE is recommended to obtain better results (BASSO et al., 2013, BATISTA et al., 1999, DO CARMO et al., 2014). The use of mass fractions was first proposed by OICHI; PRAUSNITZ, (1978) using the UNIQUAC and UNIFAC models to calculate the activity of solvents in polymers. Previous works calculated the LLE for systems with high differences between molecular weights of the compounds involved, obtaining accurate results (BASSO et al., 2012, BATISTA et al., 1999, DO CARMO et al., 2014, OICHI; PRAUSNITZ, 1978, ROCHA; FOLLEGATTI-ROMERO, 2014). LLE models using mole and mass fractions are presented in equations (4-1) to (4-3). In order to calculate the LLE in mass fraction it is necessary to express the activity coefficient in the same unit terms (γ_i^w).

$$\left(\gamma_i x_i\right)^I = \left(\gamma_i x_i\right)^{II} \qquad \textbf{(4-1)}$$

$$\left(\gamma_i^w w_i\right)^I = \left(\gamma_i^w w_i\right)^{II} \qquad \textbf{(4-2)}$$

$$\gamma_i^w = \frac{\gamma_i}{M_i \sum_j^k w_j / M_j} \qquad \textbf{(4-3)}$$

Where, x_i is the molar fraction of component i in the each phase, γ_i is the activity coefficient of component i, w_i is the mass fraction of the component i, γ_i^w is the activity coefficient of the component i expressed in mass fraction units, M_i is the molecular weight of the component i, and I, II refers to the ester-rich phase and glycerol-rich phase, respectively. To calculate γ_i^w, UNIQUAC and UNIFAC adaptations proposed by OICHI; PRAUSNITZ, (1978) must be used (Appendix A). The group volume and area parameter used in the model, R_k and Q_k, respectively, are the same as those presented by MAGNUSSEN, (1981) (Table 4.2).

Table 4-2. UNIFAC structural molecular groups (MAGNUSSEN, 1981).

Main group	Sub- Group	Volume (R_k)	Surface Area (Q_k)
	CH	0.4469	0.2280
(1) CH$_2$	CH$_2$	0.6744	0.5400
	CH$_3$	0.9011	0.8480
(2) C=C	CH=CH	1.1167	0.8670
(3) OH	OH	1.0000	1.2000
(4) COOC	CH$_2$COO	1.6764	1.4200

All the LLE were calculated using the Rachford–Rice algorithm in mass fraction (equations 4-4 to 4-7). This algorithm is an iterative procedure carried out by solving the material balance (equation 4-7), more details about this algorithm are described by LI; FIROOZABADI, (2012).

$$K_i = \frac{\left(\gamma_i^w\right)^I}{\left(\gamma_i^w\right)^{II}} \qquad i = 1, 2, 3 \qquad \textbf{(4-4)}$$

$$w_i^{II} = K_i w_i^I \qquad i = 1, 2, 3 \qquad \textbf{(4-5)}$$

$$w_i^I = \frac{Z_i}{1 + (K_i - 1)\phi} \qquad i = 1, 2, 3 \qquad \textbf{(4-6)}$$

$$\sum_{i=1}^{3} \frac{z_i (K_i - 1)}{1 + (K_i - 1)\phi} = 0 \qquad \textbf{(4-7)}$$

In these equations, K_i is the distribution coefficient for component i (ratio between activity coefficients), Z_i is the mass fraction of a component i in the overall composition, and ϕ is the glycerol-rich phase mass fraction. In this work, GIP were supposed. Then, the LLE for all the correlated database were calculated using the Rachford–Rice algorithm and the supposed GIP. Finally, the evolutionary algorithm tested different GIP and selected the GIP with the lower value in the objective function evaluation (equation 4-11).

4.2.3 Estimation of group interaction parameters

Vegetable oils and biodiesel are mixtures of TG and FAME, respectively, previous works suggested modeling biodiesel as an average molecule obtained from the fatty acid profile of the vegetable oil used for its production (BASSO et al., 2013, BATISTA et al., 1999, DO CARMO et al., 2014). To introduce biodiesel in the UNIFAC model, a pseudo molecule with the structure $(CH_3)_2(CH_2)_m(CH=CH)_n(CH)_p(OH)_pCH_2COO$ was used, where m, n and p can be non-integer numbers. The value of p is different from 0 only for the representation of biodiesel with ricinoleic fatty acid ester content. The molecular groups selected to represent the systems in the UNIFAC model were "CH$_3$", "CH$_2$", "CH", "CH=CH", "OH" and "CH$_2$COO"; the main groups are specified in Table 4-2. Parameters m, n and p were calculated according to the equations (4-8 to 4-10), where x_i is the molar fraction of the biodiesel kind i in the biodiesel mixture, obtained from the fatty acid profile, S is the number of biodiesel kinds in the biodiesel mixture, m_i is the quantity of CH$_2$ groups in the biodiesel kind i, A is the CH$_2$ quantity in the alcohol used in the biodiesel production, it is equal to 0 in the case of a methyl ester and equal to 1 in the case of an ethyl ester, n_i is the quantity of CH=CH groups in the biodiesel kind i and p_i is the quantity of CHOH groups in the biodiesel kind i.

$$m = A + \sum_{i=1}^{S} x_i m_i \qquad \textbf{(4-8)}$$

$$n = \sum_{i=1}^{S} x_i n_i \qquad \textbf{(4-9)}$$

$$p = \sum_{i=1}^{S} x_i p_i \qquad \textbf{(4-10)}$$

Once the pseudo-molecule is determined, its values are used to calculate the number of times group k is in the molecule i ($v_k^{(i)}$) (Appendix A). An example of these pseudo-molecule is presented in table 4-4. The LLE calculated was compared with non-integer values and with the values adjusted with a scientific notation to integer values. Results obtained were similar, with differences less than 1%. This behavior is explained because the change in the value is extremely low compared with the molecular size.

To improve the fit between experimental data and the UNIFAC description, those GIP were determined from the LLE experimental data. The determination of the group interaction parameters was performed via the minimization of the function shown in equation 4-11 using a DPEA programmed in MATLAB®.

$$F = \sum_{k}^{D} \sum_{j}^{M} \sum_{i}^{N} \left[\left(w_{ijk}^{I,\exp} - w_{ijk}^{I,calc} \right)^2 + \left(w_{ijk}^{II,\exp} - w_{ijk}^{II,calc} \right)^2 \right] \quad \textbf{(4-11)}$$

The average deviations between the experimental and calculated compositions in both phases were calculated according to the root mean square deviation (equation 4-12).

$$Dev = \sqrt{\frac{F}{D \cdot M \cdot N}} \qquad \textbf{(4-12)}$$

In equations 4-11 and 4-12, F is the objective function result, D is the total number of references in the database; M is the total number of tie lines in reference k; N is the total number of components in the data group; subscripts i, j and k correspond to the component, tie line and group number, respectively; exp. and calc. represent the experimental and calculated compositions (SØRENSEN et al., 1979).

4.3 Results and discussion

4.3.1 Group interaction parameters correlation

Table 4.3 presents four sets of GIP that could be applied in the description of the LLE of the system studied in this work. The first data set (1) was proposed by MAGNUSSEN, (1981); the second, third, and fourth GIP sets were obtained in this work. The second set (2) was obtained by minimizing only the GIP not related to the main group 1 ("CH=CH", "CH$_2$COO" and "OH"), and the third data set (3) was obtained by minimizing only the GIP related to the main group 1 ("CH$_3$", "CH$_2$" and "CH"). Finally, the fourth set (4) was obtained by minimizing the whole set of GIP.

Table 4-3. UNIFAC group interaction parameters. Main groups: (1) CH$_3$, CH$_2$, and CH; (2) CH=CH; (3) OH and (4) CH$_2$COO.

GIP	Set 1	Set 2	Set 3	Set 4
Minimization Condition	Magnussen et al. [32]	GIP not related with group 1	GIP related with group 1	All of the GIP
a_{12}	292.3	292.3	799.7	1351.4
a_{21}	74.54	75.54	8.5	909.7
a_{23}	470.7	1079.9	470.7	1078.5
a_{32}	724.4	821.6	724.4	867.5
a_{24}	485.6	-699.6	485.6	-292.8
a_{42}	-577.5	-669.7	-577.5	69.8
a_{13}	328.2	328.2	1495.2	1294
a_{31}	644.6	644.6	209.3	722.9
a_{34}	180.6	1261.6	180.6	667.6
a_{43}	195.6	1298.6	195.6	1040
a_{14}	-320.1	-320.1	-597.9	982.8
a_{41}	972.4	972.4	-311.4	674.3
Average deviation (%)	**0.91%**	**0.55%**	**0.31%**	**0.20%**
Maximum deviation (%)	**2.08%**	**1.38%**	**0.89%**	**0.66%**
Biodiesel for the maximum deviation	Soybean at 298.15 K	Crambe oil at 318.15 K	Jatropha at 328.15 K	Jatropha at 328.15 K

The average deviation presented in Table 4.3 is less than 1% for all of the GIP sets tested. This means that Magnussen and proposed GIP can be used with confidence in LLE calculation. The lowest average and maximum deviation (0.20% and 0.66%, respectively)

were obtained using the GIP determined in this work (Set 4) because these GIP were correlated directly with the experimental data. The average deviation for set 3 is better than that for set 2, indicating a stronger influence for the GIP related with the main group 1 ("CH$_3$", "CH$_2$" and "CH") this behavior can be explained because biodiesel molecules are composed mainly by elements of this Group (up to 90% of the molecular weight). The average deviation for set 4 is better than for the set 3, indicating the influence of the GIP not related to the main group 1 ("C=C", "OH" and "CH$_2$COO"), this is also expected since set 4 involves a lot of parameters to be regressed.

LLE in the database used in the correlation were calculated using the GIP proposed by MAGNUSSEN, (1981) (set 1) and set 4 determined in this work. Subsequently, the model calculation was compared with the experimental results, this result is presented in the Figure 4-1; both tested constants sets present an accurate fit between the experimental data and the calculated values, regardless of the biodiesel types, composition, and temperatures. Nevertheless, the proposed constants describe the experimental data with a better fit than the MAGNUSSEN, (1981) constants; in general, the fit is better in the glycerol-rich phase than in the ester-rich phase, and the fit is better in the low methanol region.

It is recommended to use the correlated GIP (set 4) in systems composed of biodiesel, glycerol, and alcohol because these parameters were obtained from experimental data including these compounds, so the result will be more accurate. On the other hand, it is recommended to use the Magnussen GIP (set 1) in systems composed of other components, for example, biodiesel, alkanes, and glycerol, because these parameters are more general and include all kind of components (MAGNUSSEN, 1981).
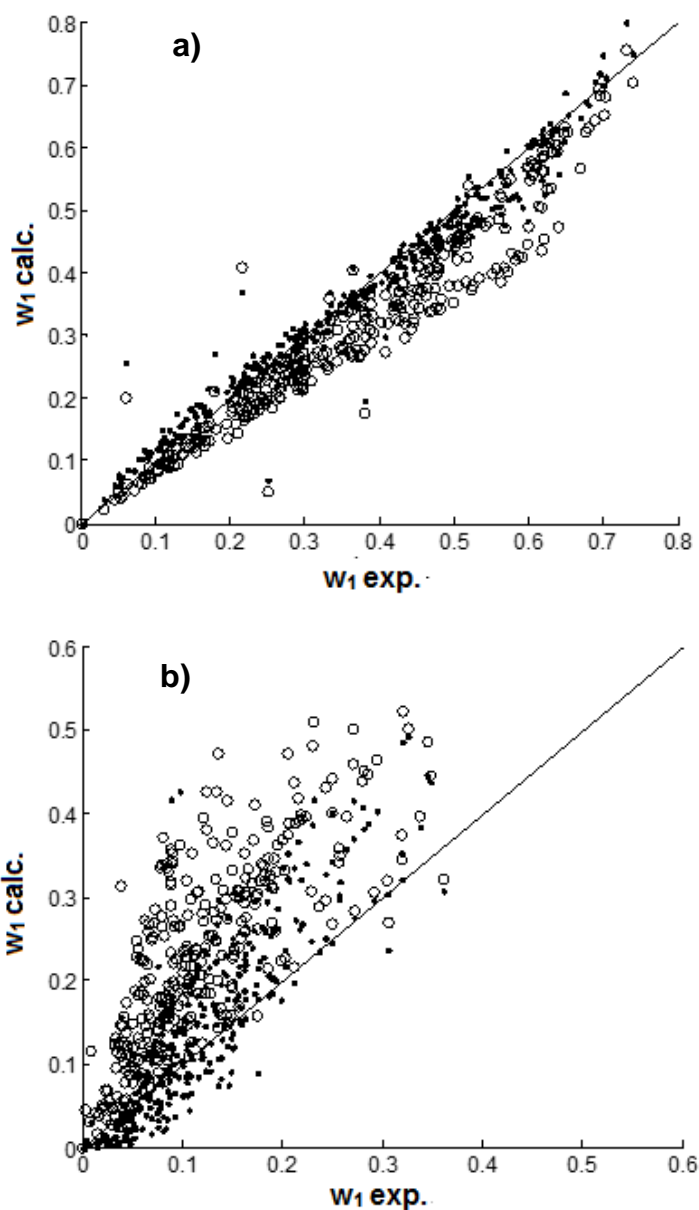
Figure 4-1. Comparison between the calculated and experimental alcohol mass fraction (w_1) for the LLE used in correlation in the **a)** glycerol-rich phase; **b)** ester-rich phase. (UNIFAC calculation using MAGNUSSEN, (1981) constants (*circles*), UNIFAC calculation using the proposed constants in this work (*points*)).

4.3.2 Group interaction parameters verification

LLE of the database used for the verification were calculated using the Set 4 of GIP determined in this work. Then, the calculated results were compared with the experimental

data, as shown in Figure 4-2. The use of the UNIFAC model with the proposed constants described accurately the LLE even in systems not included in the correlation process. This description could be obtained even for biodiesel with particular fatty acid profiles like waste fish oil biodiesel (MAGHAMI et al., 2016) or Brazil nut oil biodiesel (GONÇALVES et al., 2014).
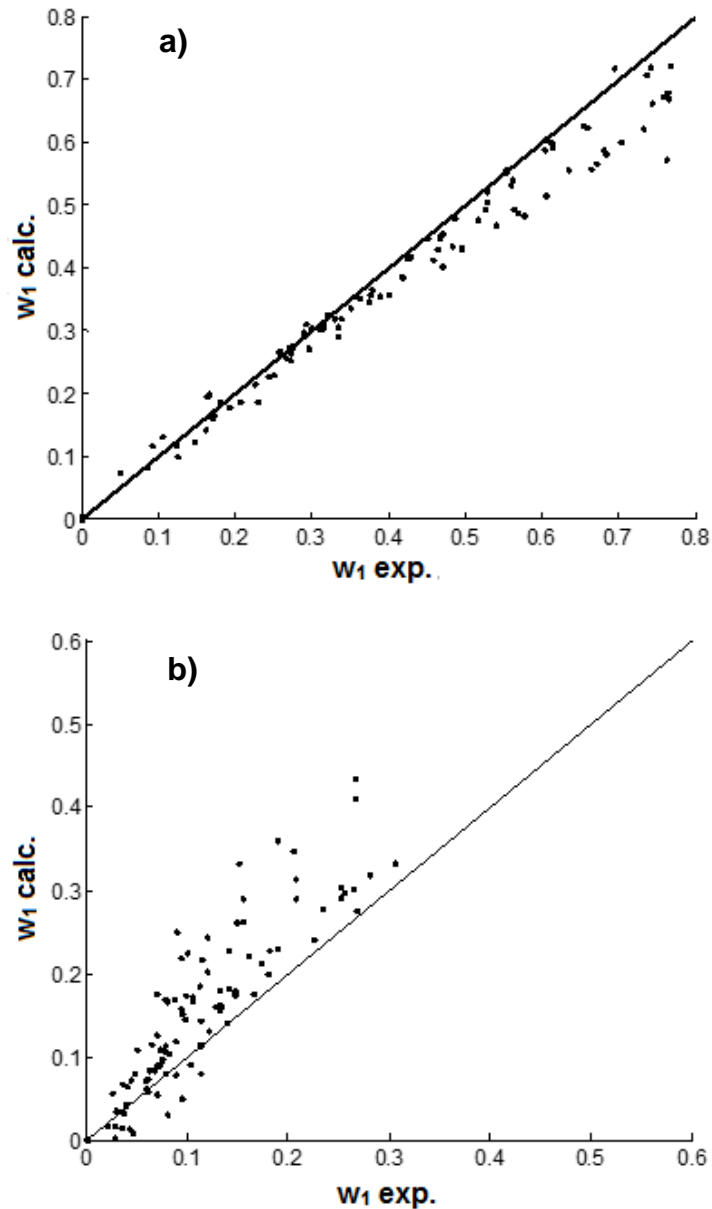
Figure 4-2. Comparison between the calculated and experimental alcohol mass fraction (w_1) for the LLE used in the UNIFAC proposed constants verification a) glycerol-rich phase; b) ester-rich phase.

4.3.3 Liquid –liquid equilibrium results

Figures 4-3a, 4-3b, 4-3c and 4-3d show the LLE ternary diagrams using the Set 4 of GIP and its comparison with the experimental data, the corresponding characteristics molecules are presented in the Table 4-4.

Table 4-4. Characteristic molecule for the LLE presented in Figure 4-3 and 4-4.

Figure	Biodiesel type	Number of groups in the characteristic molecule
		CH_3	CH_2	CH=CH	CHOH	CH_2COO
3a	Jatropha	2	12.32	1.19	0	1
3b	Palm	2	12.85	0.64	0	1
3c	Castor	2	12.03	1.01	0.91	1
3d	Waste fish oil	2	12.20	1.10	0.06	1
4a	Soybean methyl	2	11.69	1.55	0	1
4b	Soybean methyl	2	11.75	1.53	0	1
4c	Soybean ethyl	2	12.73	1.52	0	1

a)

b)

c)

d)
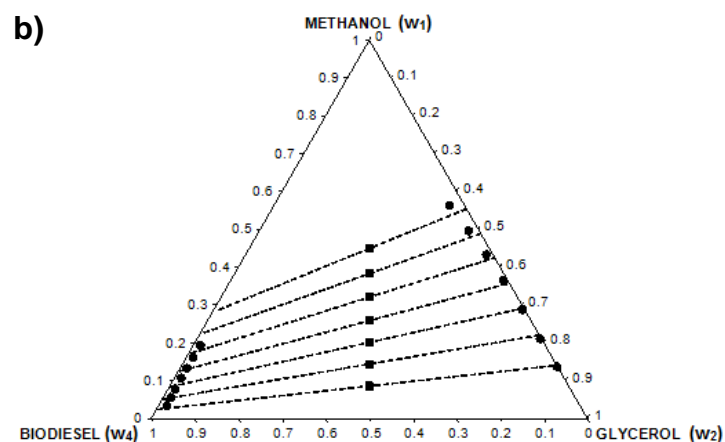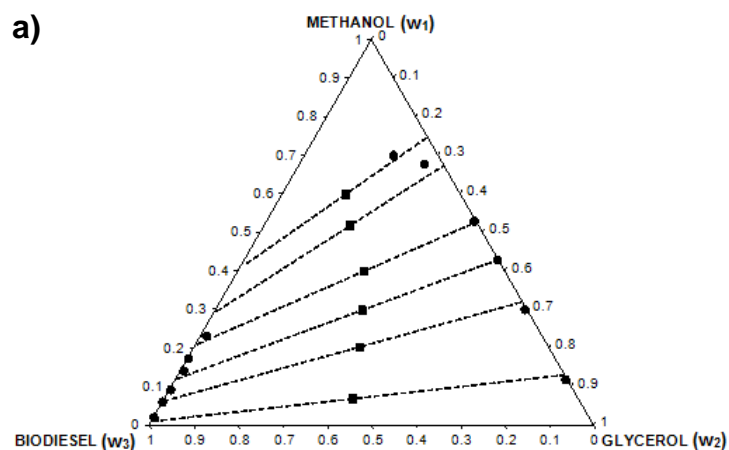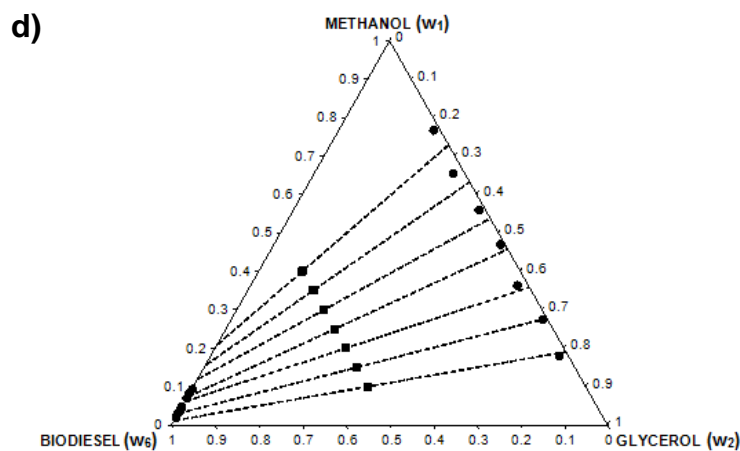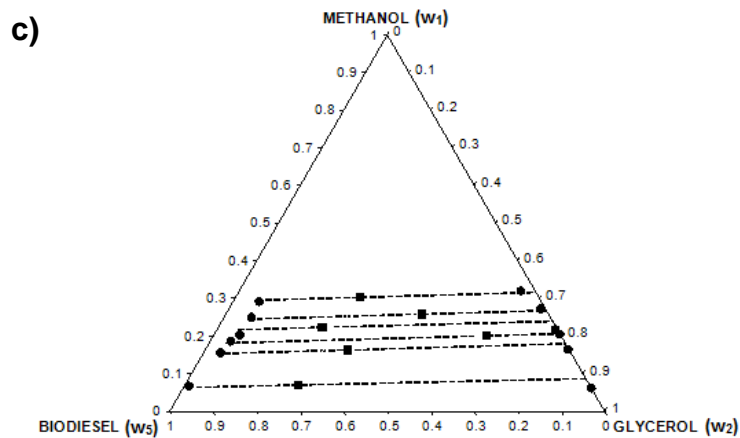
Figure 4-3. Comparison between calculated and experimental data of the LLE of the system of methanol (w_1), glycerol (w_2) and: a) Jatropha biodiesel (w_3) at 318.15 K (exp. data. (SILVA et al., 2013)), b) Palm biodiesel (w_4) at 298.15 K (exp. data. (ROCHA; FOLLEGATTI-ROMERO, 2014)), c) Castor biodiesel (w_5) at 298.15 K (exp. data. (MACHADO et al., 2011)), d) Waste fish oil biodiesel (w_6) at 328.5 K (exp. data. (MAGHAMI et al., 2016)). Note: experimental data (*filled dot*); UNIFAC (*black lines*); overall composition (*filled square*).

An accurate fit between the model descriptions and the experimental data is observed, regardless of the biodiesel composition and the presence of different functional groups in the biodiesel molecule. Waste fish oil biodiesel (Figure 4-3d) LLE was not used for the GIP correlation. However, it shows an accurate fit with the experimental data. The LLE of jatropha and soybean biodiesel systems (Figures 4-3a and 4-4a) show a similar behavior, probably explained because their chemical composition is similar (Table 4-4).

LLE results when methanol mass fraction is higher than 0.7 were not found in the literature, indicating that the limit of the binodal region is close to this composition for all the studied references. Model descriptions are closer to the experimental data at low values of the methanol molar fraction and the difference between them increases when the methanol molar fraction increases. In general, model calculations are better for the glycerol-rich phase than for the ester-rich phase. The overestimation in the alcohol content in the ester-rich phase increases with the alcohol content in the overall composition. This problem was reported previously by others authors (CHENG et al., 2009). At these conditions, the model is not able to describe the biodiesel content in the glycerol-rich phase. This situation changes the entire tie line (mass balance). This problem cannot be solved with parameters adjustment, so, this behavior is a limitation of the UNIFAC model for the description of this kind of systems.

Figures 4-4a, 4-4b and 4-4c show a comparison between the model descriptions and the experimental data in systems composed by soybean methyl biodiesel and soybean ethyl biodiesel, in these systems an accurate fit between model and experimental data was found. The experiments and calculated results are similar to the Figures 4-4a and 4-4b even when they were reported by different references. On the other hand, the comparison between the Figures shows a bigger solubility between the ethanol and the soybean ethyl biodiesel than the solubility between the methanol and the soybean methyl biodiesel.
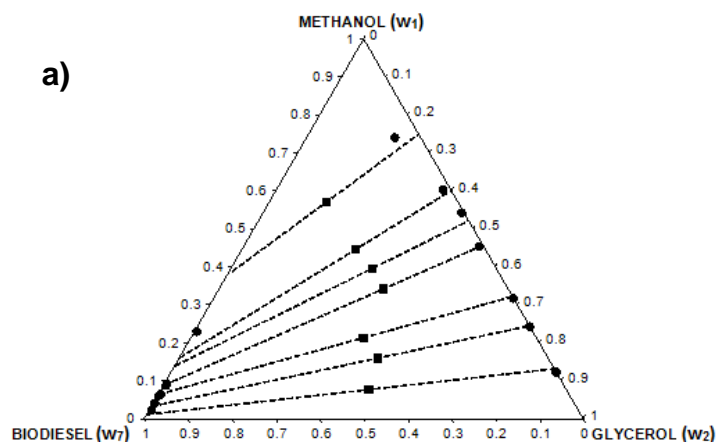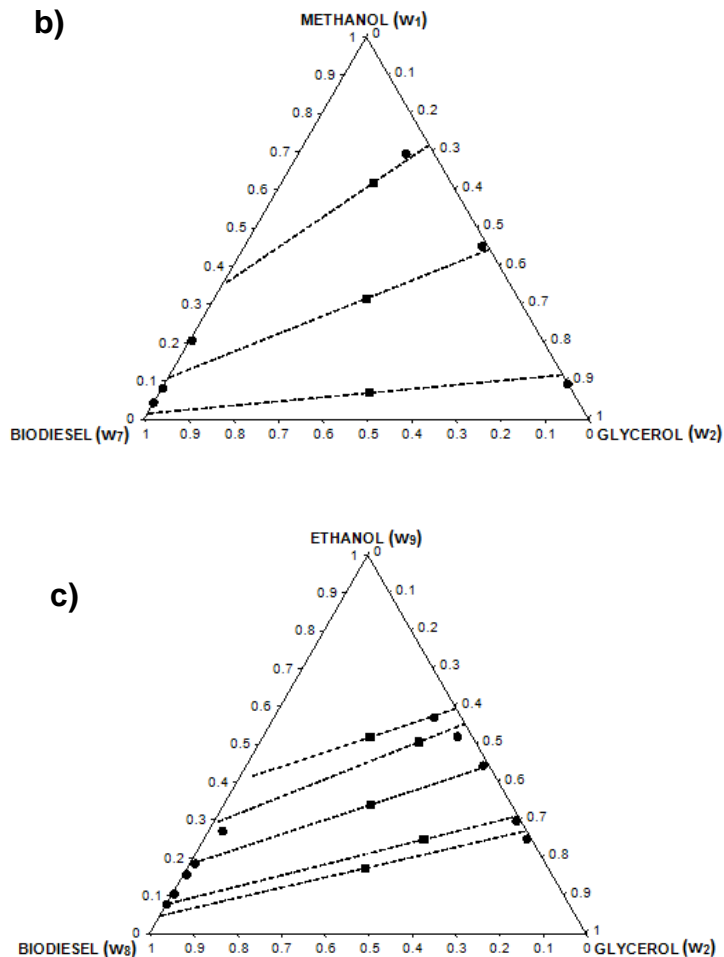
Figure 4-4. Comparison between calculated and experimental data of the LLE of the system of a) Soybean biodiesel (w_7), glycerol (w_2) and methanol (w_1) at 303.15 K. (exp. data. (MAZUTTI et al., 2013)), b) Soybean biodiesel (w_7), glycerol (w_2) and methanol (w_1) at 318.15 K (exp. data. (BENETI et al., 2014)). and c) Soybean ethyl biodiesel (w_8), glycerol (w_2) and ethanol (w_9) at 300.15 K (exp. data. (LIU et al., 2008)). Note: experimental data (*filled dot*); UNIFAC (*black lines*); overall composition (*filled square*).

LLE calculation in systems composed of biodiesel-glycerol-methanol or ethanol describes poorly the biphasic region and the tie lines close to that region. However, the correlated GIP permits an accurate description of all the experimental data when alcohol concentration is lower than 40%, which is usual in biodiesel production.

4.4 Conclusions

Using the UNIFAC model with the correlated GIP (set 4) describes the behavior for LLE of biodiesel, glycerol, and alcohol for all the references studied, regardless of the biodiesel type, composition, and temperature, with an average deviation of 0.20% and a maximum specific deviation of 0.66% (Jatropha biodiesel). The comparison between this work and the UNIFAC description using the GIP proposed in the literature indicated that the best average and specific deviation were obtained using the GIP proposed in this work. Nevertheless, it is recommended to use the correlated GIP (set 4) in systems containing only biodiesel, glycerol, and alcohol; and the Magnussen GIP (set 1) could be used in systems composed of other kinds of components. The GIP related with the UNIFAC main group 1 ("CH$_3$", "CH$_2$" and "CH") exhibits a stronger influence on the descriptions than the GIP not related with this group. For all of the cases, alcohols are distributed among the ester-rich phase and glycerol-rich phase, exhibiting higher affinity for the glycerol-rich phase. The best UNIFAC descriptions were obtained in the low methanol concentration region, and the model descriptions were better for the glycerol-rich phase than for the ester-rich phase.

4.5 List of symbols

γ_i Activity coefficient of component i

M_i Molar mass

w_i Mass fraction of component i

R   Residual part of the equation

C   Combinatorial part of the equation

$v_k^{(i)}$ Number of times that group k is in molecule i

Γ_k Residual activity coefficient of group k

Q_k Group area parameter

R_k Group volume parameter

$q_i^{'}$ Van der Waals molecular area

$r_i^{'}$ Van der Waals molecular volume

$\Theta_i^{'}$ Area fraction

$\phi_i^{'}$ Volume fraction

i, j, k   Component

a_{ij} UNIFAC Group interaction parameters

T Temperature (K)

5. Modeling of biodiesel production in liquid-liquid film reactor including mass transfer effects

5.1 Introduction

LLFRM is the product of the integration between LLFR and UF membranes, this integration is only possible with the knowledge about the transport phenomena inside the reactor, especially mass transfer effects and hydrodynamics. Besides, this knowledge permits to understand the phenomena inside the reactor, to improve its performance and to scale up the process.

This chapter presents a mathematical model for biodiesel production using an LLFR operated in co-current mode. The model includes the mass transfer limitations and describes the hydrodynamics inside the reactor. It was validated through experimental data obtained in a bench level reaction system, studying the effect of the packing fraction (5 to 60%), VO flow rate (5 to 40 g min^{-1}) and reaction length (0.25 to 1 m) on conversion and FAME yield, at constant temperature (55°C), catalyst concentration (1% w/w based on VO weight) and methanol to oil molar ratio (6:1).

5.2 Materials and methods

5.2.1 Physical background

A schematic diagram of the LLFR configuration including a differential element of volume is shown in Figure 5-1. A tubular reactor with uniform diameter (D_{Rxn}) is packed with a defined quantity of stainless steel threads (n_{Pack}) with uniform diameter (D_{Pack}).
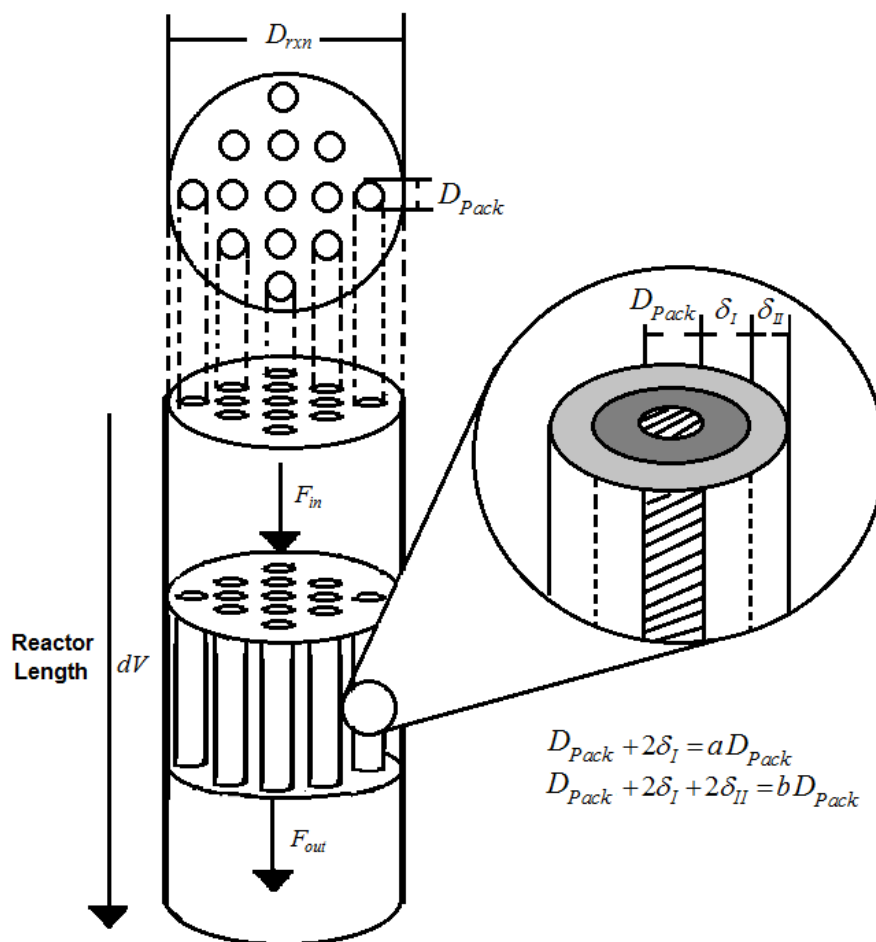
Figure 5-1. Schematic representation of an LLFR. F_{IN}: Input flow rate; F_{OUT}: Output flow rate.

This semi-structured packing makes possible to generate interfacial area between the liquid phases inside the reactor without dispersing one into the other. VO and methanol are fed at the top of the reactor. The ester-rich phase wet the packing surface, generating

a film of thickness δ^I over it. The alcoholic phase flows over the ester-rich phase forming a film of thickness δ^{II} over the ester-rich phase. Biodiesel and glycerol produced are recovered at the bottom of the reactor. The hydrodynamics of the flow inside the reactor could be explained because ester-rich phase wettability over the stainless steel packing is higher than the alcoholic phase wettability. The reaction occurs in the two films created over the threads but principally in the ester-rich phase.

5.2.2 Materials

Refined, bleached and deodorized edible grade soybean oil was obtained from SIGRA S.A. (Bogotá, D.C. Colombia). Soybean oil fatty acid profile and some specifications were shown in Table 3-1. Analytical grade methanol and sodium hydroxide were obtained from Merck (Darmstadt, Germany). Reference standards, including methyl palmitate, methyl oleate, DL-α palmitin, dipalmitin, tripalmitin, glyceryl trioleate and the silylating agent N,O-bis(trimethylsilyl) trifluoroacetamide (BSTFA) of >99% purity, were purchased from Sigma-Aldrich Chemical Company (St Louis, MO). Tricaprine was obtained from Fluka (Buchs, Switzerland) and used as the internal standard. Pyridine, isopropanol, and toluene of ACS grade were obtained from Mallinckrodt Baker Inc. (Phillipsburg, NJ, USA).

5.2.3 Reaction conditions in the LLFR

The reaction temperature, catalyst concentration, and methanol to oil molar ratio were kept constant in all the tests performed at 55 °C, 1 %wt. based on oil mass and 6:1, respectively. These values were selected according to the results of previous experiments run in an LLFR (NARVÁEZ et al., 2009). To study the effect of packing quantity, VO flow rate and reactor length on conversion and yield at the reactor outlet, a multilevel factorial experiment was designed with five levels for packing surface area to reaction volume ratio ($444 \ m^{-1}$, $1332 \ m^{-1}$, $2664 \ m^{-1}$, $3996 \ m^{-1}$ and $5333 \ m^{-1}$) and four levels of VO flow rates (5 g/min, 10 g/min, 15 g/min and 40 g/min). Additionally, different reactor lengths (0.25 m, 0.50 m, 0.80 m and 1 m) were evaluated at constant packing quantity and VO flow rates ($5333 \ m^{-1}$ and 40g/min, respectively) for a total of 24 experiments, each one performed at least in duplicate.

5.2.4 Equipment

A diagram of the experimental setup is presented in Figure 5-2. The LLFR consists of a borosilicate glass column $\left(D_{rxn} = 0.03m \right)$ packed with a semi-structured stainless steel packing (threads). The packing was custom made by adjusting the necessary quantity of stainless steel threads to obtain the desired packing surface area to reaction volume ratio of the experiment. The packing was axially aligned and homogeneously distributed fixing every thread $\left(D_{Pack} = 0.2mm \right)$ to a distribution plate at the reactor top and to a ring at the reactor bottom. A decanter (300 cm^3) located downstream the reactor separates the ester and alcohol-rich phase (6). Soybean oil was fed at the reactor top (5a) and methanol was fed 20 cm lower (5b). This configuration makes possible the VO reaches a fully developed flow before methanol contact. To maintain reaction temperature, the reactor was provided with a heating jacket, which was connected to a Heating Circulator (PolySciencePP07R-40-A12E). Soybean oil and NaOH solution in methanol were stored in two tanks installed on two balances Mettler Toledo 4000 (Mettler Toledo GmbH, Schwerzenbach, Switzerland) (1 and 2, respectively). These balances were used to determine mass flow rates of VO and methanol. The flow in the reactor was caused by gravity, but two metering pumps HMS EXT 2001 (EMEC Srl, Vazia, Italy) were used to feed the inlet streams at controlled flow rates (3a and 3b). Soybean oil and NaOH solution were independently heated up to the reaction temperature using two heating systems located just before each fed nozzle. The heating systems are equipped (4a and 4b) with silicon-shielded electric resistances and SHIMADEN SR 91 (Japan) temperature controllers (±0.1 ºC). The reactive mixture leaves the reactor through the outlet nozzle (5C) connected to the decanter (6) where the phase separation takes place. Finally, the two phases obtained from the decanter were stored in the tanks 8 and 9.
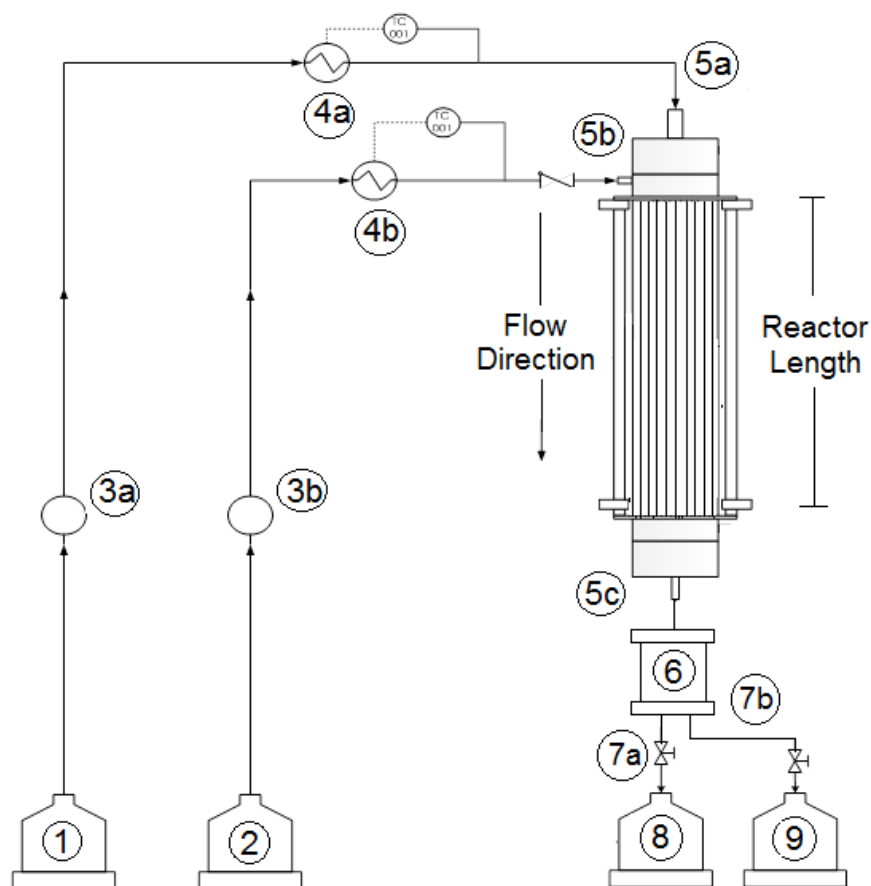
Figure 5-2. Diagram of the experimental configuration of the LLFR. 1) Oil tank; 2) NaOH in methanol solution tank; 3a) Oil metering pump; 3b) NaOH in methanol metering pump; 4a) Oil heat exchanger; 4b) NaOH in methanol heat exchanger; 5a) LLFR oil feeding nozzle; 5b) LLFR NaOH in methanol solution feeding nozzle; 5c) LLFR outlet nozzle and valve; 6) Decanter; 7a) Ester-rich phase output; 7b) Alcoholic phase output; 8) Ester-rich phase tank; 9) Alcoholic phase tank.

5.2.5 Procedure

Soybean oil and the solution of NaOH in methanol, which was prepared no more than 1 hour prior to the reaction, are added to the tanks 1 and 2, respectively. The reactor and the oil heat exchanger (4a) were preheated to 55 °C. Initially, soybean oil at the specific flow rate was fed to the reactor using the metering pump (3a). The system was operating in this form until achieving 55 °C in the oil at the reactor outlet. At that moment, the solution of NaOH in methanol was fed to the reactor using the respective metering pump (3b). The

initial time (t = 0) was set as soon as the pump began feeding the solution to the reactor and the heating systems were at 55 °C. Samples were collected at the reactor outlet (5C) each 20 min during 120 min. Samples were analyzed by gas chromatography to determine the content of FAMEs, MGs, DGs, and TGs, following the procedure described in section 3.2.7. Mass flow rates were monitored each 5 min during the experiment. At the end of each experiment, the decanter outlet streams were stored in the tanks 8 and 9 and the reactor was cleaned feeding ethanol for 10 min.

5.2.6 Identification of the model parameters

Fisher–Snedecor test of unbiased variances (section 3.2.8) was implemented for 24 experimental conditions which were used; 14 in identification, 5 in validation and 5 in replication.

The determination of the error was for each experimental condition. Average deviations between experimental and calculated compositions were calculated according to the root mean square deviation (equation 5).

$$Dev = \sqrt{\frac{\sum_{i}^{N}\left(w_i^{\exp} - w_i^{calc}\right)^2}{N}}.100\% \qquad \textbf{(5-1)}$$

In equation 5-1, *Dev* is the deviation percentage, N is the total number components in each experiment, subscripts *i* correspond to the component number and *exp* and *calc* represent the experimental and calculated compositions (SØRENSEN et al., 1979).

5.2.7 Mathematical model of liquid–liquid film reactor

The kinetic model of VO methanolysis can be described by the six differential equations presented in equations (5-2) to (5-7). The kinetic model has a set of six kinetic constants $\left(k_i\right)$ three in the forward direction, three in the backward direction and it does not include mass transfer resistance (NOUREDDINI; ZHU, 1997).

$$\frac{d[TG]}{dt} = [M]\left(-k_1[TG]\right) + [FAME]\left(k_{-1}[DG]\right) \qquad \textbf{(5-2)}$$

$$\frac{d[DG]}{dt} = [M]\left(k_1[TG] - k_2[DG]\right) - [FAME]\left(k_{-1}[DG] - k_{-2}[MG]\right) \qquad \textbf{(5-3)}$$

$$\frac{d[MG]}{dt} = [M]\left(k_2[DG] - k_3[MG]\right) - [FAME]\left(k_{-2}[MG] - k_{-3}[G]\right) \quad \textbf{(5-4)}$$

$$\frac{d[FAME]}{dt} = [M]\left(k_1[TG] + k_2[DG] + k_3[MG]\right) - [FAME]\left(k_{-1}[DG] + k_{-2}[MG] + k_{-3}[G]\right) \quad \textbf{(5-5)}$$

$$\frac{d[G]}{dt} = [M]\left(k_3[MG]\right) - [FAME]\left(k_{-3}[G]\right) \quad \textbf{(5-6)}$$

$$\frac{d[M]}{dt} = -\frac{d[FAME]}{dt} \quad \textbf{(5-7)}$$

For two-phase reaction system well mixed, the interfacial concentrations of components are equal to the bulk composition (LIKOZAR et al., 2016). Nevertheless, for systems with high mass transfer limitations the controlling reaction step is the component transport until the interface, so, the methanol consumed by the reaction is equal to the methanol transferred by diffusion from the alcohol-rich phase to the interface (equation 5-8).

At the beginning, the reaction consumes the soluble methanol inside the ester-rich phase and the methanol composition approaches to the interface composition, methanol concentration inside the ester-rich phase do not increase, because is consumed in the interface for the reaction. The methanol solubility contribution in the reaction rate can be dismissed, because its effect in the overall reaction is lower than the effect of the mass transfer limitation. These considerations were previously studied for the heterogeneous reaction, particularly with heterogeneous catalyst (H. S. FOGLER, 2006, LEVENSPIEL, 1986). The Proposed Mathematical model is an adaptation of this concept for the biodiesel production. The mass transfer limitation for the Glycerol transport until the alcoholic phase was dismissed because the kinetic constant related with the methanol is higher than the kinetic constant related with the glycerol.

$$[M]_{Int}\left(k_1[TG] + k_2[DG] + k_3[MG]\right) = k_C a_C \left([M] - [M]_{Int}\right) \quad \textbf{(5-8)}$$

Where, k_C is the global mass transfer coefficient (m/min) and a_c is the packing surface area to reaction volume ratio (m^2/m^3, Figure 5-1). This ratio is calculated according to equation 5-10. Equation 5-8 considers only the methanol consumption (direct reaction) because its rate constant is higher than the rate constant for the reverse reaction. It is possible to obtain the methanol concentration in the interface (equation 5-9) from the equation 5-8.

The ratio between the interfacial methanol concentration and the global methanol concentration was called effective transport coefficient $\left(k_{eff} \right)$ (equation 5-11) and it can be calculated according to the equation 5-12; this parameter can take values between 0 and 1. Values close to 0 indicate high mass transfer resistance (low effective transport coefficient) while values close to 1 mean low mass transfer resistance (high effective transport coefficient).

$$[M]_{Int} = \frac{k_C a_C [M]}{k_C a_C + k_1 [TG] + k_2 [DG] + k_3 [MG]} \tag{5-9}$$

$$a_C = \frac{4 n_{Pack} D_{Pack}}{D_{rxn}^2} \tag{5-10}$$

$$k_{eff}(z) = \frac{[M]_{Int}}{[M]} \tag{5-11}$$

$$k_{eff}(z) = \frac{k_C a_C}{k_C a_C + k_1 [TG] + k_2 [DG] + k_3 [MG]} \tag{5-12}$$

The LLFR behavior is described integrating the material balance in the differential section of Figure 5-1, assuming laminar flow, the system is in steady state, without radial or angular profile concentrations, without mass transfer by diffusion in the flow direction (z) and coupling the methanolysis kinetic model with the methanol transport until the interface (equations 5-13 to 5-18).

$$V_z \frac{dC_{TG}}{dZ} = [M] \left(-k_{eff} \left(k_1 [TG] \right) \right) - [FAME] \left(-k_{-1} [DG] \right) \tag{5-13}$$

$$V_z \frac{dC_{DG}}{dZ} = [M] \left(k_{eff} \left(k_1 [TG] - k_2 [DG] \right) \right) - [FAME] \left(k_{-1} [DG] - k_{-2} [MG] \right) \tag{5-14}$$

$$V_z \frac{dC_{MG}}{dZ} = [M] \left(k_{eff} \left(k_2 [DG] - k_3 [MG] \right) \right) - [FAME] \left(k_{-2} [MG] - k_{-3} [G] \right) \tag{5-15}$$

$$V_z \frac{dC_{FAME}}{dZ} = [M] \left(k_{eff} \left(k_1 [TG] + k_2 [DG] + k_3 [MG] \right) \right) - [FAME] \left(k_{-1} [DG] + k_{-2} [MG] + k_{-3} [G] \right) \tag{5-16}$$

$$V_z \frac{dC_G}{dZ} = [M] \left(k_{eff} \left(k_3 [MG] \right) \right) - [FAME] \left(k_{-3} [G] \right) \tag{5-17}$$

$$V_Z \frac{dC_M}{dZ} = [M]\left(-k_{eff}\left(k_1[TG] + k_2[DG] + k_3[MG]\right)\right) + [FAME]\left(k_{-1}[DG] + k_{-2}[MG] + k_{-3}[G]\right) \tag{5-18}$$

To solve equations 5-13 to 5-18 determining the value of k_{eff} for the whole reactor is necessary. This variable is a function of k_C which depends on the average flow velocity over the packing (V_Z, equation 5-23). The values of the dimensionless parameters C_1, C_2 and C_3 (equation 5-19) were obtained from experimental data, while methanol diffusivity in the VO rich phase was calculated using equation (5-21) (WILKE; CHANG, 1955). AAF is the transversal area available for the flow of the phases into the reactor (equation 5-27).

$$k_C(z) = C_1 Sc_I^{C_2} \operatorname{Re}_I^{C_3}\left(\frac{D_{12}}{\delta_I}\right) \tag{5-19}$$

$$\delta^I(z) = \frac{D_{Pack}(a-1)}{2} \tag{5-20}$$

$$D_{12}(z) = 7.4 \times 10^{-15} \frac{(x_2 M_2)^{1/2} T}{\mu_2 V_{MOL1}^{0.6}} \tag{5-21}$$

$$\delta^{II}(z) = \frac{D_{Pack}(b-a)}{2} \tag{5-22}$$

$$V_Z(z) = \frac{4\left(Q_{Pack}^I + Q_{Pack}^{II}\right)}{\pi D_{Pack}^2 (b^2 - 1)} \tag{5-23}$$

$$\operatorname{Re}^I(z) = \frac{V_Z^I \rho^I D_H^I}{\mu^I} \tag{5-24}$$

$$V_0 = \frac{4 n_{Pack}\left(Q_{Pack}^I + Q_{Pack}^{II}\right)}{\pi\left(D_{rxn}^2 - n_{Pack} D_{Pack}^2\right)} \tag{5-25}$$

$$Sc^I(z) = \frac{\mu^I}{\rho^I D_{12}} \tag{5-26}$$

$$AAF(z) = \frac{D_{rxn}^2 - 4 n_{emp}\left(\frac{D_{Pack}}{2} + \delta^I + \delta^{II}\right)^2}{D_{rxn}^2} \tag{5-27}$$

$$Q_{Pack}^I = \frac{Q^I}{n_{Pack}} \tag{5-28}$$

Variables described by the equations 5-19 to 5-28 are a function of the reactor length. Consequently, they must be calculated for each integration step (Figure 5-3). The velocity is a function of the film thickness, the density and the viscosity for the both phases ($V_z = f\left(\delta_z, \rho_z, \mu_z\right)$), at the same time $\rho_z = f\left(C_i^z\right)$ and $\mu_z = f\left(C_i^z\right)$. Consequently, the velocity is a function of the concentration and the reactor length and must by calculated for each integration step. To calculate the velocity for all the reactor (equation 5-23) it is

necessary to find the ester and alcoholic film thickness in contact with each thread (δ^I, δ^{II}), which can be calculated by solving simultaneously the force balances over the cylindrical thread for both phases (alcohol and ester-rich phases) (equations 5-29 to 5-30).

$$2a^2 - a^4 - 1 + 2\beta a^2 \left(2\ln(a) - 1 + \frac{1}{a^2}\right) - \frac{128\mu_I Q^I_{Pack}}{\pi\rho_I g D^4_{Pack}} = 0 \qquad \textbf{(5-29)}$$

$$2\lambda\left((b/a)^2 - 1\right) - \left((b/a)^4 - 1\right) + 2b^2\left((b/a)^2\left(2\ln(b/a) - 1\right) + 1\right) - \frac{128\mu_{II} Q^{II}_{Pack}}{\pi\rho_{II} g D^4_{Pack}} = 0 \qquad \textbf{(5-30)}$$

$$\beta = \left(b^2\frac{\rho_{II}}{\rho_I} + a^2\left(1 - \frac{\rho_{II}}{\rho_I}\right)\right) \qquad \textbf{(5-31)}$$

$$\lambda = \left(a^2 + \frac{\rho_I \mu_{II}}{\rho_{II} \mu_I}\left(1 - a^2 + 2\beta\ln(a)\right)\right) \qquad \textbf{(5-32)}$$

where, μ_I and μ_{II} are the viscosities, ρ_I and ρ_{II} are the mass densities, g is the gravity, Q^I_{emp} and Q^{II}_{emp} are the volumetric flow rates around each thread, a and b are a function of the thickness of the oil and alcoholic film adjacent to each thread and subscripts I, II refers to the ester-rich phase and alcoholic-rich phase, respectively.

Figure 5-3 shows the solution algorithm to solve the differentiable system (equations 5-13 to 5-18) which describes the LLFR behavior. First, with the initial reactor concentration the viscosity, density and film thickness for both phases are calculated for the first length step solving simultaneously equations 5-29 to 5-32, with this information the k_{eff} is calculated (equation 5-12), then the concentrations for the next length step is calculated (equations 5-13 to 5-18) and this information is used to calculated the next viscosity, density, thickness for the both phases. The procedure is repeated until it covers the reactor length. This solution algorithm allows the user to describe the LLFR profiles of conversion, yield, compositions, viscosities, densities, average velocities, effective transport coefficient, thickness films for both the ester and alcoholic phases along the whole reactor. The differential equation system does not have an analytical solution but it can be solved with any differential equation integrator. For this work differential equation system was solved using MATLAB® tool ODE15S.

Initial Variables

$$C_n, Q_{emp}^I, Q_{emp}^{II}, T, L$$

↓

Estimation of initial layers thickness and velocity

$$\mu_n^I, \mu_n^{II}, \rho_n^I, \rho_n^{II}, a_n, b_n, \delta_n^I, \delta_n^{II}, V_{z-n}^I, V_{z-n}^{II}, V_{z-n}$$

↓

Estimation of mass transfer efficiency

$$D_{12,n}, S_{C,n}, \text{Re}_n, k_{C,n}, k_{eff,n}$$

↓

Estimation of the concentration in the next iteration step

$$C_{n+1}$$

$$z_{n+1} = z_n + \Delta z$$

↓

$z_{n+1} \geq L$ — **No** → $n = n+1$ (loop back)

Yes ↓

Final of the integration
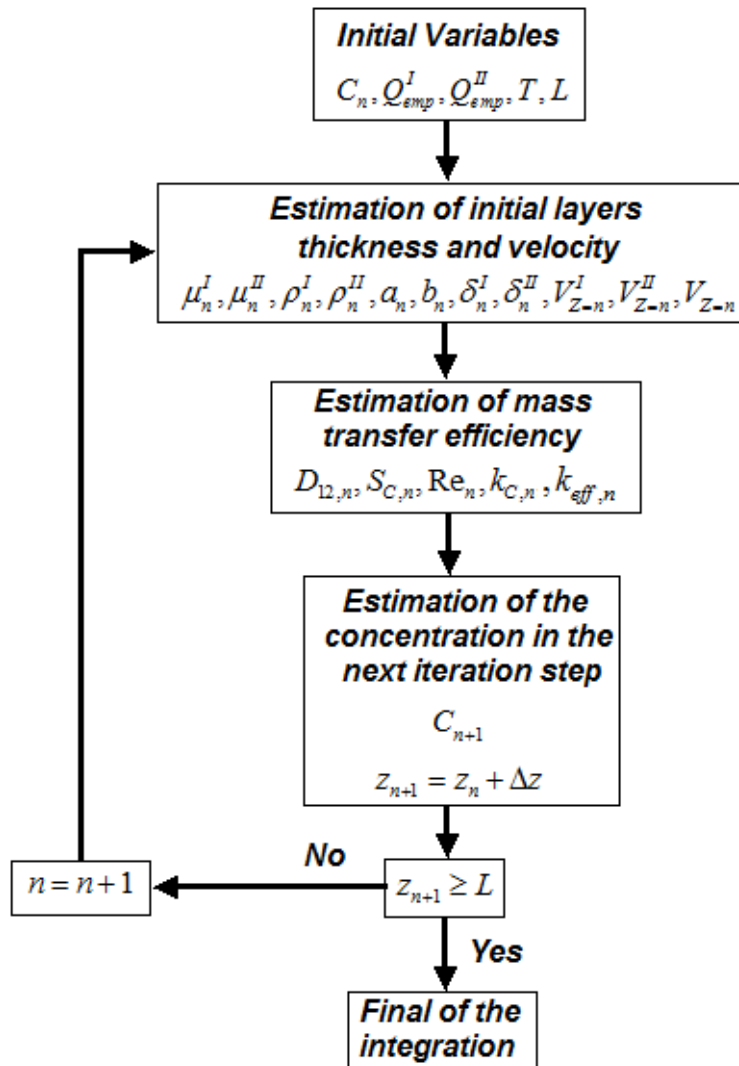
Figure 5-3. Global algorithm for the mathematical model.

5.3 Results and discussion

5.3.1 Packing fraction and flow rate effects on LLFR performance

Experimental results obtained in this work were used to adjust the dimensionless mass transfer parameters of equation 5-19 (C_1, C_2, and C_3). Results presented in Table 5-1 show the strong influence of Reynolds (Re) and Schmidt (Sc) numbers on the mass transfer coefficient (k_C, equation 5-19).

Table 5-1. Dimensionless parameters of the mass transfer coefficient for the soybean oil methanolysis in an LLFR.

C_1	5×10^{-6}
C_2	1.62
C_3	0.99

Figure 5-4 shows the packing quantity effects on the conversion and yield, comparing the experimental results with model predictions and the confidence interval of the 99% is reported too (Bounds). The increment in the packing quantity increases conversion and yield in the LLFR, which can be explained by k_{eff} augmenting (equation 5-12). Higher the packing quantity, larger the mass transfer area and lower film thickness. The difference between experimental results and model prediction were a consequence of the experimental results variability. However, the majority of the model simulations are in the confidence interval of 99%, indicating accurate fit with the experimental results.
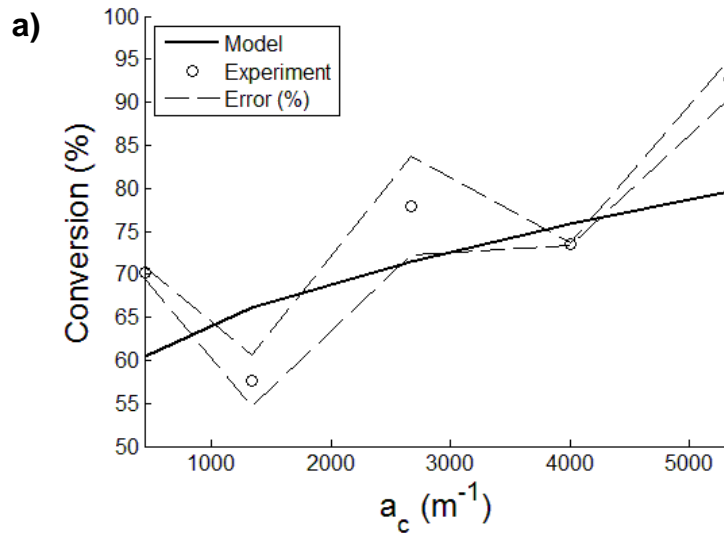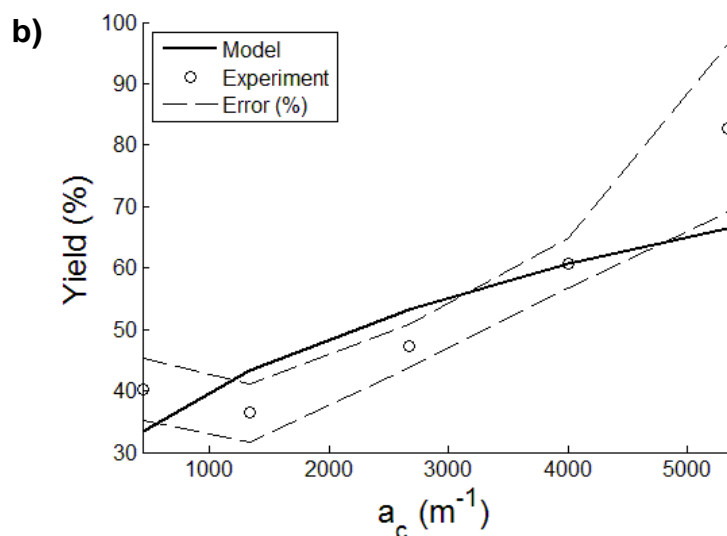
Figure 5-4. Packing quantity effects on (a) conversion; (b) FAME yield. Reactor length 25cm and Flow rate 5 g/min.

Figure 5-5 shows VO mass flow rate effects on the conversion and yield, comparing experimental results with model predictions. The increment of flow rate promotes an increase in conversion and yield in the LLFR, because k_C (equation 5-19) increases when Reynolds number augments (Figure 5-5c). This effect is stronger between 5 g/min and 15 g/min because at these conditions mass transfer limitations are stronger. Without this limitation, a flow rate increase does not improve LLFR behavior.
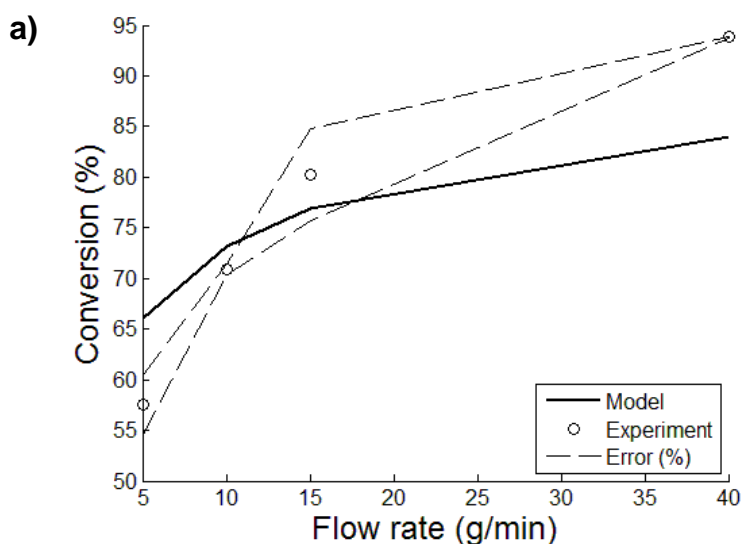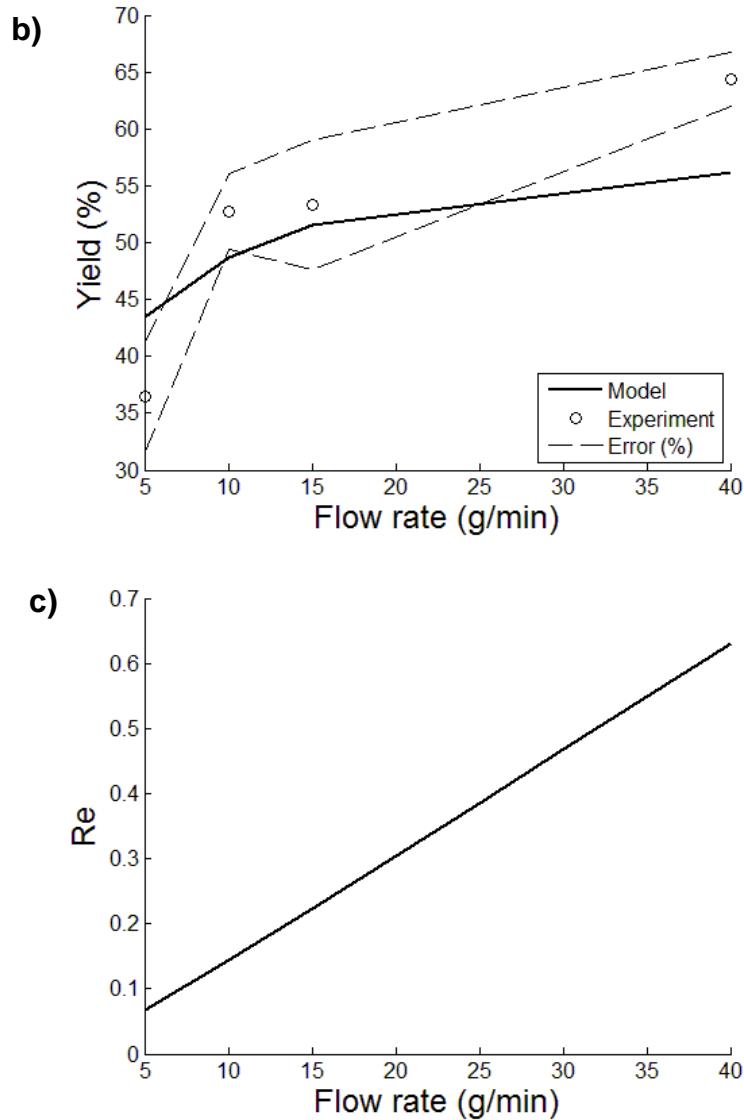
Figure 5-5. Flow rate effects on the conversion (a), FAME yield (b) and Reynolds number (c). Reactor length 25cm and a_C of 1333 m^{-1}.

Model predictions are presented in Figures 5-6 to 5-11. Figure 5-6 presents the effect of flow rate and packing quantity on conversion, yield, k_{eff} and productivity. The increment of flow rate or packing quantity promotes the increase of the k_C values and, therefore, in k_{eff} values, indicating a reduction in the mass transfer resistance. This effect can be observed in the region where mass transfer resistance is important (Low flow rate or low packing quantity). The majority of the model simulations of this effect are in the confidence interval of 99%, indicating accurate fit with the experimental results.

a)

b)
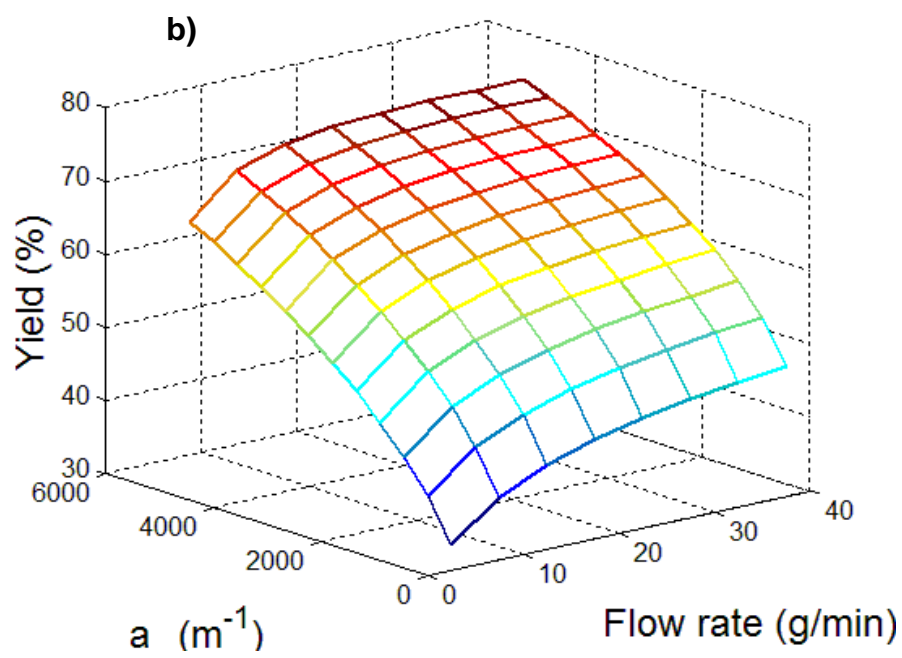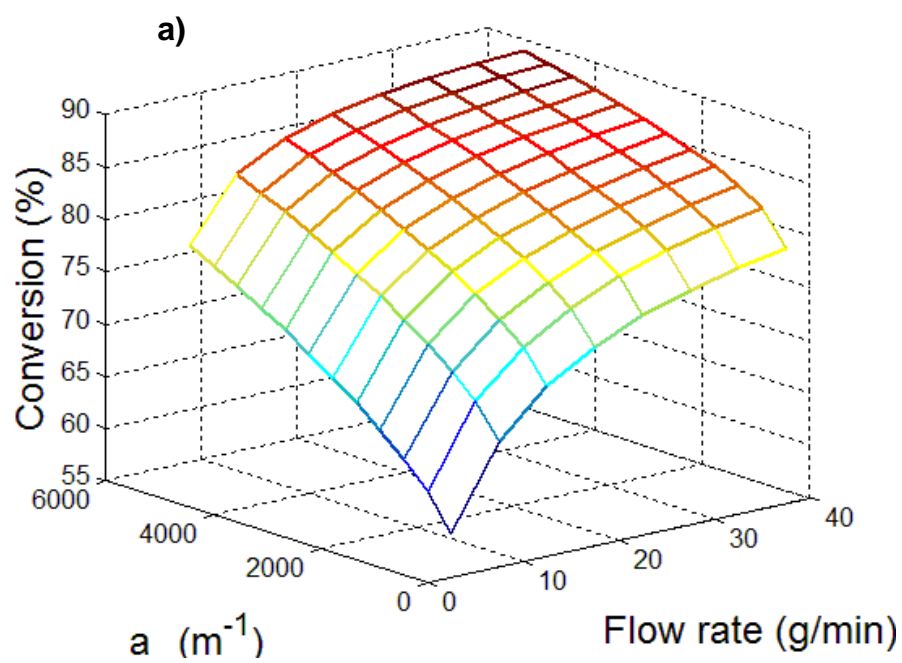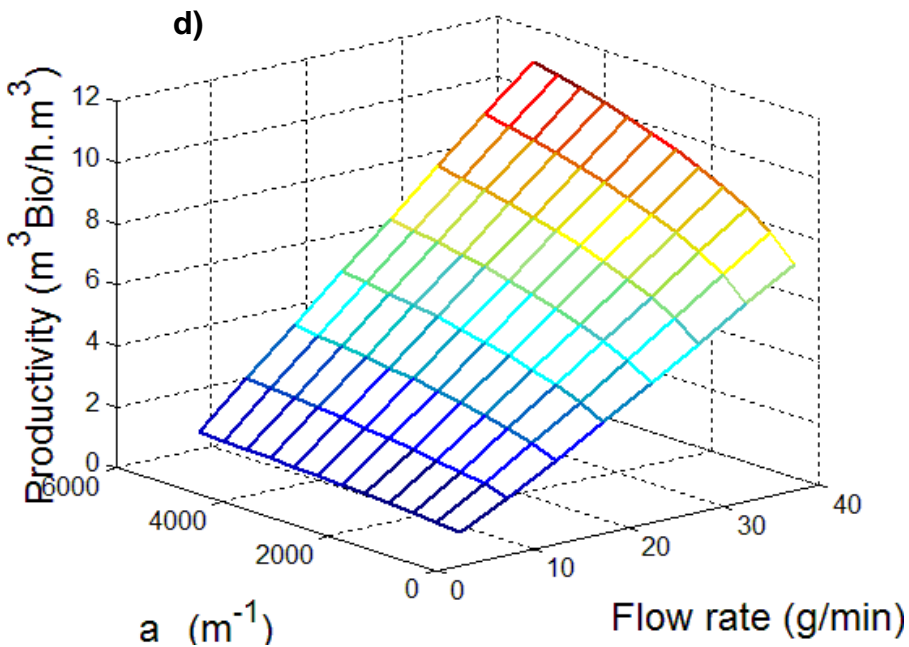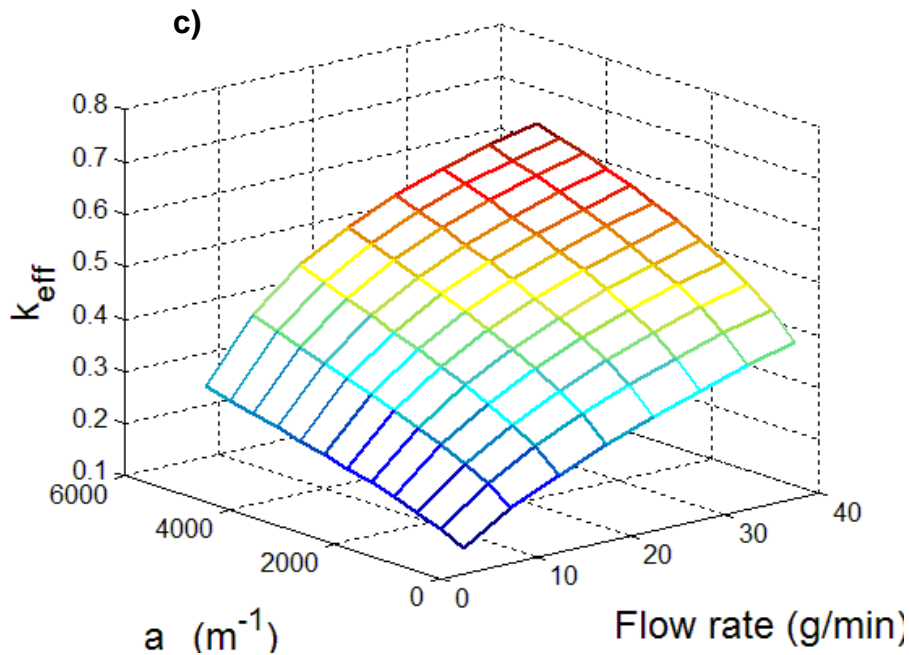
Figure 5-6. Packing quantity and VO flow rate effects on the conversion (a), FAME yield (b), effective transport coefficient (c) and productivity (d). Reactor length 25 cm.

If conversion, yield and flow rate increase, reactor productivity (m³ Biodiesel m⁻³ h⁻¹) increases for the same reactor volume, as shown in Figure 5-6d. Productivity found in this work is higher than the reported in a conventional BSTR (Table 5-2).This behavior is explained because LLFR shows low mass transfer limitations, and high conversion and

yield is achieved even at high flow rates (NARVÁEZ, P. C. et al., 2009). Moreover, as the process in an LLFR is continuous, charge and discharge times are reduced and decantation time typical in a BSTR is reduced.

Table 5-2 shows that previous results, where productivity in the LLFR is 4 times higher than the BSTR (NARVÁEZ, P. C. et al., 2009). In this work LLFR productivity was improved increasing the packing quantity and flow rates (12 times in comparison to a BSTR). However, FAME yield at that condition was 95%, value 2% lower than the reported for a BSTR (97%).

As described in section 5.2.4, a decanter (300 cm^3) was located downstream the reactor to separate the ester-rich and the alcohol-rich phases. FAME yield after decantation was 97%, meaning residence time in the decanter was enough to achieve the reaction equilibrium. If LLFR and decanter volume were considered as reaction volume to calculate the productivity, the value obtained is 8 times the productivity reported for a BSTR (Table 5-2). Decanter increases the reaction time, so, the biodiesel quality is improved but reactor productivity is reduced. LLFR coupled to decanter as reaction system fulfills biodiesel quality requirements with a productivity very attractive for industrial implementation.

Table 5-2. Productivity of biodiesel from soybean oil obtained for LLFR and for BSTR at 55 °C, using NaOH as catalyst (1 %wt.).

Variable	BSTR (CADAVID et al., 2013)	LLFR (NARVÁEZ, P. C. et al., 2009)	LLFR (this work)	LLFR with decanter (this work)
Conversion (%)	99.9	97.5	99.5	99.9
Yield (%)	97.1	92.2	95.1	97.2
Productivity $\left(\dfrac{m^3 FAME}{h \cdot m^3 reactor} \right)$	0.3	1.2	3.5	2.5
Flow rate (g/min)	N.A*	9	40	40
Packing surface to volume (a_c , m^{-1})	N.A*	444	5333	5333

* Not Applicable.

Figures 5-7a and 5-7b present simulation results for flow rate and packing quantity effect on the ester film thickness and average velocity, respectively. Mass flow rate is

proportional to volumetric flow, which depends on the threads surface area and quantity, film thickness and average velocity. Consequently, according to the continuity equation a rise in the flow rate increases the ester film thickness and the average velocity. On the other hand, the ester film thickness and the average velocity decrease when the packing quantity increases, because the reactive mixture mass is distributed over more threads (equation 5-28).
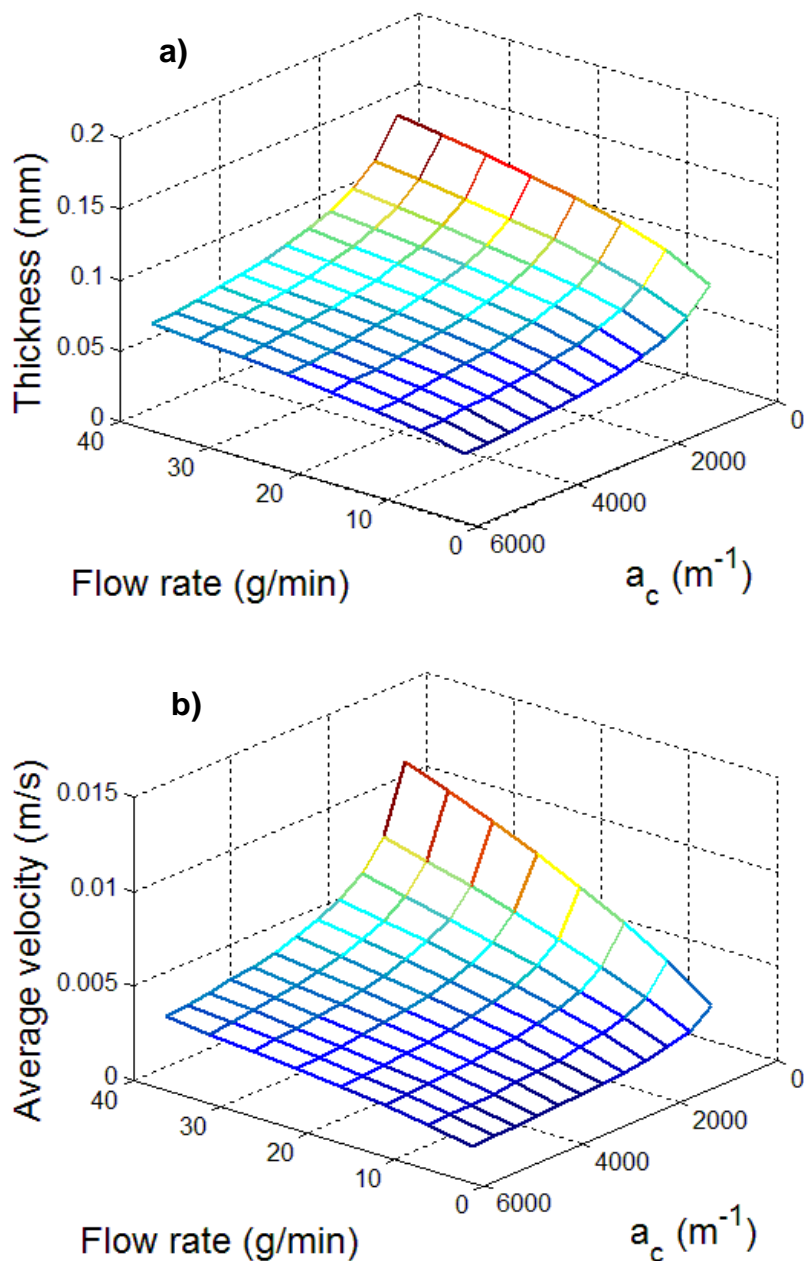
Figure 5-7. Packing quantity and flow rate effects on the ester film thickness (a) and the average velocity (b). Reactor length 25 cm.

Figure 5-8 presents packing and flow rate effects on the AAF. High packing quantity reduces AAF (equation 5-27), while increment in flow rate augments film thickness and reduces AAF (Figure 5-8). These effects were previously observed by NARVÁEZ et al., (2009) and supported by the residence time analysis of the reactor.

The LLFR operates as a film reactor until AAF is zero. At this condition, films are not formed and the behavior is similar to a plug flow reactor (PFR). To model this condition, it was necessary to replace V_Z in equations (5-23) by V_O (equation 5-25). Previously, residence time distribution in the LLFR was studied showing strong similarities between this reactor and a PFR (NARVÁEZ et al., 2009). The maximum VO flow rate used in this work was 40 g/min and the maximal packing quantity was 5333 m^{-1}due to the system design. Nevertheless, Figure 5-8 shows these conditions are close to a AAF value equal to zero, indicating the upper boundary of the film behavior inside the reactor.
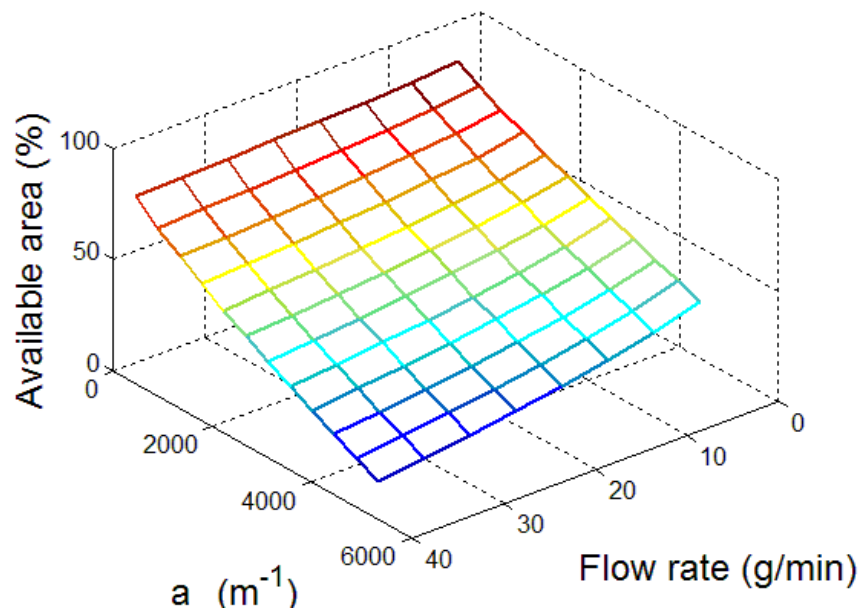
Figure 5-8. Packing quantity and VO flow rate effects on the area available for flow. Reactor length 25 cm.

5.3.2 Reactor length effects on the LLFR performance

Reactor length effect on the LLFR was evaluated and presented in Figure 5-9. Conversion and yield increase with the reactor length because residence time increases too. This behavior was previously described by (NARVÁEZ et al., 2009). Experimental data and model predictions as a function of the reactor length adjust adequately. The maximum conversion and yield experimentally determined were 99.5% and 95.1% respectively, using a 1 m reactor length. When a decanter was placed downstream the reactor, final conversion and yield increased to 99.5% and 97.5%, respectively, corresponding to the transesterification reaction equilibrium values. The highest reaction rate in the reactor was observed in the first 0.06 m. After 0.06 m, reaction rate decreases but conversion and yield continue increasing. This behavior was also observed in a BSTR (NOUREDDINI; ZHU, 1997) and it means the reaction was controlled by mass transfer for the first 10% of the reactor length (measured from the top) and by the reaction kinetics in the following 90% (Figure 5-10c).
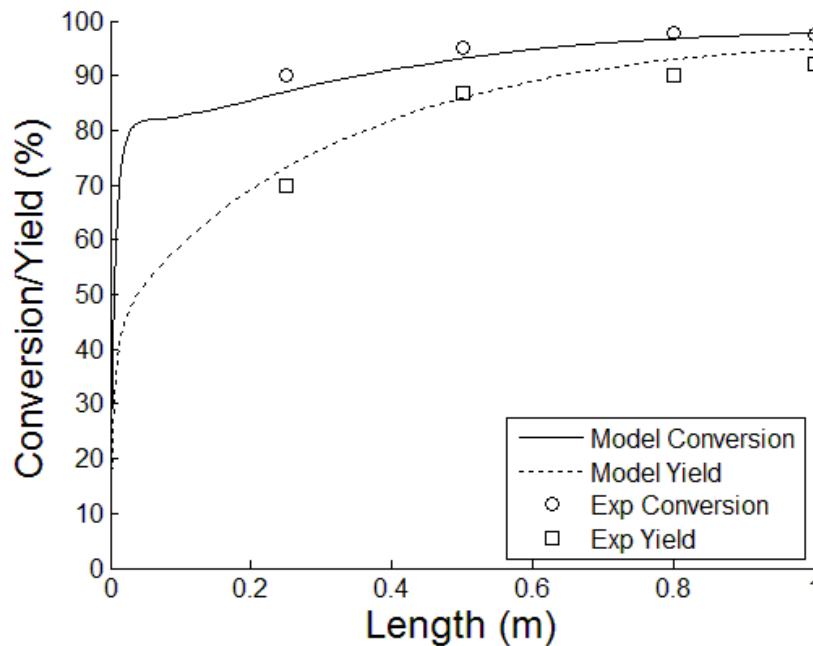
Figure 5-9. Reactor length effect on the conversion and FAME yield. VO flow rate 40g min^{-1} and a$_C$ of 5333 m^{-1}.

Mathematical model predicts changes in thickness film, average velocity, and mass transfer coefficient as a function of reactor length (Figure 5-10). At the reactor input, the ester-rich phase is soybean oil. As the ester-rich phase flows down, soybean oil is

consumed and biodiesel is formed. As a consequence, viscosity, film thickness and Schmidt number decrease along the reactor length (reaction progress), whereas the average velocity and the Reynolds number increase. An opposite behavior is observed for the alcoholic phase.

Alcoholic phase has the highest average velocity because it flows over the ester-rich phase. Then, its minimal velocity is in the interface with the ester-rich phase and its maximal velocity is on the surface (figure 5-10b) also the viscosity is higher for the ester-rich phase than the alcoholic phase. Therefore, the highest thickness was for the ester-rich phase because it shows lower average velocity and because its volumetric flow was higher than the volumetric flow for the alcoholic phase (figure 5-10a). However, Figure 5-10c presents a little reduction in the k_{eff} in the first 5% of the reactor length. This behavior can be attributed to the reduction of viscosity which increases Re number and reduces Sc number. In fact, in this section Sc number influence on k_C was higher than the Re number influence (equation 5-19). Beyond this section, Re number influence on k_C was predominant and k_{eff} increased progressively with reactor length.
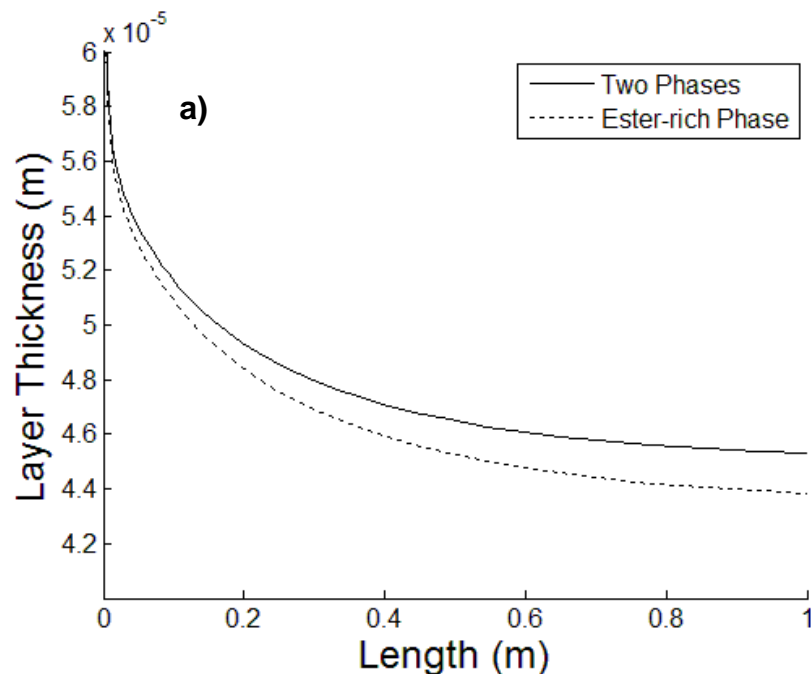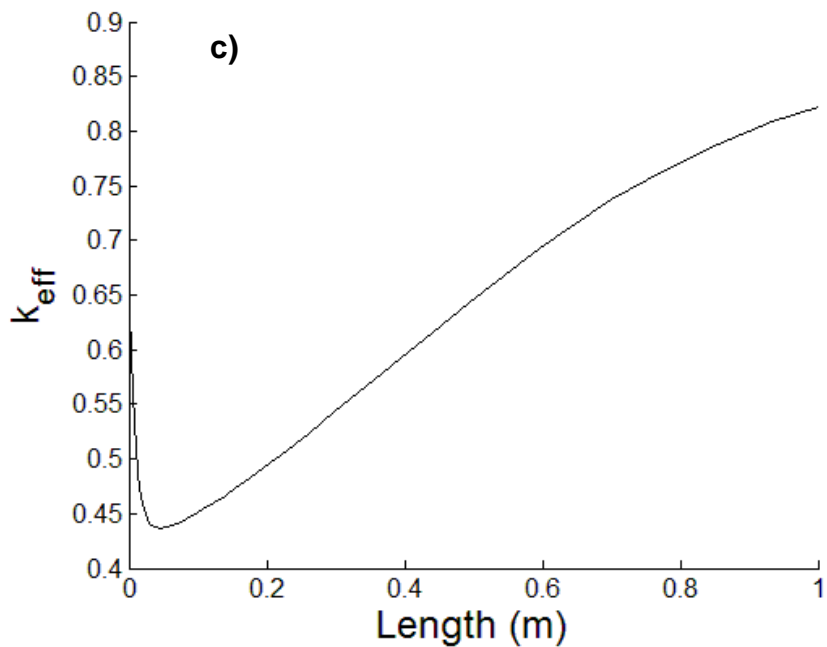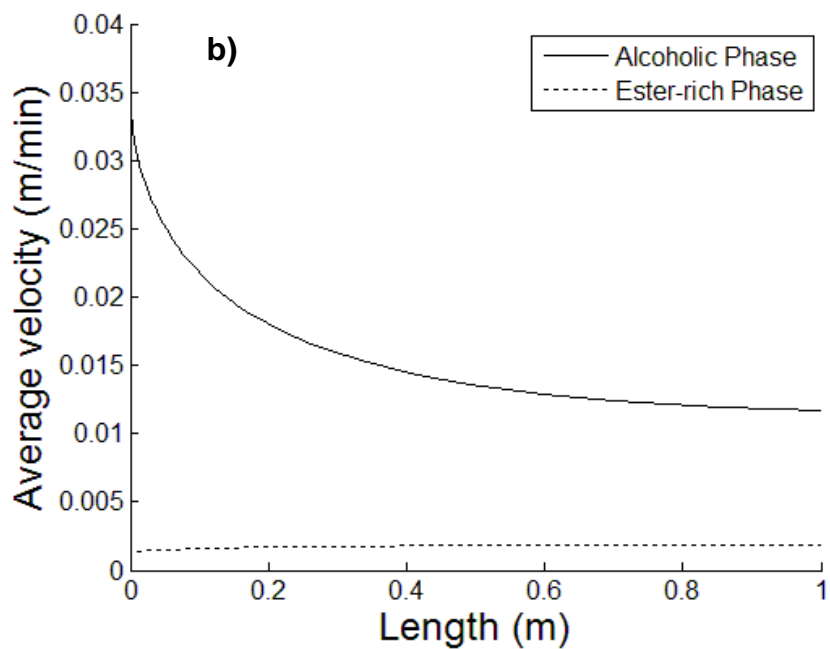
Figure 5-10. Reactor length effect on the (a) film thickness, (b) average velocity and (c) effective transport coefficient. VO flow rate 40g min^{-1} and a_C of 5333 m^{-1}.

5.3.3 Model validation

Table 5-3 shows the Fisher-Snedecor unbiased variances test for experimental FAMEs, TGs, DGs and MGs data obtained in the experiments. The Validation/Identification test

proved the quality of the model. Similarly, the Replication/Identification test proved the quality of the experimental procedure. According to the results shown in Table 5-3, the model accurately predicted the experimental compositions of FAMEs, TGs, DGs and MGs with 95% reliability.

Table 5-3. Fisher-Snedecor test of unbiased variances for the identification, validation, and replication of the LLFR.

Test relation	Category	V_1/V_2	Freedom degrees (n1 and n2)	$1/F_{0.025}(n_2, n_1)$ Min.	$F_{0.025}(n_1, n_2)$ Max.
Validation/ Identification	**FAME**	0.63	(5 and 7)	0.0523	12.03
	MG	19.81			
	DG	0.67			
	TG	0.71			
Replication/ Identification	**FAME**	9.12	(4 and 7)	0.0322	12.73
	MG	4.12			
	DG	1.79			
	TG	5.20			

Model predictions were compared with LLFR experimental results. The comparison is presented in Figure 5-11.There was a satisfactory fit between regardless the experimental conditions tested. The main deviation was observed for high flow rate and packing quantity predictions. However, the maximal deviation between model prediction and the experimental data was 10,14% (Table 5-4), this indicates an accurate fit between them.
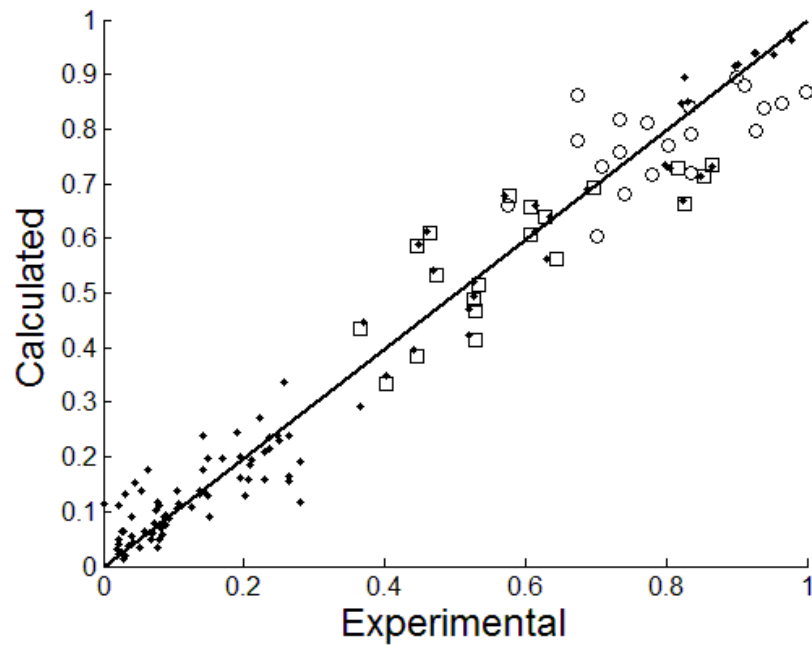
Figure 5-11. Comparison between the calculated and experimental results in the LLFR. Points: mass fraction; Circles: Conversion; Squares: Yield.

Table 5-4 shows deviation percentage between experimental and calculated results. The lowest average and maximum deviations were 1.41% and 10.14% for 5g/min with 3996 m^{-1} and 40 g/min with 2664 m^{-1}, respectively. The deviation percentages are lower for low package quantity. Nevertheless, the proposed mathematical model shows an accurate fit for the experimental results.

Table 5-4. Deviation percentage between experimental and calculated data for different flow rate and package quantity.

	444 m^{-1}	1332 m^{-1}	2664 m^{-1}	3996 m^{-1}	5333 m^{-1}
5 g/min	5.00%	5.32%	6.99%	1.41%	9.80%
10 g/min	3.38%	3.13%	8.76%	4.44%	8.60%
15 g/min	6.83%	1.67%	9.47%	6.64%	6.95%
40 g/min	3.59%	5.52%	10.14%	1.78%	8.25%

5.4 Conclusions

The mathematical model proposed in this work described adequately soybean oil methanolysis in the LLFR as validated by the Fisher-Snedecor test of unbiased variances. This model described mass transfer limitations, hydrodynamics inside the LLFR, as well as packing quantity and flow rate effects on LLFR performance. The increase in packing quantity and flow rate improved the LLFR conversion, yield, and productivity because it reduced the mass transfer resistance in the reactor. Improvements of both conditions increased LLFR productivity up to 8 times the average productivity reported by a traditional BSTR. However, these two conditions reduced the *AAF*. When the empty fraction in the reactor was close to zero, the LLFR work as a packing PFR and its hydrodynamic and mathematical model changed. The highest conversion of soybean oil methanolysis in the LLFR and its FAME yield were 99.9% and 97.5%, respectively at the following conditions: 55 °C, 1 %wt. NaOH, 1m of reactor connected to a final decanter, packing surface area to reaction volume ratio of 5333 m^{-1}, 40 g/min of VO flow rate and 6:1 methanol to oil molar ratio.

5.5 List of symbols

k_i Kinetic constant $\left(\dfrac{L}{gmol \cdot \min} \right)$

L Reactor length (m)

k_C Global mass transfer coefficient (m/min)

a_c Packing surface area to reaction volume ratio (m^2/m^3)

C_1, C_2, C_3 Parameters of the mass transfer coefficient (Dimensionless)

n_{Pack} Number of threads

D_{Pack} Thread diameter (m)

D_{rxn} Reactor diameter (m)

k_{eff}	Effective transport coefficient
AAF	Area available for flow
δ^I	Ester film thickness (m)
δ^{II}	Alcoholic film thickness (m)
V_Z	Average flow velocity over the packing (m/min)
V_0	Average flow velocity in the reactor (m/min)
D_{12}	Methanol diffusivity in the ester-rich phase (m^2/s)
Q^I_{Pack}	Volumetric flow rates ester-rich phase around each thread (m^3/min)
Q^{II}_{Pack}	Volumetric flow rates alcoholic phase around each thread (m^3/min)
Q^I	Volumetric flow rates of the ester-rich phase (m^3/min)
Q^{II}	Volumetric flow rates of the alcoholic phase (m^3/min)
Re	Reynolds number
Sc	Schmidt number
D_H	Hydraulic diameter
a	Ratio between the ester film diameter and the thread diameter
b	Ratio between the alcoholic film diameter and the thread diameter

6. Biodiesel – Glycerol – Methanol mixtures separation using membranes

6.1 Introduction

In this chapter, Biodiesel - Glycerol - Methanol mixtures separation using poly(ether sulfone) hollow fiber membranes (PES-HFM) is studied. This study gives information about the performance of the membranes in the separation of the components present in the outlet stream from an LLFR where methanolysis is carried out.

This chapter assesses the LLE influence in the biodiesel phase separation and presents a mathematical model to describe the membrane separation performance. The model parameters were adjusted from experimental data and it was validated using another set of bench scale results. A mathematical model describes the flux through the PES-HFM by using transport equations of ultrafiltration, where permeate composition is dependent of the LLE without fouling effects. Experimental validation included the evaluation of Pressure difference through the membrane (ΔP, 0 to 0.6 bar), flow rate (5 to 40 g min^{-1}), feed bulk composition and Ester-rich phase mass fraction (0 to 0.8) effects on permeability and permeate composition.

6.2 Materials and methods

6.2.1 Materials

Analytical grade methanol, glycerol, and hexane were obtained from Merck (Darmstadt, Germany). Biodiesel was produced from soybean oil (SIGRA S.A. Bogotá, D.C. Colombia) following the procedure previously described by NARVÁEZ et al., (2007).

6.2.2 Membrane characterization

Ultrafiltration PES-HFM (50 kDa) were provided by PAM Membranas Seletivas Ltda. (Río de Janeiro, Brazil). This membrane was selected by its chemical and mechanical resistance for the biodiesel reaction (BELLO et al., 2016). The affinity between the membrane and the studied components (M, G, and FAME) was evaluated through contact angle determination using an Optical Contact Angle Measuring Instrument OCA 10 (Dataphysics Instruments, Filderstadt, Germany). Water was used as a reference. Membrane morphology was evaluated by scanning electron surface micrographs (SEM) of surface and cross sections using an FEI Quanta 200. Samples were coated with a gold film with a thickness of approximately 2–4 nm to produce an electrically conductive surface.

6.2.3 Equipment

To evaluate the separation of the mixture biodiesel/methanol/glycerol a bench-scale membrane system was designed, constructed and used. A basic scheme of the system is presented in Figure 6-1 The equipment consists of a stainless steel column (Inner diameter 1 inch) packed with a semi-structured stainless steel packing (threads). The packing was custom made by placing the quantity of stainless steel and PES-HFM threads axially aligned. Only a section of the total length of the equipment was packed with PES-HFM. Then, the system was divided into two zones: an inert region (IR) and a membrane region (MR). The equipment length (L_{max} in Figure 6-1) was 0.7 m and the membrane was located at 0.3 m from the bottom (L_{mem} in Figure 6-1). Each packing thread had a diameter of 0.3 mm and it was fixed to a distribution plate located at the top and to a central core at the bottom of the system. To maintain the temperature, the system was provided with a thermal oil bath equipped with a temperature controller SHIMADEN SR 91 (Shimaden Co. Ltd., Tokyo, Japan), capable of maintaining the temperature within ±0.1 ºC. Ester-rich phase and Alcohol-rich phase were stored in two tanks (1 and 2, respectively) placed on two balances Mettler Toledo 4000 (Mettler Toledo GmbH, Schwerzenbach, Switzerland). These balances were used to determine the mass flow rate. Other two balances were used to determine the mass flow rate of permeate and retentate (7 and 6, respectively). Two metering pumps HMS EXT 2001 (EMEC Srl, Vazia, Italy) were used to feed both phases at controlled flow rates (3a and 3b). Before entering the equipment, both phases were independently heated up to test temperature using heating systems equipped with

silicon-shielded resistances (4a and 4b) and SHIMADEN SR 91 temperature controllers (Shimaden Co. Ltd., Tokyo, Japan), capable of maintaining the temperature within ±0.1 °C. ΔP was fixed according to the experimental design using a diaphragm vacuum pump (8) (vacuubrand ME 2 NT) located in the downstream permeate storage tank (7).
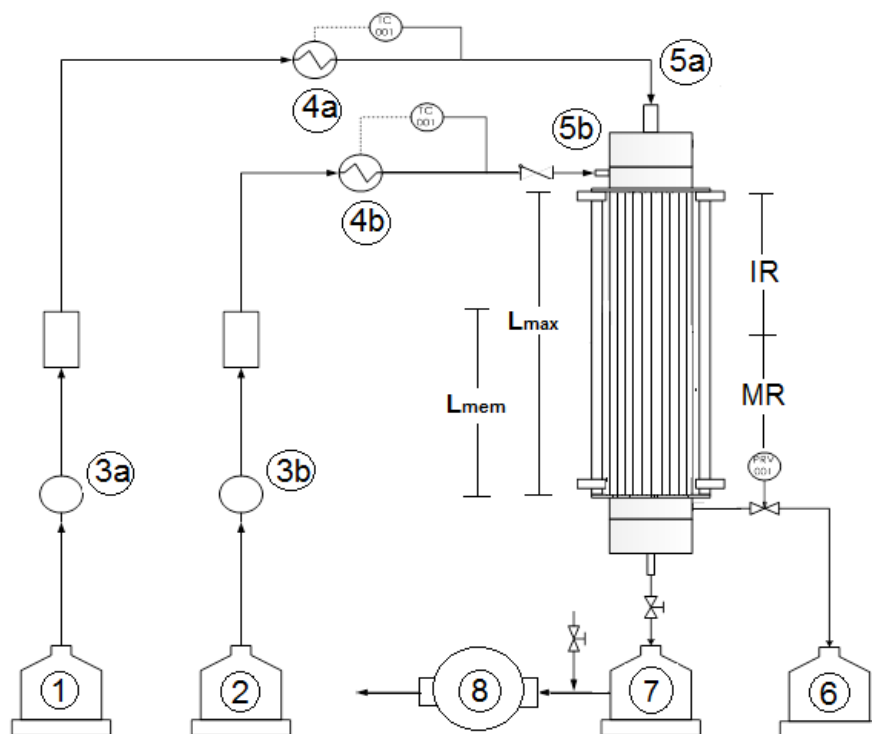
Figure 6-1. Diagram of the experimental membrane system. 1) Biodiesel phase tank; 2) Alcoholic phase tank; 3a) Biodiesel phase metering pump; 3b) Alcoholic phase metering pump; 4a) Ester-rich phase heat exchanger; 4b) Alcoholic phase heat exchanger; 5a) Biodiesel phase feeding nozzle; 5b) Alcoholic phase feeding nozzle; 6) Retentate; 7) Permeate; 8) Vacuum pump.

6.2.4 Experimental conditions

Evaluation of PES-HFM performance was made for pure methanol, methanol-glycerol mixtures, and M/G/FAME mixtures (Table 6-1), keeping constant membrane area and temperature at 4.52×10^{-2} m^2 and 40 °C, respectively. ΔP, Biodiesel-rich phase mass fraction, and flow rate effects on permeate flux and permeate composition were tested at the following intervals: 0 to 0.6 bar, 0 to 0.8, and 5 to 40 g min^{-1}, respectively. Thirteen

experiments were performed, each one at least twice. Experimental conditions are presented in Table 6-1. Compositions of Ester-rich phase correspond to the typical product composition for biodiesel production after the first reaction stage. For example, experimental conditions of the tests 5, 6 and 7 correspond to typical product composition when the molar ratio methanol to oil at the first reaction stage are 6:1, 12:1 and 18:1, respectively, considering 100% conversion. The other experimental conditions want to evaluate the influence of the Ester-rich phase mass fraction on the permeate flux and composition.

Table 6-1. Experimental conditions for the biodiesel phase separation. Temperature: 40ºC, Membrane area: 4.52×10^{-2} m^2.

Test	Biodiesel-rich phase mass fraction	Feed composition (%wt.)		
		M (%wt.)	G (%wt.)	FAME (%wt.)
1	0	100	0	0
2	0	40	60	0
3	0	63	37	0
4	0	78	22	0
5	0.855	9.58	8.61	81.81
6	0.781	22.96	7.33	69.71
7	0.704	33.48	6.33	60.19
8	0.401	26.12	35.50	38.38
9	0.412	43.55	19.69	36.76
10	0.385	53.94	13.06	33.00
11	0.181	34.13	48.54	17.32
12	0.211	54.75	26.42	18.83
13	0.252	62.51	15.89	21.60

6.2.5 Experimental procedure

The membrane previously preserved in methanol was installed in the system (Figure 6-1). Before each test, the system was preheated at 40 °C. A single component or a mixture was fed to the system using one or two metering pumps (3a and 3b in Figure 6.1). When the retentate starts to flow, the vacuum pump (8) was turned on at the first ΔP. The initial

time (t = 0) was set as soon as permeate started to flow. Feed, retentate, and permeate flow rates were measured (see 6.2.3 section) and samples were collected each 20 minutes to determine their FAME composition using the EPA method 1664 (OW, 1999). Glycerol and methanol content were evaluated using a gravimetric method, evaporating the methanol at 60 °C until constant weight.

6.2.6 Mathematical model of ultrafiltration in biodiesel phase separation

The flux through the membrane was calculated with the Hagen-Poiseuille equation including membrane resistance and fouling effects (equation 6-1).

$$J_M = \frac{\Delta P}{\mu_M^{mem}\left(R_m + R_f\right)}$$
(6-1)

Where J_M is the membrane flux, ΔP the promoter of membrane transport, is the difference of pressures on each side of the hollow fiber membrane (outside the fiber and in the bore), μ_M^{mem} is the alcohol-rich phase viscosity, R_m is the membrane resistance and R_f is the fouling resistance. R_f was assumed dependent on the cake layer resistance created when macromolecules and particulates are deposited on the surface of the membrane which results in higher ΔP (BAKER, 2004). It can be assumed that the cake layer resistance was directly proportional to the material accumulated on the surface of the membrane as given in equation 6-2 (FALAHATI; TREMBLAY, 2011, KOVALSKY et al., 2009). Then, fouling resistance increases with the Ester-rich phase mass fraction $\left(\phi\right)$ and the permeate flux $\left(J_M\right)$.

$$R_f = k\phi J_M$$
(6-2)

Including the fouling effect in the UF expression, equation (6-1) is transformed into equation (6-3).

(6-3)
$$J_M = \frac{\Delta P}{\mu_M^{mem}\left(R_m + k\phi J_M\right)}$$

The values of the parameters R_m and k for equation 6-3 have to be obtained from experimental data. LLE has to be predicted in order to calculate the permeate composition

that permeate through the membrane (alcoholic-rich phase) and to calculate the retentate composition. LLE was calculated using UNIFAC with the group interaction parameters and the solution algorithm presented in Chapter 4, using the global feed composition and temperature. These compositions were used to determine the permeate viscosity $\left(\mu_M^{mem}\right)$ using the equations (6-4 to 6-8) in the Table 6-2. Then, ϕ can be determined. Finally, J_M was calculated using equation (6-3).

Table 6-2. Viscosity (cP) dependence of temperature (°C).

Component	Equation	Reference	
Methanol	$\ln\left(\mu_{Met}\right) = -0.8173 \cdot \ln\left(T\right) + 2.233$	(GONZÁLEZ et al., 2007)	**(6-4)**
Glycerol	$\ln\left(\mu_{Gly}\right) = -2.889 \cdot \ln\left(T\right) + 16.1181$	(SEGUR; OBERSTAR, 1951)	**(6-5)**
Biodiesel	$\ln\left(\mu_{EM}\right) = -0.8677 \cdot \ln\left(T\right) + 4.6787$	(NARVAEZ P.C, RINCON S.M, 2008)	**(6-6)**
Biodiesel Phase Viscosity	$Ln\left(\mu_{MIX}\right) = \sum_{i=1}^{n} x_i Ln\left(\mu_i\right)$	(NARVAEZ P.C, RINCON S.M, 2008)	**(6-7)**
Alcoholic Phase Viscosity	$\mu_{MIX} = \left(\sum_{i=1}^{n} x_i \mu_i^{0.24}\right)^{4.1667}$	(SEGUR, 1953)	**(6-8)**

6.3 Results and discussion

6.3.1 Membrane characterization

Higher the affinity between the component and the membrane surface, smaller the contact angle, resulting in higher degree of surface wetting. The contact angle for water, biodiesel, glycerol and methanol were 58.8, 10.23, 50.7 and 12.2, respectively. The water contact angle was lower than 90, which means the PES - HFM is hydrophilic. Methanol and biodiesel contact angles show a strong affinity for the membrane surface. However,

glycerol shows lower affinity with the membrane than methanol, in consequence, the affinity between the membrane and the alcoholic phase was mainly due to the methanol presence.

Figure 6-2 shows SEM photographs of surface and cross sections for PES – HFM. Figure 6-2a shows the external diameter of 752.5 μm. The membrane was anisotropic with a porous substructure of ranging 182 to 190 μm thick and an upper less porous layer of 4.5 to 5.5 μm thick (Figures 6-2b and 6-2c). The pore size distribution at the surface was apparently not broad with an average porous diameter at the surface of 93 nm, being pore shapes quite asymmetric (Figure 6-2d).
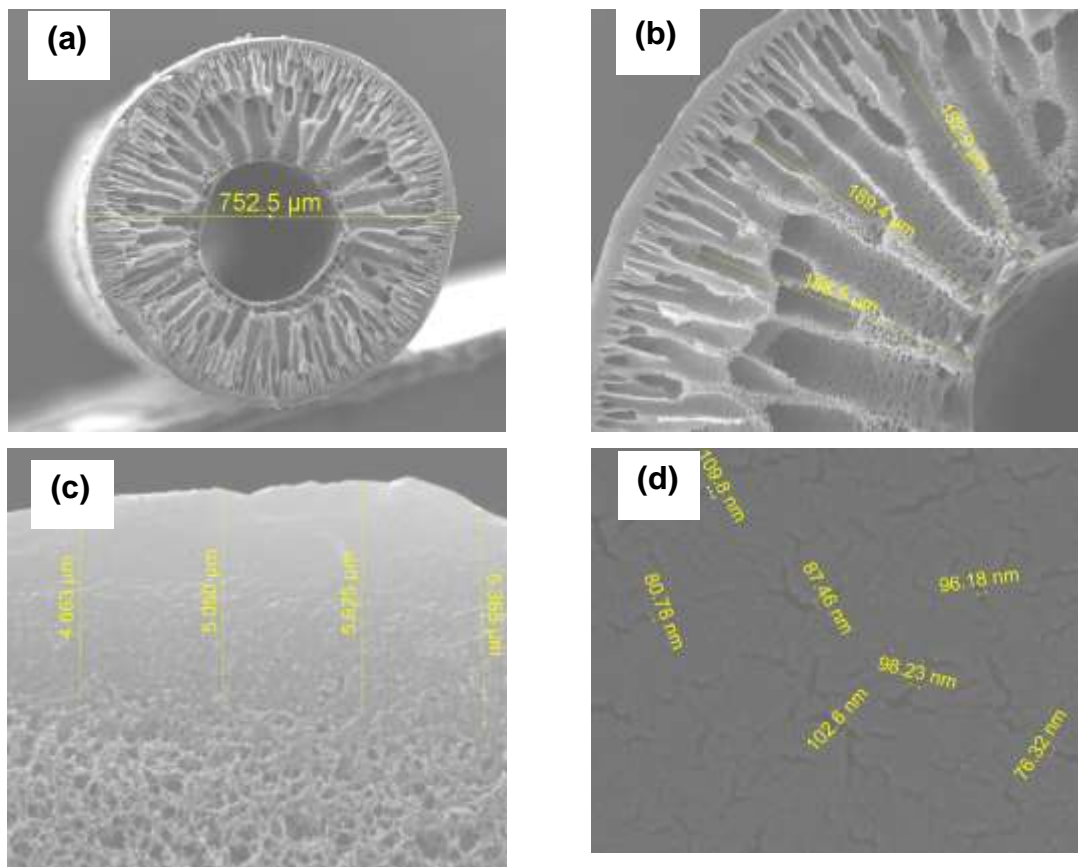
Figure 6-2. SEM of PES-HFM. a) hollow fiber; b) porous substructure; c) upper less porous layer; d) membrane surface.

6.3.2 Feed composition effect on methanolysis reaction mixture separation using membranes

Figure 6-3 shows the experimental composition for permeate and retentate. This figure also shows the LLE of the system M/FAME/G for the different overall composition tested (Table 6-1). A comparison between the experimental results and the LLE prediction reveals that membrane separation is close to the LLE. As a matter of fact, the LLE determinate the permeate composition because only the alcoholic phase was able to permeate the membrane. Figure 6-3 also shows that different overall compositions in the same tie line promote the same alcoholic phase composition. Therefore, the same permeate composition. This means that the only way to change the permeate composition was changing the feed composition or the temperature, according with the LLE. The membrane presence did not modify the LLE. However, it allowed a faster phase separation reducing the plant volume and increasing the process productivity.
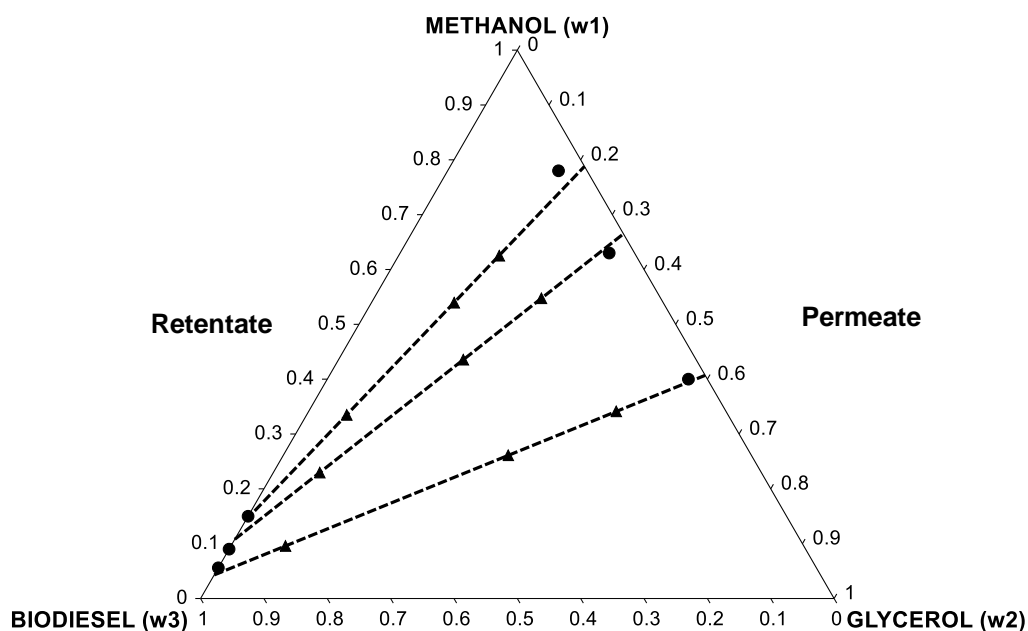
Figure 6-3. Comparison between experimental permeate and retentate with the LLE of Methanol (w_1), FAME (w_3) and Glycerol (w_2) for different molar feed. Temperature: 40 °C. Membrane Area: 4.52×10^{-2} m². ΔP : 0.6 bar. Note: Experimental Data (*filled dot*); Calculated tie lines (*Continuous lines*); Overall composition (*filled triangle up*).

6.3.3 Alcoholic feed stream flow rate and pressure effects on methanolysis reaction mixture separation using membranes

To determine the real flux it was necessary to increase the feed stream flow rate until a constant flux was obtained. This flow rate defines the minimal feed stream flow rate to develop the experiments. In order to determine these values, conditions 1, 2, 3 and 4 in Table 6.1 were evaluated. Figure 6-4 shows the results of these experiments. Once the minimal feed stream flow rate was reached its increment did not augment the membrane flux. The minimal feed stream flow rate decreases when the content of glycerol and viscosity in the alcoholic phase increases, following Hagen-Poiseuille law. Also, at feed stream flow rates higher than the minimal membrane flux did not change indicating there were not fouling effects.
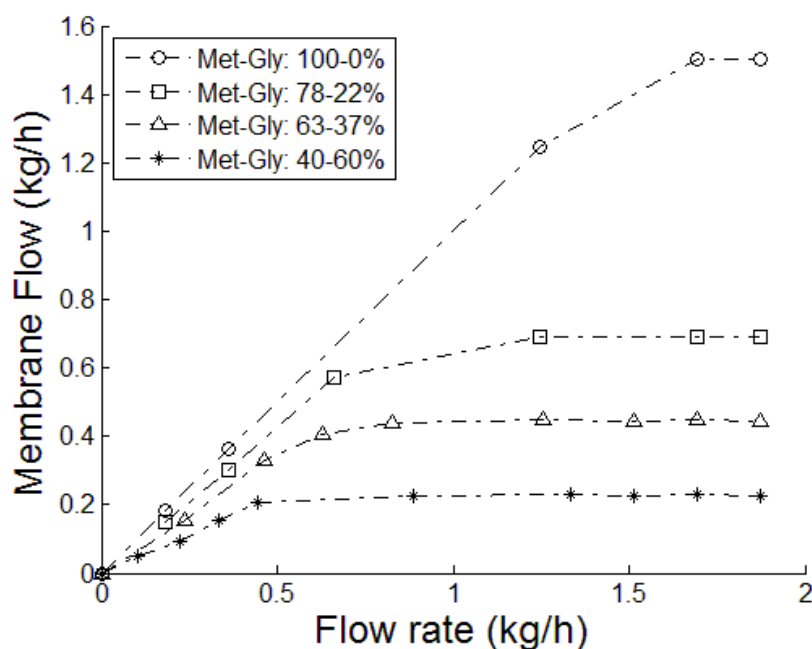
Figure 6-4. Alcoholic phase flow rate effect on the membrane flux. Temperature: 40 °C; Membrane Area: 4.52×10^{-2} m^2; ΔP : 0.6 bar.

In order to calculate the permeability, it was developed a minimization of the deviation between the experimental and the calculated flux for each composition, the results are show in the table 6 -3. The deviation increase with the methanol content in the alcoholic

phase, this deviation is related with the experimental error, as consequence of the boiling of the methanol.

Table 6-3. Permeabilities

Methanol-Glycerol Composition (%)	Permeability $\left(\dfrac{kg}{h \cdot bar \cdot m^2}\right)$	Deviation (%)
100 - 0	88.3	14.35
78 - 22	33.2	10.72
63 - 37	15.2	7.86
40 - 60	7.8	8.02

Figure 6-5a shows ΔP effect on the membrane flux for the experimental data and the correlated permeability (Table 6-3). Membrane flux increases linearly with the ΔP. This effect was higher at low viscosities following Hagen-Poiseuille law. Linearity decreases with the increment of the methanol content, indicating a possible boiling effect in the experiment. However, figure 6-5b shows good linearity between permeability and the inverse of the viscosity indicating Hagen-Poiseuille law applicability (Equation 6-3). Finally, using the permeability experimental results was possible to find a value for R_m (equation 6-11).
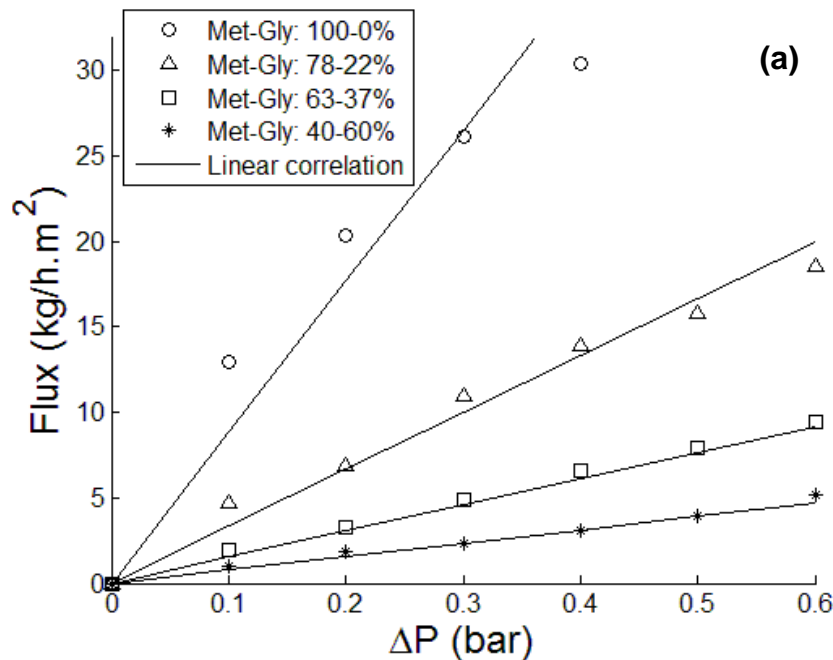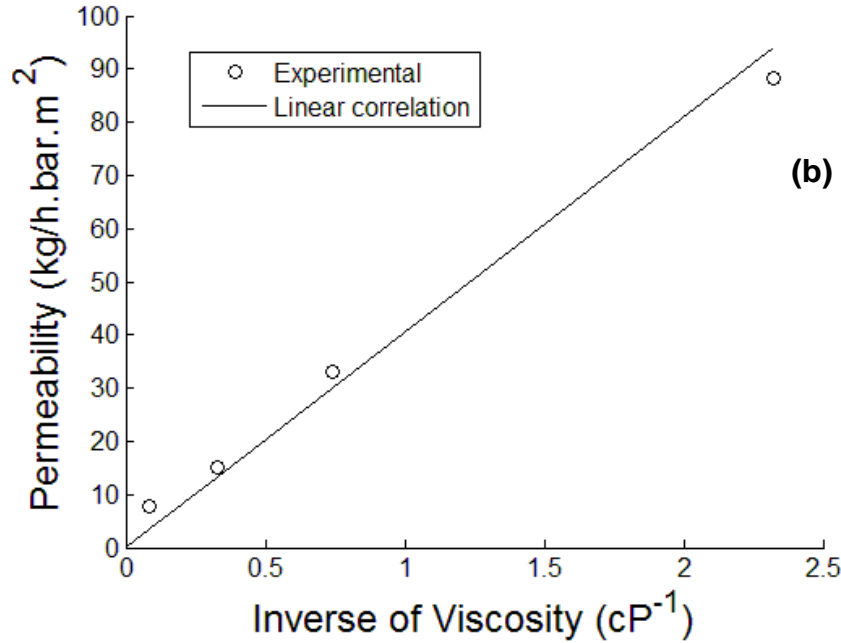
Figure 6-5. a) ΔP effect on the Membrane flux and b) Effect of the alcoholic phase viscosity on the permeability. Temperature: 40 °C; Membrane Area: 4.52×10^{-2} m²; Flow rate: 1.7 kg/h.

$$P_i = \frac{40.5}{\mu_i} \tag{6-9}$$

$$J_i = 40.5 \frac{\Delta P}{\mu_i} \tag{6-10}$$

$$R_m = 0.0247 \tag{6-11}$$

6.3.4 Biodiesel mass fraction effects in phase separation using membranes

Membrane flux was evaluated for different biodiesel-rich phase mass fraction (ϕ) in order to identify fouling effects (Conditions 2 to 13, Table 6-1) according with the equation 6.2. Figure 6-6 shows membrane flux did not change with ϕ. This means that fouling effects were not observed for all the conditions tested.

105
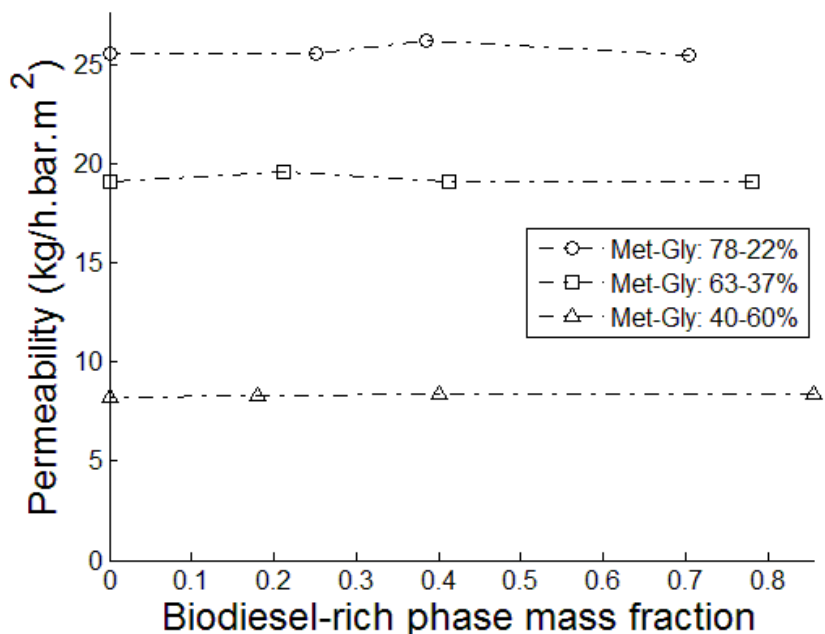
Figure 6-6. Effect of mass fraction on membrane permeability. Temperature: 40 °C; Membrane Area: 4.52×10^{-2} m^2; Flow rate: 1.7kg/h; ΔP : 0.6 bar.

6.3.5 Sensibility analysis on methanolysis reaction mixture separation using membranes

Figures 6-7a, 6-7b, and 6-7c, show a simulation of the temperature and methanol to oil molar ratio effect on biodiesel content of the retentate, glycerol content of the permeate and for the alcoholic phase permeability, respectively. These predictions were made using the proposed mathematical model and algorithm as explained in section 6.2.6.

Results show that an increase in methanol ratio produce a strong reduction in biodiesel and glycerol content because methanol is distributed in both phases. On the other hand, an increase in the temperature does not produce an observable effect in the glycerol content in the permeate or biodiesel content in the retentate. If the methanol ratio or the temperature were extremely high, the system was to be located outside the LLE and the membrane is not going to be able to separate both phases. This effect was previously described by CHENG et al., (2009) in systems composed by Oil/FAME/M.

The increment in the methanol ratio produces an increase in permeability (figure 6-7c) as a consequence of the permeate viscosity reduction. However, it increases the methanol content in permeate and retentate (figure 6-7 a, and b). This increase is higher in the permeate stream (figure 6-7 b). When temperature increases, permeability increases slightly because of the permeate viscosity reduction.
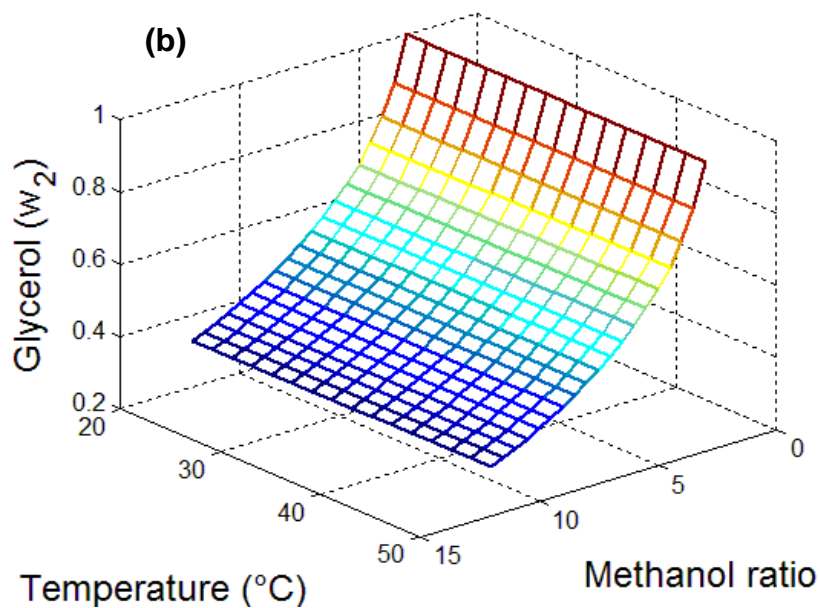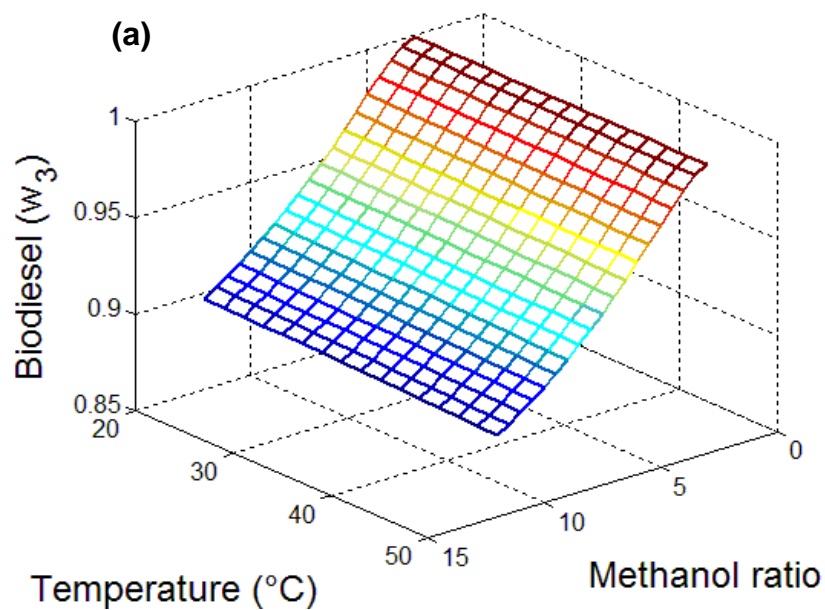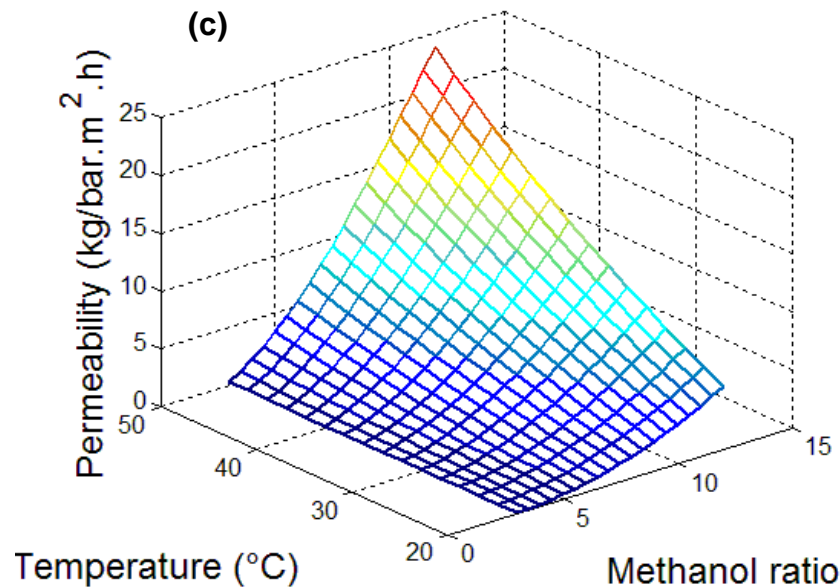
Figure 6-7. Temperature and methanol ratio effects on a) biodiesel composition for the retentate; b) glycerol composition for the permeate; c) permeability.

6.4 Conclusions

PES – HFM was able to remove the alcoholic phase selectively. The permeate composition was a function of the LLE, so the only way to change the permeate composition was dislocating the feed composition to another LLE tie line (changes in the fed composition or temperature). Fouling effects were not observed. The permeate flux follows Hagen-Poiseuille law, where an increment in the driving force (ΔP) promotes an increase in the membrane flux. An increase in the viscosity reduces its permeability. Glycerol content in permeate and biodiesel content in retentate decreased when methanol content in the feed diminishes, following the LLE. The increment in the methanol ratio increases permeability because of the methanol content augment in permeate reducing permeate viscosity. In the same way, an increment in temperature increases permeability because it reduces permeate viscosity. Methanol content in the fed increase membrane flux but the methanol content in permeate and retentate increase too. PES - HFM used in the reactor or the settling, successfully allows a faster removal of the alcoholic-rich phase, reducing the plant volume and increasing the process productivity. The use of membrane technology could be extended to others LLE systems, for the same reasons.

6.5 List of symbols

ΔP Pressure difference through the membrane (bar)

J_M Membrane flux $\left(\dfrac{kg}{h \cdot \mathrm{m}^2}\right)$

μ_M^{mem} Alcohol-rich phase viscosity (cP)

R_m Membrane resistance $\left(\dfrac{h \cdot \mathrm{m}^2 \cdot bar}{kg \cdot cP}\right)$

R_f Fouling resistance $\left(\dfrac{h \cdot \mathrm{m}^2 \cdot bar}{kg \cdot cP}\right)$

P_i Membrane Permeability $\left(\dfrac{kg}{h \cdot bar \cdot \mathrm{m}^2}\right)$

ϕ Biodiesel-rich phase mass fraction

T Temperature (°C)

w Mass fraction

7. Biodiesel production in a liquid-liquid film reactor integrated with membranes

7.1 Introduction

LLFRM was investigated in order to improve the performance of the LLFR incorporating simultaneous reaction and separation in the same device. This technology could overcome limitations in conversion and yield when LLFR is operated in co-current and operation and control, problems when it is operated in counter-current. Besides, membrane system integration eliminates the necessity of a decanter downstream the reactor. The LLFRM conserves the advantages of an LLFR and simultaneously removes glycerol-rich phase from the reaction.

In this chapter, a mathematical model to predict the behavior of an LLFRM was developed and validated through a set of experiments developed in a bench-scale system. A sensitivity analysis was performed to better understand the membrane reactor behavior. The model describes the falling film reactor with mass transfer limitations and the flux through the membrane by transport equations properly used to describe ultrafiltration, where the membrane selectivity depends on the LLE. Validation through experimental data included the effect of lateral methanol percentage (0 to 50%) after membrane separation, methanol to oil molar ratio (6:1 to 12:1), oil fed flow rate (10 to 30 g min^{-1}) and catalyst concentration (0.2 to 1% w/w based on VO weight) on product concentration (FAME %) and membrane flux.

7.2 Materials and methods

7.2.1 Configuration and transport model for biodiesel production in an LLFRM

Figure 7-1a shows the experimental configuration of the bench scale LLFRM system. The oil and the solution of NaOH in methanol are fed on the column top (locations 1 and 2, respectively). Then, the reactive mixture passes through the first packed zone, reacting and producing biodiesel and glycerol. Downstream, the reactive mixture flows into the simultaneous reaction and separation section where the alcoholic phase is removed by the membrane. At the end of this zone, fresh methanol is fed to the reactor (location 5) and the reactive mixture goes into the final reaction zone. The final biodiesel is collected as retentate on the column bottom (location 4). Figure 7-1b illustrate the generation, migration and removal of components in each phase of the proposed transport model inside the reactor, where the membrane completely removes the alcoholic phase. This assumption is based on the behavior modeled and validated in chapter 6.

Reaction occurs mainly in the ester-rich phase and at the interface. Then reaction products migrates to each phase, following the LLE distribution, while, simultaneously the alcoholic phase mainly composed of methanol and glycerol is removed through the membrane.
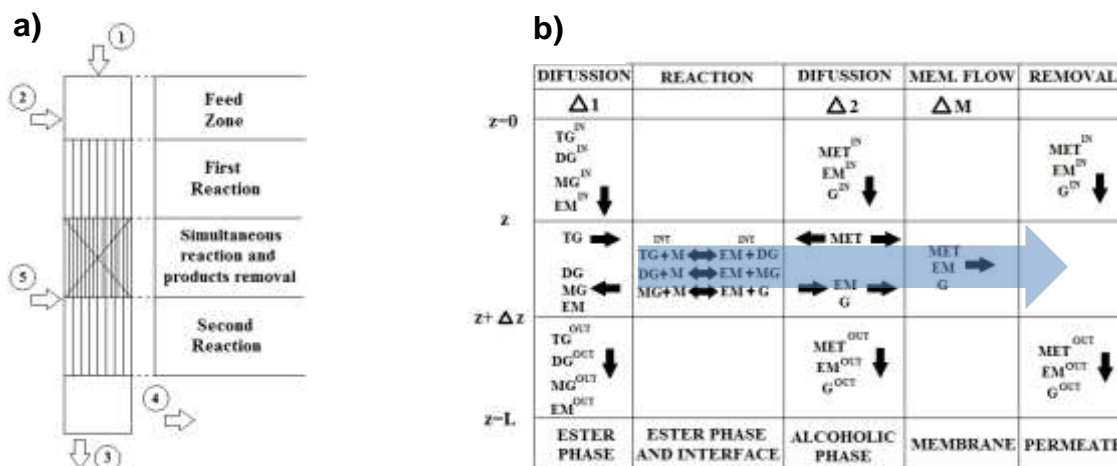
Figure 7-1. a) Diagram of the LLFRM. b) Schematic transport model in the LLFRM.

A schematic diagram of the LLFRM configuration including a differential element of volume is shown in Figure 7-2. The ester-rich phase wet the packing surface and the alcoholic phase flows down between the ester-rich phase and the membrane. The hydrodynamics of this flow is explained because the wettability over the package is higher for the ester-rich phase and the wettability over the membrane is higher for the alcohol-rich phase.
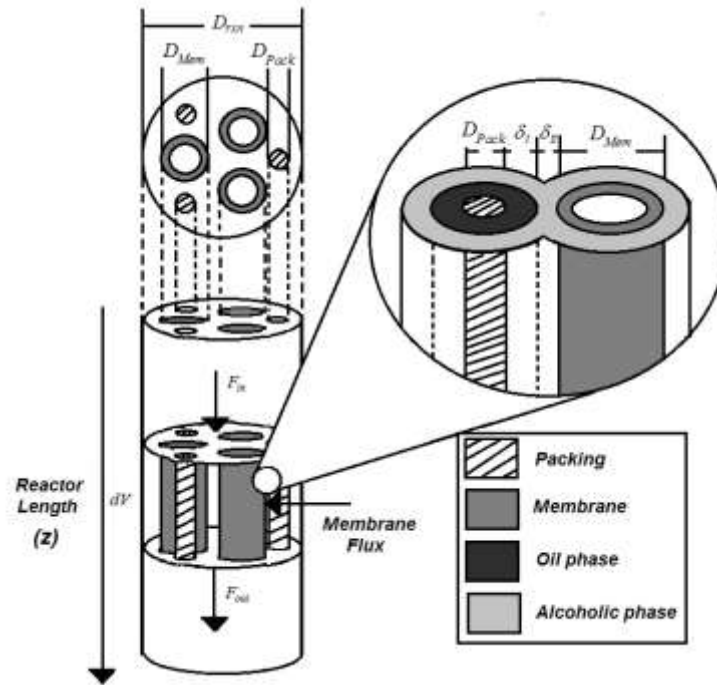
Figure 7-2. Configuration of the Liquid-Liquid Film Reactors Integrated with Membranes. F_{IN}: Input flow rate; F_{OUT}: Output flow rate.

7.2.2 Mathematical model of biodiesel production using LLFRM

Integrating the mathematical model for the LLFR (section 5.2.7) and the mathematical model for the UF membrane (section 6.2.6), equation (7-1) describes the LLFRM behavior.

$$V_Z \frac{dC_i}{dZ} = r_i \cdot \frac{\pi D_{rxn}^2}{4} \left(1 - \Omega_{Mem} - \Omega_{Pack}\right) - J_i^M \cdot \pi n_{Mem} D_{Mem} \qquad i = 1,2,3...,6 \qquad \text{(7-1)}$$

$$\Omega_{Mem} = n_{Mem} \left(\frac{D_{Mem}}{D_{rxn}}\right)^2 \qquad \text{(7-2)}$$

$$\Omega_{Pack} = n_{Pack} \left(\frac{D_{Pack}}{D_{rxn}}\right)^2 \qquad \text{(7-3)}$$

Where, Ω_{Mem} is the cross sectional fraction area occupied by the membranes (equation 7-2) and Ω_{Pack} is the cross sectional fraction area occupied by the packing (equation 7-3), then, the cross sectional area occupied by the packing and the membrane hollow fiber cannot exceed the cross sectional reactor area, as defined by equation 7-4.

$$\Omega_{Mem} + \Omega_{Pack} \leq 1 \qquad \textbf{(7-4)}$$

Figure 7-3 shows the algorithm implemented to solve the differential equations system (equation 7-1) which describes the LLFRM behavior. First, using the initial reactor concentration the LLE was calculated using UNIFAC with the set 4 of GIP and the solution algorithm presented in chapter 4, (NORIEGA et al., 2016). Having mass composition of both phases, it is possible to calculate viscosities, densities and membrane flux. Then, these properties permit to calculate the film thickness, the film velocity and k_{eff}. Concentrations obtained permit to calculate the next length step. The procedure is repeated until it covers the reactor length.

This solution algorithm allows the user to describe the LLFRM profiles of conversion, yield, compositions, viscosities, densities, membrane flux, flux composition, average velocities, mass transfer efficiency, and thickness film for both the ester and alcoholic phases along the whole reactor. Solution algorithm modified excluding the terms that describe membranes behavior into the model was used to solve the model of the LLFR, as shown in Chapter 5, section 5.2.7. In that case, differential equations related to the membrane behavior takes a value of zero (equations 5-13 to 5-18) and the new differential equation system solution is easier than the differential equation system including membranes (equation 7-4). Rate constants used were presented in Table 3.1.

Initial Variables

$C_n, Q_{emp}^{I}, Q_{emp}^{II}, T, L$

Estimation of the Liquid - Liquid Equilibrium

w_i^{I}, w_i^{II}, ϕ

Estimation of layers thickness velocity and propierties

$\mu_n^{I}, \mu_n^{II}, \rho_n^{I}, \rho_n^{II}, a_n, b_n, \delta_n^{I}, \delta_n^{II}, V_{Z-n}^{I}, V_{Z-n}^{II}, V_{Z-n}$

Estimation of mass transfer efficiency

$D_{12,n}, S_{C,n}, \mathrm{Re}_n, k_{C,n}, k_{eff,n}$

Estimation of membrane flux

J_i^{M}

Estimation of the concentration in the next iteration step

C_{n+1}

$z_{n+1} = z_n + \Delta z$

No

$n = n+1$

$z_{n+1} \geq L$

Yes

Final of the integration

Figure 7-3. Global algorithm for the mathematical model.

7.2.3 Materials

Refined, bleached and deodorized edible grade soybean oil obtained from SIGRA S.A. (Bogotá, D.C. Colombia) was used, with the properties presented in Table 3-1. Analytical grade methanol and sodium hydroxide were obtained from Merck (Darmstadt, Germany). Reference standards, including methyl palmitate, methyl oleate, DL-α palmitin, dipalmitin, tripalmitin, glyceryltrioleate and the silylating agent N,O-bis(trimethylsilyl) trifluoroacetamide (BSTFA) of >99% purity, were purchased from Sigma-Aldrich Chemical Company (St Louis, MO). Tricaprine was obtained from Fluka (Buchs, Switzerland) and used as the internal standard. Pyridine, isopropanol, and toluene of ACS grade were obtained from Mallinckrodt Baker Inc. (Phillipsburg, NJ, USA). Ultrafiltration PES-HFM (50

kDa and an external diameter of 0.9 mm) was provided by PAM Membranas Seletivas Ltda (Río de Janeiro, Brasil).

7.2.4 Equipment

A bench scale LLFRM system was used. A basic scheme of the system is presented in Figure 7.4. The equipment consists of a stainless steel column (Inner diameter 1 inch) packed with a semi-structured stainless steel packing (threads). The packing volume fraction of the reactor was kept constant at 60% (packing surface area to reaction volume ratio 5333 m^{-1}). The packing was custom made by placing the quantity of stainless steel and PES-HFM threads axially aligned. Only a section of the total length of the equipment was packed with PES-HFM. Thus, the reactor is divided into three zones: the first reaction zone (RR1) without membranes with 0.7 m of length where only reaction occurs; the second zone was a combined reaction separation zone (RSR) with 0.1 m of length and membrane area of 0.2513 m^2; finally, the third zone was a second reaction zone (RR2) with 0.2 m. Each packing thread had a diameter of 0.3 mm and it was fixed to a distribution plate located at the top and to a central core at the bottom of the reactor. A thermal oil bath equipped with a temperature controller SHIMADEN SR 91 (Shimaden Co. Ltd., Tokyo, Japan), was used to maintain the temperature within ±0.1 ºC. The soybean oil and the solution of NaOH in methanol were stored in three tanks (1, 2 and 3 respectively) installed on three balances Mettler Toledo 4000 (Mettler Toledo GmbH, Schwerzenbach, Switzerland). These balances were used to determine the mass flow rates of VO and methanol. Three metering pumps HMS EXT 2001 (EMEC Srl, Vazia, Italy) were used to feed the soybean oil and the solution of NaOH in methanol at controlled flow rates (4a, 4b, and 4c). Before entering the reactor, the soybean oil, and the solution were independently heated up to the reaction temperature using a heating system equipped with silicon-shielded electric resistances and SHIMADEN SR 91 (Japan) temperature controller (±0.1 ºC) (5a and 5b). The VO was fed into the reactor on the reactor top (6a). The solution of NaOH in methanol was fed to the reactor through two different inputs (6b and 6c). The ratio between the molar flow of the input 5c and the total molar flow fed in the reactor was called lateral methanol percentage. The other two balances were used to determine the mass flow rate of permeate and retentate (7 and 9, respectively). Membrane operating pression diference (ΔP) was fixed at 0.6 bar using a diaphragm vacuum pump (10) (Vacuubrand ME 2 NT) located downstream the permeate collection tank (9).
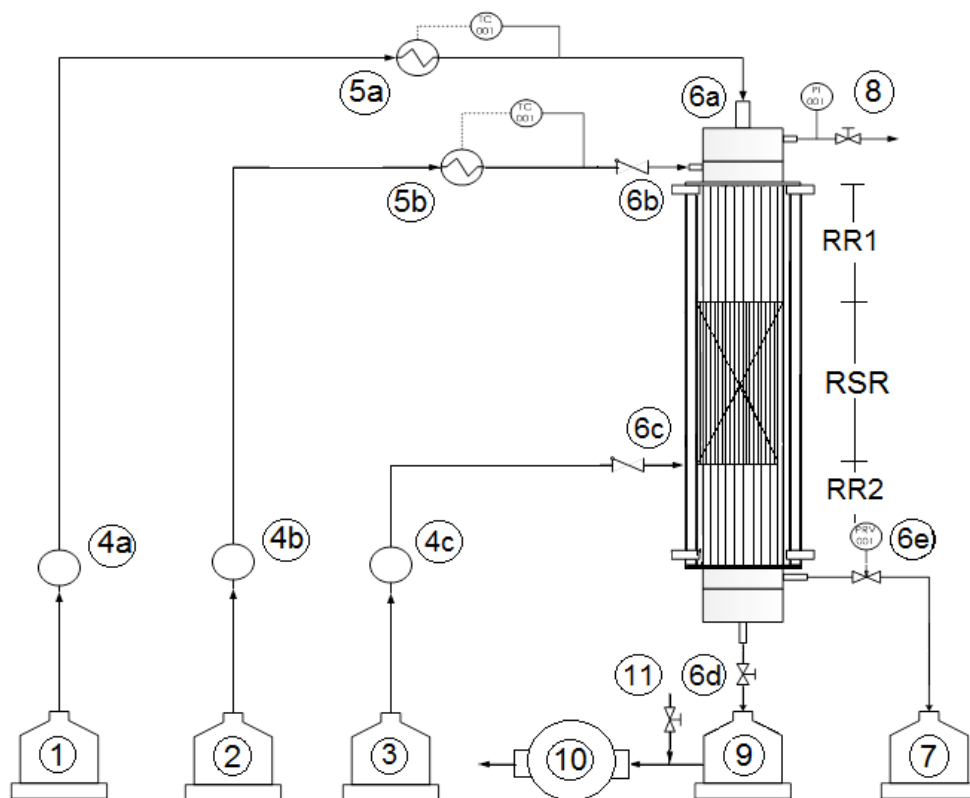
Figure 7-4. Diagram of the experimental configuration of the LLFRM. 1) Oil tank; 2) NaOH in methanol solution tank; 3) NaOH in methanol solution tank; 4a) Oil metering pump; 4b) NaOH in methanol metering pump; 4c) NaOH in methanol metering pump; 5a) Oil heat exchanger; 5b) NaOH in methanol metering pump; 6a) LLFRM oil feeding nozzle ; 6b) LLFRM NaOH in methanol solution feeding nozzle; 6c) Lateral fed of LLFRM NaOH in methanol solution feeding nozzle; 6d) LLFRM Permeate outlet nozzle and valve; 6e) LLFRM retentate outlet nozzle and valve; 7) LLFRM retentate tank. 8) Purge valve; 9) LLFRM permeate tank; 10) Vacuum pump; 11) Air valve. Solid lines represent reaction zone (RR); High-density line represents reaction separation zone (RSR).

7.2.5 Experimental conditions

Evaluation of LLFRM was made keeping the reactor length, membrane area, temperature and pressure difference (ΔP) constants at 1m, 0.2513 m^2, 55 ºC and 0.6 bar, respectively, and varying flow rate from 10 to 30 g min^{-1}, methanol to oil molar ratio in the feed between 6:1 to 12:1, lateral methanol percentage between 0 to 50% and the catalyst concentration

between 0.2 to 1%wt. NaOH based on the mass of soybean oil. Experimental conditions are presented in Table 7-1.

Table 7-1. Experimental conditions in the biodiesel production with LLFRM.

Experiment	Oil flow rate (g/min)	Methanol to oil molar ratio	Lateral methanol (%)	Catalyst (% wt. based on oil)	Rep
1	20	6	0	1	4
2	20	12	50	1	1
3	20	6	25	1	1
4	20	9	33	1	1
5	10	9	50	1	4
6	20	9	50	1	2
7	30	9	50	1	2
8	10	6	25	0.2	1
9	20	6	25	0.2	1
10	30	6	25	0.2	1
11	10	6	25	0.4	1
12	20	6	25	0.4	1
13	30	6	25	0.4	1
14	10	6	25	0.6	1
15	20	6	25	0.6	1
16	30	6	25	0.6	1

7.2.6 Procedure

The hollow fibers membranes previously preserved in methanol were installed in the system. Each experiment was run during 240 min. The first 120 min correspond to the reactor evaluation without membrane (LLFR) and the following 120 min for the reactor evaluation with the membrane (LLFRM). Before each test, the system was preheated to 55 °C. Initially, the oil was fed to the reactor using the metering pump 4a. When the oil flow rate reached the desired value, the solution of sodium hydroxide in methanol, which was prepared no more than 1 hour prior to the start of the reaction, was fed to the reactor using metering pump 4b and 4c for the case of the lateral fed. The heating systems for each feed stream were set at 55°C (5a and 5b, respectively). The initial time (t = 0) was set as soon as the metering pump 4b began feeding the methoxide solution. The stream flow rates were determined (as described in section 7.2.4) and recorded. Samples were collected at 20 min intervals, during 120 min, therefore adding up 6 samples for each run to determine their concentration following the procedure described in section 3.2.7. Then, the vacuum was turned on, keeping constants the other operation conditions and the

evaluation of the membrane effect on the reactor start. Samples were collected each 20 min for a total of 120 min to determine their concentration following the procedure described in section 3.2.7. So, for each experiment were collected 12 samples, 6 without membrane and 6 with the membrane. Steady state conditions were verified by measuring the product biodiesel output mass flow, usually observed after no more than 40 min operation.

7.3 Results and discussion

7.3.1 Model validation

Model predictions were compared to the experimental results for the LLFR and the LLFRM. The comparison is presented in Figure 7-5. There was a satisfactory fit between experimental data and predicted values, regardless the experimental conditions tested. The maximum deviation between the model prediction and the experimental data was 9.5% for FAME content in the product, indicating an accurate fit between them. The proposed mathematical model predicted the LLFR and the LLFRM behavior. The model fit was better for high FAME%.
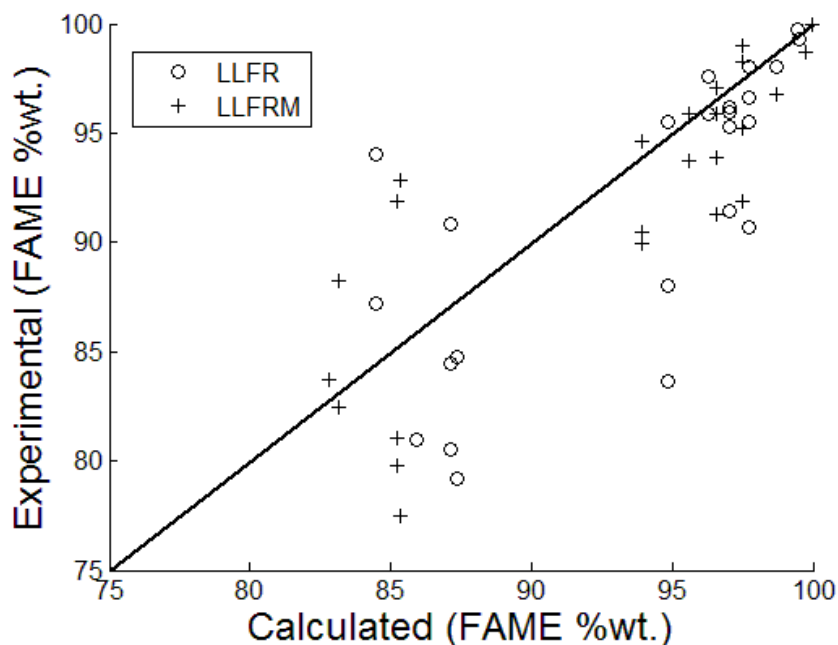
Figure 7-5. Comparison between the experimental and calculated results.

7.3.2 Reactor length and flow rate effects on the LLFRM performance

Figure 7-6 shows simulation results to describe the overall concentration for M, FAME, G and TG at the end of the first reaction zone (0.7 m). FAME and G were produced meanwhile TG and M were consumed, then, in the simultaneous reaction and separation zone (between 0.7 m and 0.8 m) the membrane removed the alcoholic phase. Methanol remained in the ester-rich phase obeying the LLE distribution. Finally, for the second reaction zone (between 0.8 m and 1 m), fresh methanol was fed to the reactor and the reaction continue without the presence of glycerol. At these conditions was possible to achieve complete conversion of TG to FAME. The concentration of glycerol in the biodiesel-rich outlet stream is low because most of the glycerol was removed through the membrane in the second zone. Therefore, for an industrial application, the decanter after LLFRM is not necessary.

Most of the reaction proceeded in the first reaction zone. The behavior of this zone was simulated by the LLFR model presented in chapter 5. The length of this section depends on the reaction conditions (flow rate, methanol: oil molar ratio, catalyst concentration, temperature and packing area). The behavior of the section of simultaneous reaction and membrane separation (II) can be simulated by the LLFRM model presented in this chapter and depends on operating conditions of the membrane system (ΔP, methanol: oil molar ratio and membrane area installed). Finally, the length of the second reaction zone (III) can be simulated by the LLFR model and depends on the reaction conditions. Figure 7-6 shows that the membrane area was enough for the alcoholic phase removal which required only 20% of the installed membrane area (as observed from z=0.70 to z=0.72 m).
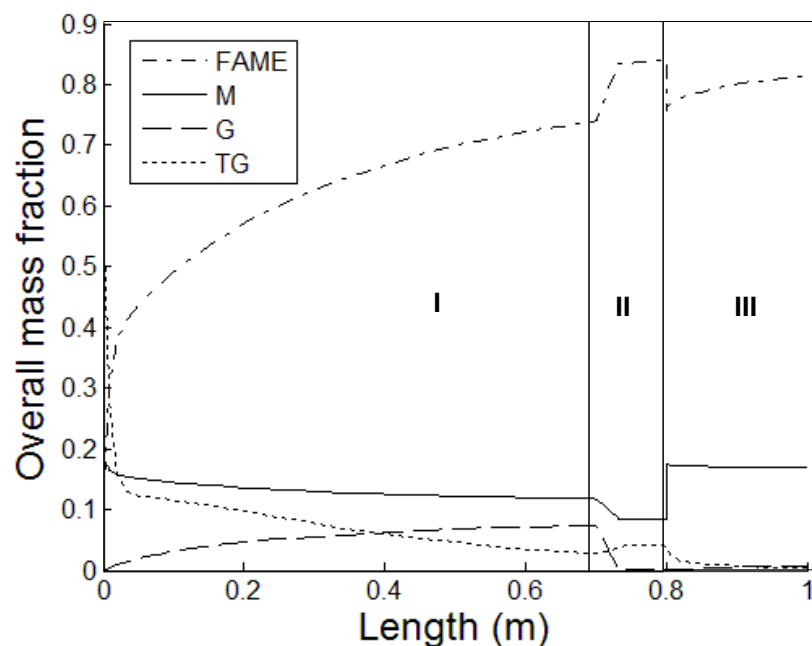
Figure 7-6. Performance of the LLFRM over the reactor length as predicted by the model. Temperature 55 °C, Catalyst concentration 1 %wt., VO flow rate 20g min⁻1, 9:1 methanol to oil molar ratio and 33% Lateral methanol.

Simulations for conversion and yield as a function of the LLFRM length are presented in Figure 7-7. Conversion and yield increase with the reactor length because residence time increases too. This behavior was previously described by NARVÁEZ et al., (2009) and it was presented in section 5.3.2. The maximum conversion and yield experimentally determined were 99.7% and 99.3% respectively, using a 1 m reactor length. The highest reaction rate in the reactor was observed in the first 0.06 m. After that, the reaction rate decreases but conversion and yield continue increasing. In the simultaneous reaction separation zone (from 0.7 m to 0.8 m) conversion and yield remains constant due to the methanol removal. Finally, in the third zone when make-up methanol is fed (from 0.8 m to 1 m) proceeded, achieving almost total TG conversion and FAME yield.
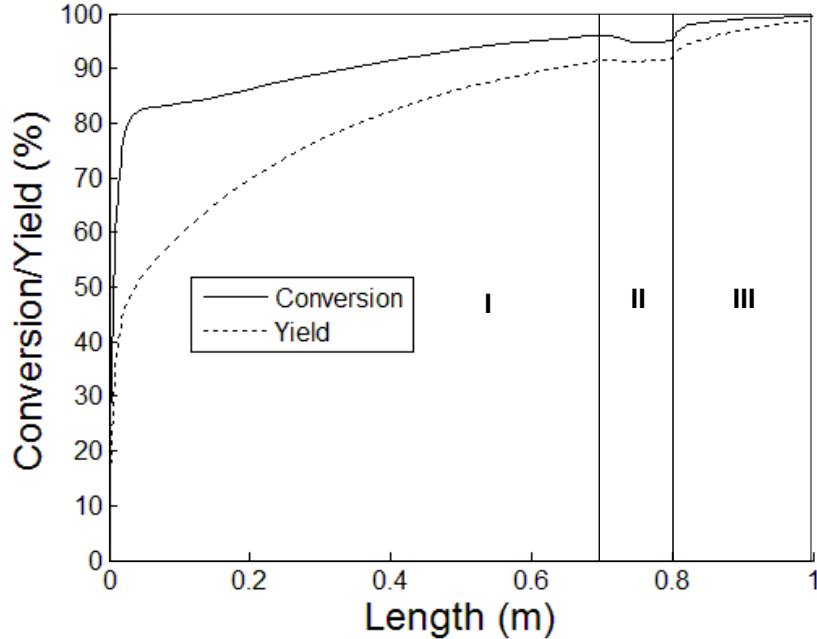
Figure 7-7. Model prediction of conversion and FAME yield in a LLFRM. Temperature 55 °C, Catalyst concentration 1 %wt., VO flow rate 20g min^{-1}, 9:1 methanol to oil molar ratio and 33% Lateral methanol.

Figure 7-8 shows a simulation of the LLFRM evaluating the effect of the length and the oil flow rate. It shows an increment in the final biodiesel content when the reactor length increases and the oil flow rate diminishes. Both effects were a consequence of the increase of residence time.

Table 7-2 shows the comparison between the performance for LLFRM, LLFR, and BSTR. LLFRM productivity was higher than the LLFR because the membrane presence avoids the necessity of a decanter downstream the LLFR, this reduces the final equipment volume. LLFRM productivity was 12 times the productivity reported for the BSTR.
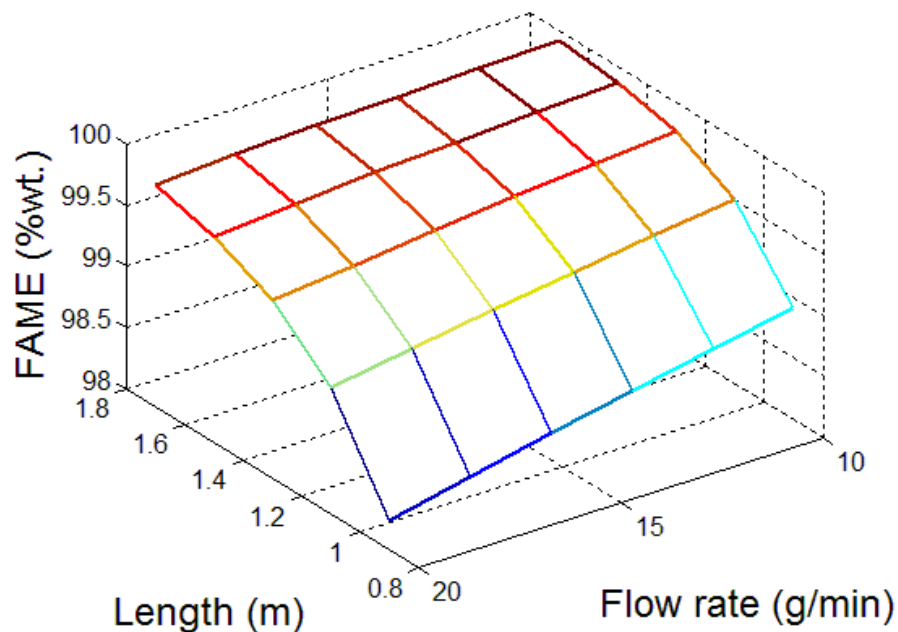
Figure 7-8. Model prediction of reactor length and flow rate effects on the final FAME concentration. Temperature 55 °C, Catalyst concentration 1 %wt., methanol to oil molar ratio 9:1 and lateral methanol of 33%.

Table 7-2. Productivity of biodiesel from soybean oil obtained for LLFR, LLFRM, and BSTR at 55 °C, using NaOH as catalyst (1 %wt.).

Variable	BSTR (CADAVID et al., 2013)	LLFR with decanter (Chapter 5)	LLFRM (this work)
Conversion (%)	99.9	99.9	99.7
Yield (%)	97.1	97.2	99.3
Productivity $\left(\dfrac{m^3\,FAME}{h \cdot m^3\,reactor}\right)$	0.3	2.5	3.5

7.3.3 Methanol ratio and lateral methanol percentage effects on the LLFRM performance

The product removal through the membrane was a function of the LLE inside the reactor. The alcohol-rich phase was the only phase able to permeate the membrane, as it was demonstrated in chapter 6. High lateral methanol percentage reduces the reaction rate (reduction in methanol fed through the input 6b) but produces permeate with high glycerol

and low methanol content (Figure 7-9). FAME concentration increases when the methanol to oil molar ratio increases and when less methanol (percentage of the total) is fed into the third zone of the LLFRM. Methanol to oil molar ratio 9:1 and feeding 33% of the methanol to the third zone of the LLFRM was enough to achieve the final product requirements for the biodiesel production.
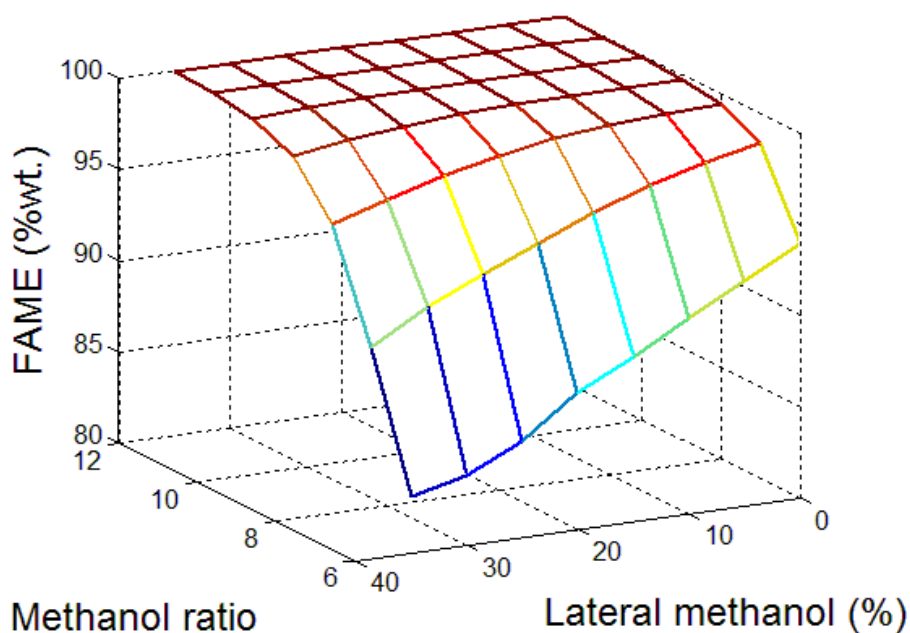
Figure 7-9. Model prediction of methanol ratio and lateral methanol effects on the final FAME concentration. Temperature 55 °C, Catalyst concentration 1 %wt., Reactor length 1m and VO flow rate 20 g min^{-1}.

Figure 7-10 shows the effect of methanol to oil molar ratio on conversion and yield for the LLFRM, according to experimental results. Conversion and yield increase when methanol to oil molar ratio augments. The maximal conversion and yield (99.7% and 99.3% respectively) were achieved when the methanol to oil molar ratio was 12:1. Coupling the membrane system did not change the final conversion and yield but allowed the complete alcoholic phase removal, avoiding the requirement of a final decanter. Consequently, process productivity increased.

Figure 7-11 shows the correlation between methanol concentration in the final biodiesel product with the final conversion and yield. When methanol content in biodiesel was higher

than 10% final conversion and yield were 99.7% and 99.3%, respectively. That condition was achieved at the highest methanol to oil molar ratio (12:1).
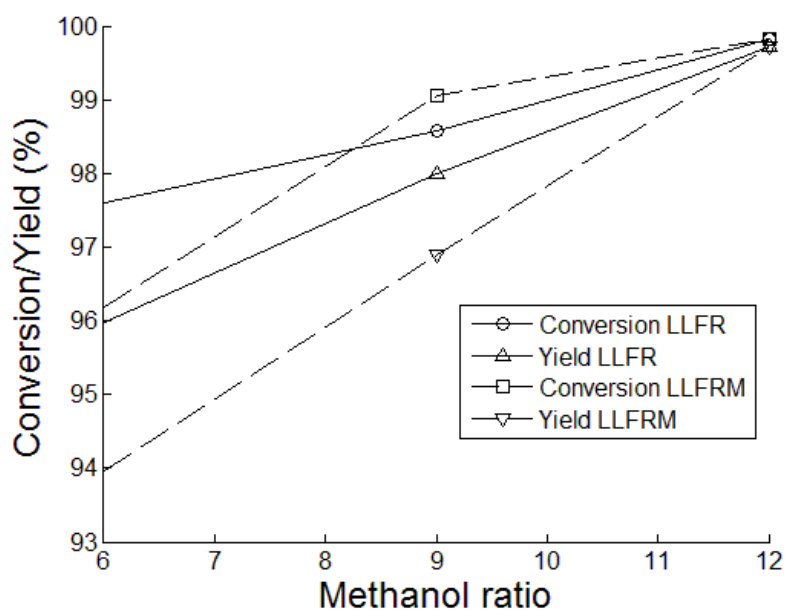
Figure 7-10. Experimental results of the LLRFM operation: Methanol ratio effect on the conversion and yield. Temperature 55 °C, Catalyst concentration 1 %wt., package fraction 60%, VO flow rate 20 g min⁻¹ and 100cm reactor length.
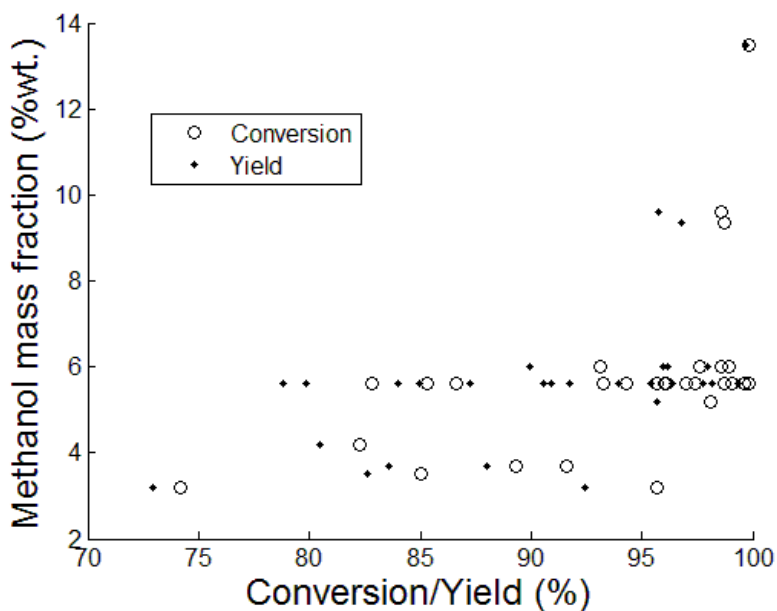
Figure 7-11. Purity of biodiesel obtained in the LLRFM operation: correlation of the final methanol content in the ester-rich phase effect with conversion and yield.

Figure 7-12a shows that glycerol content in the permeate diminishes if methanol to oil molar ratio increases (input 6b). In the same sense, it increases when the lateral methanol percentage in the third reactor section increases (input 6c), because, high methanol content in the reactor promotes high methanol content in the permeate following the LLE behavior. Therefore, a high glycerol concentration in the film adjacent to the hollow fiber will be more viscous, reducing the membrane permeability (Figure 7-12b).

As mentioned in the section 1.1, soaps and gels may be produced in the reactor. Emulsified biodiesel molecules may permeate the membrane, and gels may cause a drastic fouling of the membrane. These effects were avoided reducing the catalyst concentration to 0.6 %wt. NaOH based on the mass of soybean oil.
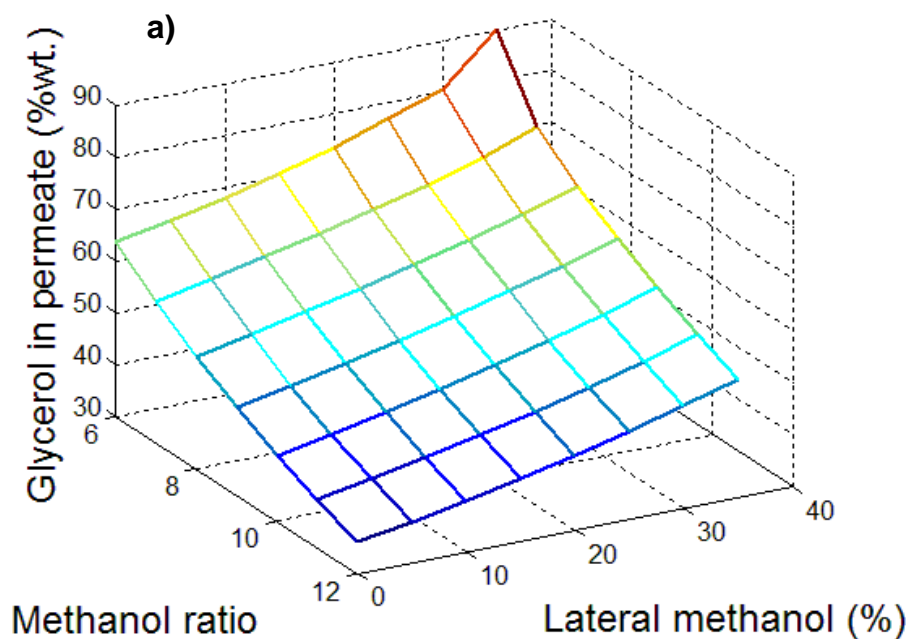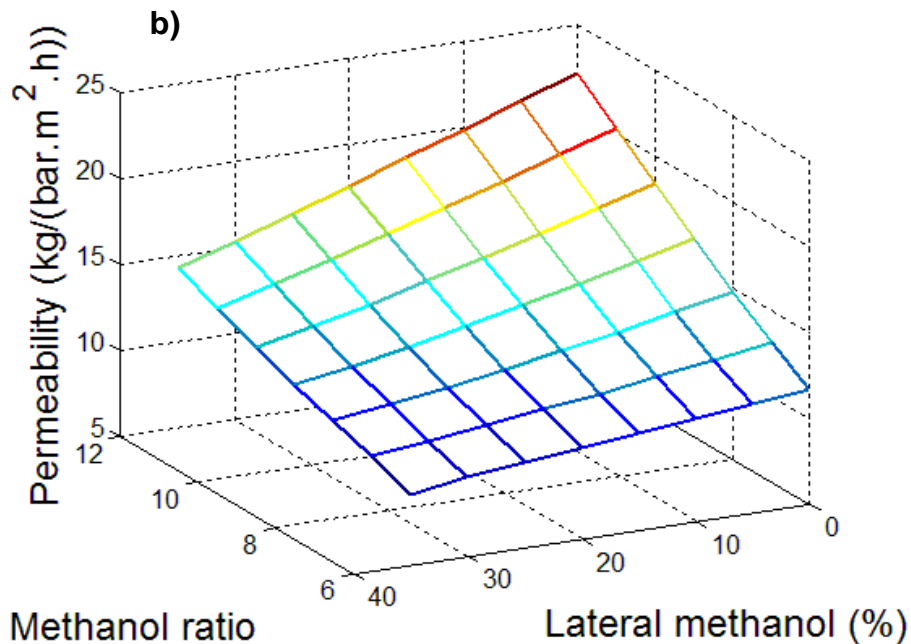
Figure 7-12. Model prediction of methanol ratio and lateral methanol effects on the a) Glycerol mass fraction in permeate. b) Membrane permeability of the alcoholic phase. Temperature 55 °C, Catalyst concentration 1 %wt., Reactor length 1m and VO flow rate 20 g min^{-1}.

7.3.4 Process evaluation: comparing LLFR with LLFRM performance

Figure 7-13 shows how coupling a membrane separation system to a LLFR influence on the reaction product for experimental conditions in Table 1. Data on the drawn line represent no changes. Figure 7-13a shows predicted results from the model and Figure 13b shows experimental results. The proposed mathematical model predicts the same biodiesel concentrations for the LLFR and for the LLFRM (Figure 7-13a), indicating just a small reduction in the reaction rate in the latter, as a consequence of the methanol removal through the membrane. The experimental results did not show membrane effects on the reactor (Figure 7-13b). The deviation for the experimental results between the LLFR and LLFRM were dues to experimental error. Reduction in the reaction rate for the membrane presence was not observed for high methanol content on the fed. The validation of the reactor model with and without membrane was successful. It is necessary

used the proposed mathematical model to optimize the reactor configuration and the operation variables.
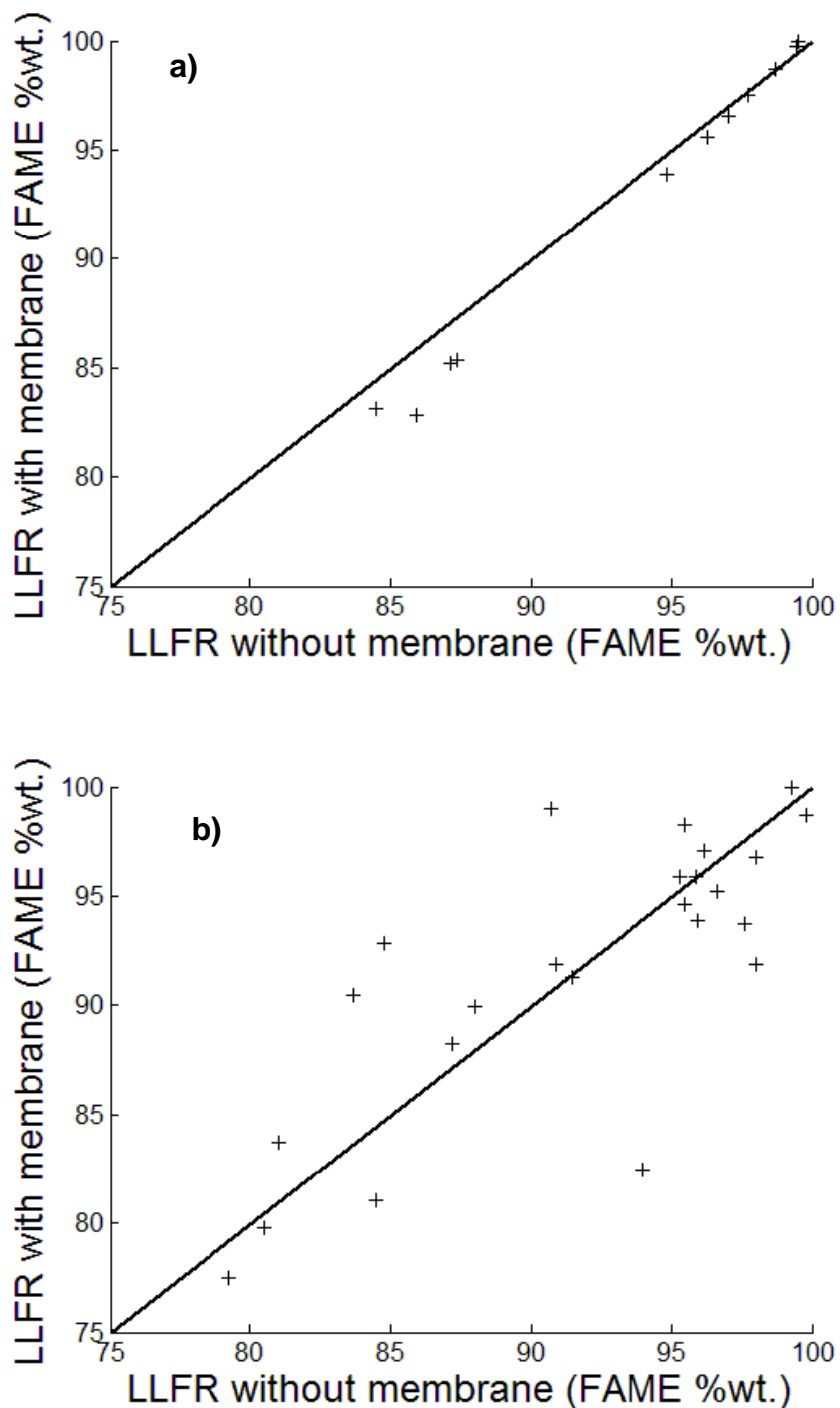
Figure 7-13. Membrane influence for the FAME production using the LLFRM. a) Simulation results. b) Experimental results.

7.4 Conclusions

The mathematical model proposed in this work described adequately soybean oil methanolysis in the LLFRM. The increase in methanol ratio improved the LLFR and LLFRM conversion, yield and productivity because it increases the methanol content in the ester-rich phase increasing the reaction rate. The increment in the percentage of methanol fed in the third zone of the LLFRM reduces the biodiesel content because reduces the methanol content in the feed. The increment in the reactor length or reduction in the flow rate, increases the final biodiesel content. The coupling of a membrane separator in the LLFR did not change the biodiesel content in the final product. However, the removal of the alcoholic phase inside the reactor eliminates the requirement of a final decanter and, consequently, the LLFRM productivity increases until 12 times the productivity reported for the BSTR. The proposed mathematical model predicts adequately the behavior of the LLFR and the LLFRM. Methanol to oil molar ratio (9:1) and 33% of the total methanol fed to the third reaction zone are enough to achieve a complete oil conversion to biodiesel. Soaps and gels produced in the reactor permeate through the membrane dragging biodiesel to permeate and fouling the membrane. Low catalyst concentration was necessary for operating the LLFRM in order to avoid fouling problems and biodiesel dragging to the permeate.

7.5 List of symbols

r_i Reaction rate

k_i Kinetic constant $\left(\dfrac{L}{gmol \cdot \min} \right)$

L Reactor length (m)

n_{Pack} Number of threads

D_{Pack} Thread diameter (m)

D_{Mem} Membrane diameter (m)

D_{rxn} Reactor diameter (m)

k_{eff} Effective transport coefficient

Ω_{Mem} Fraction area occupied by the membranes

Ω_{emp} Fraction area occupied by the packing

V_Z Average flow velocity over the packing (m/min)

V_0 Average flow velocity in the reactor (m/min)

J_M Membrane flux $\left(\dfrac{kg}{h \cdot m^2} \right)$

8. Conclusions and recommendations

Biodiesel production presents mass transfer limitations and equilibrium limitations. In order to increase the process productivity and profitability was necessary overcome these limitations. The main objective of this study was to evaluate theoretically and experimentally the performance of a liquid – liquid film reactor assisted by membranes in biodiesel production. The hypothesis of this work stated the possibility of increase the liquid – liquid film reactor productivity integrating membranes within the reactor. If membranes permit selective removal of reaction products, it will shift the equilibrium towards the biodiesel formation, promoting an increment in conversion, yield, and productivity, fulfilling the required quality standards in a single reaction step.

Liquid – liquid film reactor productivity was increased integrating UF hollow fiber membranes within the reactor. Membranes permit the selective removal of the alcoholic phase, eliminating the necessity of a decanter downstream the reactor. The required quality standards were achieved in a single reaction step. This integrated reactor showed a productivity up to 12 times the average productivity reported by a traditional BSTR. These results were validated experimentally and simulated using a mathematical model developed and validated in this work. Effects of the alcoholic phase removal on chemical equilibrium were not observed. Therefore, for this work, membranes presence in the reactor increases biodiesel productivity as a consequence of the elimination of further reaction steps including a decanter between them, as well as the decanter downstream the reactor and not because of the equilibrium shifts towards to the biodiesel formation.

The findings addressed in this thesis can be divided into five interrelated subjects: Kinetics of oil methanolysis, LLE description using UNIFAC, LLFR modeling, simulation and validation, biodiesel – glycerol – alcohol separation with membranes and LLFRM modeling, simulation, and validation.

Initially, in the third chapter was presented the kinetics methanolysis for Jatropha soybean and palm oil. An expression to describe the catalyst and temperature influence in the reaction rate was validated experimentally. The increase in the temperature on vegetable oil methanolysis improves the reaction rate and the final FAME yield. This effect is stronger during its first ten minutes of reaction. The reaction rate is very slow at a catalyst concentration of 0.2 %wt. Nevertheless, an increase in the catalyst concentration from 0.2 %wt. to 0.6 %wt. enhanced the reaction rate. Based on activation energies, an increase in reaction temperature favors the production of DG from TG and MG.

Fourth chapter showed a correlated set of group interaction parameters for the UNIFAC model that describes the LLE for systems biodiesel-glycerol-methanol and ethanol regardless biodiesel origin and temperature. In order to describe the LLE for these systems with the proposed method, only is required the fatty acid profile. The comparison between this work and the UNIFAC description using the GIP proposed in the literature indicated that the best average and specific deviation were obtained using the GIP proposed in this work. The GIP related with the UNIFAC main group 1 ("CH$_3$", "CH$_2$" and "CH") exhibits a stronger influence on the descriptions than the GIP not related with this group. For all of the cases, alcohols are distributed among the ester-rich phase and glycerol-rich phase, exhibiting higher affinity for the glycerol-rich phase. The best UNIFAC descriptions were obtained in the low methanol concentration zone, and the model descriptions were better for the glycerol-rich phase than for the ester-rich phase.

The fifth chapter presented the mathematical model of the liquid - liquid film reactor. This model described mass transfer limitations, hydrodynamics inside the LLFR, as well as packing quantity and flow rate effects on LLFR performance. The increase in packing quantity and flow rate improved LLFR conversion, yield, and productivity because it reduced mass transfer resistance in the reactor. Improvements of both conditions increased LLFR productivity up to 8 times the average productivity reported by a traditional BSTR. When the empty fraction in the reactor was close to zero, the LLFR operates like a packing PFR and its hydrodynamic and mathematical model changed. The highest conversion of soybean oil methanolysis in the LLFR and its FAME yield were 99.9% and 97.5%, respectively.

Sixth chapter described biodiesel – glycerol – methanol mixtures separation using hollow fiber membranes. Permeate concentration was a function of the LLE. The only way to change permeate concentration was dislocating the feed composition to another LLE tie line (changes in the fed concentration or temperature). Permeate follows Hagen-Poiseuille law, where an increase in the viscosity reduce permeability. Fouling effects were not observed. Glycerol content in permeate and biodiesel content in retentate decreased when methanol content in the feed increases, following the LLE. An increment in the methanol ratio increases permeability. It can be explained by methanol concentration increment in permeate that reduces its viscosity. In the same way, an increment in temperature has the same effect on permeate viscosity. Methanol content increase membrane flux but the methanol content in permeate and retentate increase too. PES - HFM could be employed in the reactor or the settling to remove the alcoholic rich phase faster, reducing the plant volume and increasing the process productivity.

Finally, the seventh chapter showed the integration between LLFR and UF membranes. All the concepts presented in the previous chapters were condensed and used in this chapter. The removal of the alcoholic phase inside the reactor eliminates the requirement of multiple reaction steps with decantation between them. Consequently, the LLFR productivity increases up to 12 times the average productivity reported by a traditional BSTR. It was possible to obtain biodiesel fulfilling the quality requirements with a single reaction stage. The increase in methanol ratio improved the LLFR and LLFRM conversion, yield and productivity because it increases the methanol content in the ester-rich phase increasing the reaction rate. Increments in the reactor length or reduction in the flow rate increase the final biodiesel content. The membrane presence in the LLFR did not change the biodiesel content in the final product. However, the removal of the alcoholic phase inside the reactor eliminates the requirement of a final decanter and, consequently, the LLFR productivity increases. Methanol to oil molar ratio (9:1) and 33% of the total methanol fed to the third reaction zone are enough to achieve a complete oil conversion to biodiesel. Low catalyst concentration was necessary for the LLFRM in order to avoid fouling problems and biodiesel dragging to the alcoholic phase.

This work revealed important relations between reaction mechanism, concentration, interfacial area, flow rate, catalyst concentration and temperature in an LLFR with and

without membranes. These relations and its mathematical expressions are excellent tools to analyze biodiesel production in LLFR, including strategies to improve the productivity reported in this work.

LLFRM increases biodiesel productivity promoting a reduction in biodiesel process fixed and variable cost. In order to transfer this technology to industry, several steps are necessary. In future works, it is recommended to assess the effect of scale-up the process and to use the information collected to evaluate the profitability of the process using LLFRM.

The LLFR and the LLFRM reduce mass transfer limitations and its product separation is fast. These process characteristics are useful for reaction with two or more liquid phases as other esterification reactions and separation operations with two or more liquid phases as liquid-liquid extraction. The proposed reactor and its mathematical model could be evaluated for these and other applications. Finally, it is necessary to develop more studies for the phase separation using membranes. This technology has a lot of applications in the process integration and plant size reduction.

9. Appendix A: Mathematical model

9.1 Force balance over the packing

Figure 5.1 shows the schematic representation used for developing the force balance for both films over the packing. Equation 1 shows the force balance over the packing.

$$2\pi rL\tau_{rz}\big|_r - 2\pi rL\tau_{rz}\big|_{r+\Delta r} + \left(2\pi r\Delta r\upsilon\right)\rho\upsilon\big|_{r=0} - \left(2\pi r\Delta r\upsilon\right)\rho\upsilon\big|_{r=L} + 2\pi rL\Delta r\rho g = 0 \quad (1)$$

The force profile is mainly radial, but it exists two different films, so, the force balance must be done for both films.

$$\frac{d}{dr}\left(r\tau_{rz}^{I}\right) = \rho_I gr \quad (2) \qquad \frac{d}{dr}\left(r\tau_{rz}^{II}\right) = \rho_{II} gr \quad (3)$$

After integration of equation 2 and 3, it is possible to get the equations 4 and 5.

$$r\tau_{rz}^{I} = \frac{\rho_I gr^2}{2} + C_1^I \quad (4) \qquad r\tau_{rz}^{II} = \frac{\rho_{II} gr^2}{2} + C_1^{II} \quad (5)$$

The first frontier condition was $r = aR_{emp}$ $\tau_{rz}^{I} = \tau_{rz}^{II}$, and $r = bR_{emp}$ $\tau_{rz}^{II} = 0$ (Figure 5.1), so, it is possible to obtain the integration constants 10 and 11.

$$C_1^I = C_1^{II} + \frac{ga^2 R_{Pack}^2}{2}\left(\rho_{II} - \rho_I\right) \quad (7) \qquad C_1^{II} = -\frac{\rho_{II} gR_{Pack}^2 b^2}{2} \quad (11)$$

$$C_1^I = -\frac{\rho_I gR_{Pack}^2}{2}\left(b^2 \frac{\rho_{II}}{\rho_I} + a^2\left(1 - \frac{\rho_{II}}{\rho_I}\right)\right) \quad (8)$$

$$\beta = \left(b^2 \frac{\rho_{II}}{\rho_I} + a^2\left(1 - \frac{\rho_{II}}{\rho_I}\right)\right) \quad (9)$$

$$C_1^I = -\frac{\rho_I g R_{Pack}^2}{2} \beta \qquad (10)$$

If both films show Newtonian behavior, the equations 2 and 3, change to the equations 12 and 13.

$$r\left(-\mu_I \frac{dV_Z^I}{dr}\right) = \frac{\rho_I g r^2}{2} - \frac{\rho_I g R_{Pack}^2 \beta}{2} \quad (12) \qquad r\left(-\mu_{II} \frac{dV_Z^{II}}{dr}\right) = \frac{\rho_{II} g r^2}{2} - \frac{\rho_{II} g R_{Pack}^2 b^2}{2} \quad (13)$$

Leaving the equation 12 and 13, as a function of the velocity, it is possible to obtain the equations 14 and 15.

$$\frac{dV_Z^I}{dr} = \frac{\rho_I g}{2\mu_I}\left(\frac{R_{Pack}^2 \beta}{r} - r\right) \qquad (14) \qquad \frac{dV_Z^{II}}{dr} = \frac{\rho_{II} g}{2\mu_{II}}\left(\frac{R_{Pack}^2 b^2}{r} - r\right) \qquad (15)$$

Integrating the differential equation 14 and 15, it is possible to obtain the equations 16 and 17.

$$V_Z^I = \frac{\rho_I g}{2\mu_I}\left(R_{Pack}^2 \beta \ln(r) - \frac{r^2}{2} + C_2^I\right) \qquad (16) \qquad V_Z^{II} = \frac{\rho_{II} g}{2\mu_{II}}\left(R_{Pack}^2 b^2 \ln(r) - \frac{r^2}{2} + C_2^{II}\right) \quad (17)$$

Using the frontier condition of not slide $r = R_{Pack}$ $V_Z^I = 0$, it is possible to obtain the second constant for the first film (equation 18)

$$C_2^I = \frac{R_{Pack}^2}{2} - R_{Pack}^2 \beta \ln(R_{Pack}) \qquad (18)$$

Using C$_2$ (equation 18) in the equation 16, it is possible to obtain the velocity profile for the first film (equation 19).

$$V_Z^I = \frac{\rho_I g R_{Pack}^2}{4\mu_I}\left(1 - \left(\frac{r}{R_{Pack}}\right)^2 + 2\beta \ln\left(\frac{r}{R_{Pack}}\right)\right) \qquad (19)$$

The second frontier condition for the second film is $r = a R_{Pack}$ $V_Z^I = V_Z^{II}$, this means that the velocity for both films is equal in the interface. So, using this condition and equaling the equations 17 and 19 for the interface, it is possible to obtain the second integration constant for the second film (equation 20).

$$C_2^{II} = R_{Pack}^2 \left(\frac{a^2}{2} - b^2 \ln \left(aR_{Pack} \right) + \frac{\rho_I \mu_{II}}{2\rho_{II}\mu_I} \left(1 - a^2 + 2\beta \ln (a) \right) \right) \tag{20}$$

Using the second integration (equation 20) constant in the velocity equation for the second film (equation 17), it is possible to obtain the velocity profile for the second film (equation 21).

$$V_z^{II} = \frac{\rho_{II} gR_{Pack}^2}{4\mu_{II}} \left(a^2 + 2b^2 \ln \left(\frac{r}{aR_{Pack}} \right) - \left(\frac{r}{R_{Pack}} \right)^2 + \frac{\rho_I \mu_{II}}{\rho_{II}\mu_I} \left(1 - a^2 + 2\beta \ln (a) \right) \right) \tag{21}$$

It is possible to obtain the first film from the velocity profile integration (equation 22).

$$Q_{emp}^I = \int_0^{2\pi} \int_{R_{Pack}}^{aR_{Pack}} V_z^I r \, dr \, d\theta \tag{22}$$

The first integration of the equation (22) change to the equation (23).

$$Q_{Pack}^I = \frac{\pi \rho_I gR_{Pack}^2}{2\mu_I} \int_{R_{Pack}}^{aR_{Pack}} \left(1 - \left(\frac{r}{R_{Pack}} \right)^2 + 2\beta \ln \left(\frac{r}{R_{Pack}} \right) \right) r \, dr \tag{23}$$

In order to integrate the equation (23), it is necessary to change the integration variable $\frac{r}{R_{Pack}} = \alpha$, then, the equation (23) change to the equation (24).

$$Q_{Pack}^I = \frac{\pi \rho_I gR_{Pack}^4}{2\mu_I} \int_1^a \left(\alpha - \alpha^3 + 2\beta\alpha \ln (\alpha) \right) d\alpha \tag{24}$$

The equation (25) is the integration result of the equation (24).

$$Q_{Pack}^I = \frac{\pi \rho_I gR_{Pack}^4}{2\mu_I} \left[\frac{\alpha^2}{2} - \frac{\alpha^4}{4} + \beta \frac{\alpha^2}{2} \left(2\ln (\alpha) - 1 \right) \right]_1^a \tag{25}$$

The equation (25) is reorganized and describe the volume flow for the first film over each packing thread (equation (26)).

$$Q^I_{Pack} = \frac{\pi \rho_I g R^4_{Pack}}{8 \mu_I} \left(2a^2 - a^4 - 1 + 2\beta a^2 \left(2\ln(a) - 1 + \frac{1}{a^2} \right) \right) \qquad (26)$$

If both films have the same composition, the properties of both films are equal and $a = b$ .Therefore, $\beta = a^2$, and the volume flow equation is the equation for film description over a cylinder, previously presented by Bird (BIRD et al., 2002) (equation 27).

$$Q^I_{Pack} = \frac{\pi \rho_I g R^4_{Pack}}{8 \mu_I} \left(4a^2 - 3a^4 - 1 + 4a^4 \ln(a) \right) \qquad (27)$$

The equation (26) is reorganized and change to the equation (28).

$$2a^2 - a^4 - 1 + 2\beta a^2 \left(2\ln(a) - 1 + \frac{1}{a^2} \right) - \frac{8 \mu_I Q^I_{Pack}}{\pi \rho_I g R^4_{Pack}} = 0 \qquad (28)$$

Following the previous procedure for the first film, it is possible to obtain the volume flow for the second film, after the integration of the equation (29).

$$Q^{II}_{Pack} = \int_0^{2\pi} \int_{aR_{Pack}}^{bR_{Pack}} V^{II}_Z \, r \, dr \, d\theta \qquad (29)$$

It is necessary to change the integration variable $\dfrac{r}{R_{Pack}} = \alpha$, then, the equation (29) change to the equation (30).

$$Q^{II}_{Pack} = \frac{\pi \rho_{II} g R^4_{Pack}}{2 \mu_{II}} \int_1^{b/a} \left(\alpha \lambda - \alpha^3 + 2b^2 \alpha \ln(\alpha) \right) d\alpha \qquad (30)$$

$$\lambda = \left(a^2 + \frac{\rho_I \mu_{II}}{\rho_{II} \mu_I} \left(1 - a^2 + 2\beta \ln(a) \right) \right) \qquad (31)$$

After integration the equation (30) change to the equation (32).

$$Q^{II}_{Pack} = \frac{\pi \rho_{II} g R^4_{Pack}}{2 \mu_{II}} \left[\frac{\lambda \alpha^2}{2} - \frac{\alpha^4}{4} + \frac{b^2 \alpha^2}{2} \left(2\ln(\alpha) - 1 \right) \right]_1^{b/a} \qquad (32)$$

The equation (32) is reorganized and describe the volume flow for the second film over each packing thread (equation (33)).

$$Q_{Pack}^{II} = \frac{\pi \rho_{II} g R_{Pack}^4}{8\mu_{II}} \left(2\lambda \left(\left(b/a\right)^2 - 1 \right) - \left(\left(b/a\right)^4 - 1 \right) + 2b^2 \left(\left(b/a\right)^2 \left(2\ln\left(b/a\right) - 1\right) + 1 \right) \right) \quad (33)$$

If both films have the same composition, the properties of both films are equal and $a = b$, the use of this expression in the equation (33) give as result that $Q_{Pack}^{II} = 0$. Finally, it is possible to reorganize the equation (33) as the equation (34).

$$2\lambda \left(\left(b/a\right)^2 - 1 \right) - \left(\left(b/a\right)^4 - 1 \right) + 2b^2 \left(\left(b/a\right)^2 \left(2\ln\left(b/a\right) - 1\right) + 1 \right) - \frac{8\mu_{II} Q_{Pack}^{II}}{\pi \rho_{II} g R_{Pack}^4} = 0 \quad (34)$$

It is possible to obtain the values a, b after simultaneous solution of the equations (28) and (34). This can be made using the Newton-Raphson method for two variables. With the values, a, b it is possible to obtain the thickness for both films from the equations (35) and (36).

$$\delta^I = R_{Pack}\left(a - 1\right) \quad (35) \qquad \delta^{II} = R_{Pack}\left(b - a\right) \quad (36)$$

It is possible to calculate the flow area for both phases with the equations (37) and (39).

$$A^I = \pi R_{Pack}^2 \left(a^2 - 1\right) \quad (38) \qquad A^{II} = \pi R_{Pack}^2 \left(b^2 - a^2\right) \quad (39)$$

The average velocity for each film is obtained from the equations (40) and (41).

$$V_m^I = \frac{Q_{Pack}^I}{\pi R_{Pack}^2 \left(a^2 - 1\right)} \quad (40) \qquad V_m^{II} = \frac{Q_{Pack}^{II}}{\pi R_{Pack}^2 \left(b^2 - a^2\right)} \quad (41)$$

Finally, these values can be used to calculate others flow conditions with the equations (42) to (47).

$$Q_{Pack}^I = Q^I \Big/ n_{Pack} \quad (42) \qquad \mathrm{Re}^I = \frac{V_m^I \rho^I D_H^I}{\mu^I} \quad (43) \qquad D_H^I = 2R_{Pack}\left(a^2 - 1\right) \quad (44)$$

$$Q_{Pack}^{II} = Q^{II} \Big/ n_{Pack} \quad (45) \qquad \mathrm{Re}^{II} = \frac{V_m^{II} \rho^{II} D_H^{II}}{\mu^{II}} \quad (46) \qquad D_H^{II} = 2R_{Pack}\left(b^2 - a^2\right) \quad (47)$$

9.2 Mass balance over each package

The continuity equation in cylindrical geometry has the form of the equation (48) (BIRD et al., 2002).

$$\frac{\partial C_i}{\partial_t} + \left(V_r \frac{\partial C_i}{\partial r} + \frac{V_\theta}{r} \frac{\partial C_i}{\partial \theta} + V_z \frac{\partial C_i}{\partial z} \right) = -\left[\frac{1}{r} \frac{\partial (rJ_{ir})}{\partial r} + \frac{1}{r} \frac{\partial (J_{i\theta})}{\partial \theta} + \frac{\partial (J_{iz})}{\partial z} \right] + r_i \quad (48)$$

Assuming the system is in steady state, without radial or angular profile concentrations and without mass transfer by diffusion, the equation (48) takes the form of equation (49).

$$V_z \frac{\partial C_i}{\partial z} = r_i \quad (49)$$

From the equation (49) $V_z = f(\delta_z, \rho_z, \mu_z)$, $\rho_z = f(C_i^z)$ and $\mu_z = f(C_i^z)$, them, the velocity change with the reactor length and must be calculated in each integration step. The system is considered a falling film reactor only if the transversal area occupied by the two films are lower than the transversal area available in the reactor (equation 50), above this value the velocity of the film is not a function of the gravity, the velocity is a function of the input velocity and the reactor behaves as a plug flow reactor. The equations (51) and (52) are another expression of the same constraints.

$$A^R \geq n_{Pack} \left(A^I + A^{II} \right) \quad (50)$$

$$\pi \left(R_{Rxn}^2 - n_{Pack} R_{Pack}^2 \right) \geq \pi n_{Pack} R_{Pack}^2 \left(a^2 - 1 \right) + \pi n_{Pack} R_{Pack}^2 \left(b^2 - a^2 \right) \quad (51)$$

$$R_{Rxn}^2 - n_{Pack} R_{Pack}^2 b^2 \geq 0 \quad (52)$$

The reactor behaves as a falling film reactor for low package quantity, low package radio, low flow rate and high reactor radio (equation 52). Figure 2 shows the molar balance for the plug flow reactor with the package, useful when the reactor operation variables are above the available area constraint (equation 52).

From a differential element with the reaction in figure 5-1 is possible to obtain the equation (53).

$$F_i^V - F_i^{V+\Delta V} + r_i \cdot \Delta V = 0 \quad (53)$$

The reaction volume is the reactor volume (cylinder) without the volume occupied by the package (Equation 54).

$$\Delta V = (\pi R_1^2 - n_{Pack}\pi R_2^2) \cdot \Delta Z \tag{54}$$

$$F_i^V - F_i^{V+\Delta V} + r_i(\pi R_1^2 - n_{Pack}\pi R_2^2) \cdot \Delta Z = 0 \tag{55}$$

$$\frac{F_i^V - F_i^{V+\Delta V}}{\Delta Z} + r_i(\pi R_1^2 - n_{Pack}\pi R_2^2) = 0 \tag{56}$$

Finally from the equation (56) is possible obtain the differential equation system for the reactor (equation 57).

$$\frac{dF_i}{dz} = r_i(\pi R_1^2 - n_{Pack}\pi R_2^2) \qquad\qquad i = 1, 2, 3 ..., 6 \tag{57}$$

Where R_1 is the reactor ratio, R_2 is the package ratio, n_{Pack} is the package threads number, z is the reactor length and F_i are the molar flows for components. As a normal PFR, the velocity inside the reactor is not a function of the length, so it is possible to obtain the equation 59.

$$Q_0 \frac{dC_i}{dz} = r_i(\pi R_1^2 - n_{Pack}\pi R_2^2) \qquad\qquad i = 1, 2, 3 ..., 6 \tag{58}$$

$$V_0 \frac{dC_i}{dz} = r_i \qquad\qquad i = 1, 2, 3 ..., 6 \tag{59}$$

The equation (59) for the PFR description is similar to the equation (49) for the LLFR. However, the velocity for LLFR is a function of reactor length meanwhile the velocity for PFR is constant for the entire reactor length.

9.3 Kinetic of oil methanolysis with mass transfer efficiency for the LLFR

Triacylglycerol (TG) Triacylglycerol (TG) methanolysis consists of three stepwise reversible reactions: partial methanolysis of TG to form diacylglycerol (DG), partial methanolysis of DG to form monoacylglycerol (MG) and partial methanolysis of MG to form glycerol (G). A molecule of fatty acid methyl ester (FAME) is released and a molecule of methanol (M) is consumed in each of the three reactions (NARVÁEZ et al., 2007, NORIEGA et al., 2014, NOUREDDINI; ZHU, 1997). The kinetics model of VO methanolysis can be described by the six differential equations presented in equations

(60) to (65). The kinetics model has a set of twelve parameters and does not include mass transfer resistance (NORIEGA et al., 2014).

$$\frac{d[TG]}{dt} = -k_1[TG][M] + k_{-1}[DG][EM]$$ (60)

$$\frac{d[DG]}{dt} = k_1[TG][M] - k_{-1}[DG][EM] - k_2[DG][M] + k_{-2}[MG][EM]$$ (61)

$$\frac{d[MG]}{dt} = k_2[DG][M] - k_{-2}[MG][EM] - k_3[MG][M] + k_{-3}[G][EM]$$ (62)

$$\frac{d[EM]}{dt} = k_1[TG][M] - k_{-1}[DG][EM] + k_2[DG][M] \ldots\ldots\ldots$$

$$\ldots\ldots\ldots - k_{-2}[MG][EM] + k_3[MG][M] - k_{-3}[G][EM]$$ (63)

$$\frac{d[G]}{dt} = k_3[MG][M] - k_{-3}[G][EM]$$ (64)

$$\frac{d[M]}{dt} = -\frac{d[EM]}{dt}$$ (65)

The low miscibility between TG and alcohols promote the presence of two phases in the entire reaction, the alcohol diffuses into the ester-rich phase, while triglycerides diffuse into the alcohol-rich phase, assuming that the reaction is developed mainly in the ester-rich phase, the methanol has strong mass transfer limitations because to react it have to travel until the ester-rich phase, so, the methanol in the reaction is lower than the overall methanol and correspond to the methanol available in the interface. Therefore, the overall methanol in the kinetic expression (equations 61 to 65) has to be replaced by the methanol available in the interface $[M]_{Int}$ (equations 66 to 71).

$$\frac{d[TG]}{dt} = [M]_{Int}\left(-k_1[TG]\right) - [EM]\left(-k_{-1}[DG]\right)$$ (66)

$$\frac{d[DG]}{dt} = [M]_{Int}\left(k_1[TG] - k_2[DG]\right) - [EM]\left(k_{-1}[DG] - k_{-2}[MG]\right)$$ (67)

$$\frac{d[MG]}{dt} = [M]_{Int}\left(k_2[DG] - k_3[MG]\right) - [EM]\left(k_{-2}[MG] - k_{-3}[G]\right)$$ (68)

$$\frac{d[EM]}{dt} = [M]_{Int}\left(k_1[TG] + k_2[DG] + k_3[MG]\right)\ldots\ldots$$

$$\ldots\ldots\ldots - [EM]\left(k_{-1}[DG] + k_{-2}[MG] + k_{-3}[G]\right)$$ (69)

$$\frac{d[G]}{dt} = [M]_{Int} \left(k_3 [MG] \right) - [EM] \left(k_{-3} [G] \right) \tag{70}$$

$$\frac{d[M]}{dt} = -[M]_{Int} \left(k_1 [TG] + k_2 [DG] + k_3 [MG] \right).......... \tag{71}$$

$$............ + [EM] \left(k_{-1} [DG] + k_{-2} [MG] + k_{-3} [G] \right)$$

For high mass transfer limitations, the methanol consumed in the reaction is equal to the methanol transported until the interface (equation 72).

$$[M]_{Int} \left(k_1 [TG] + k_2 [DG] + k_3 [MG] \right) = k_C a_C \left([M] - [M]_{Int} \right) \tag{72}$$

For the methanol description, the forward reaction is higher than the backward reaction, so, the methanol backward reaction is avoided in the equation (72). From the equation (72) is possible obtain the expression for the methanol available in the interface (equation 73).

$$[M]_{Int} = \frac{k_C a_C [M]}{k_C a_C + k_1 [TG] + k_2 [DG] + k_3 [MG]} \tag{73}$$

Where, k_C is the global mass transfer coefficient (m/min) and a_c is the packing surface area to reaction volume ratio (m^{-1}). The reactor and the packing threads are cylinders and the surface area is proportional to the number of threads (n_{emp}). a_c is calculated according to the equation (74 to 76). Where r_{Pack} is the packing thread ratio, r_{rxn} is the reactor ratio and H_{rxn} is the reactor height.

$$a_C = \frac{Surface\_Area}{Reactor\_Volume} \tag{74}$$

$$a_C = \frac{n_{emp} 2\pi r_{emp} H_{rxn}}{\pi r_{rxn}^2 H_{rxn}} \tag{75}$$

$$a_C = \frac{2 n_{emp} r_{emp}}{r_{rxn}^2} \tag{76}$$

The mass transfer coefficient (k_C) depend on the system geometry, the hydrodynamics characteristics, and the reaction condition. However, the mass transfer coefficient has a strong relation with the Sherwood number, so, it is possible to use this relation for the mass transfer coefficient calculus (equation 77), where the parameters α, β and λ must

be calculated from the experimental results obtained in the specific characteristics of geometry, hydrodynamics, and reaction.

$$k_C = \alpha Sc^{\beta} \, \text{Re}^{\lambda} \left(\frac{D_{12}}{\delta} \right)$$

(77)

The film thickness must be calculated from the equation (35) because the model assumes that the reaction is developed in the ester-rich phase and the diffusivity in this phase is calculated according to the equation (78) (WILKE; CHANG, 1955).

$$D_{12} = 7,4 \cdot 10^{-15} \frac{\left(x_2 M_2 \right)^{1/2} T}{\mu_2 V_1^{0.6}}$$

(78)

Where D_{12} (m²/s) is the methanol diffusivity in the ester-rich phase, M_2 (g/mol) is the molar mass of the ester-rich phase, μ_2 (kg/m.s) is the ester-rich phase viscosity, T (K) is the temperature, V_1 is the molar volume to the boiling point (cm³/mol) and x_2 is the association parameter in this equation has a value of one. Using the interfacial methanol expression (equation 73) in the kinetic system (equations 66 to 71) it is possible to obtain the new kinetic equation set (equations 79 to 71).

$$\frac{d[TG]}{dt} = [M] \left(\frac{-k_C a_C k_1 [TG]}{k_C a_C + k_1 [TG] + k_2 [DG] + k_3 [MG]} \right) - [EM] \left(-k_{-1} [DG] \right)$$

(79)

$$\frac{d[DG]}{dt} = [M] \left(\frac{k_C a_C \left(k_1 [TG] - k_2 [DG] \right)}{k_C a_C + k_1 [TG] + k_2 [DG] + k_3 [MG]} \right) - [EM] \left(k_{-1} [DG] - k_{-2} [MG] \right)$$

(80)

$$\frac{d[MG]}{dt} = [M] \left(\frac{k_C a_C \left(k_2 [DG] - k_3 [MG] \right)}{k_C a_C + k_1 [TG] + k_2 [DG] + k_3 [MG]} \right) - [EM] \left(k_{-2} [MG] - k_{-3} [G] \right)$$

(81)

$$\frac{d[EM]}{dt} = [M] \left(\frac{k_C a_C \left(k_1 [TG] + k_2 [DG] + k_3 [MG] \right)}{k_C a_C + k_1 [TG] + k_2 [DG] + k_3 [MG]} \right) \ldots \ldots$$

$$\ldots \ldots \ldots - [EM] \left(k_{-1} [DG] + k_{-2} [MG] + k_{-3} [G] \right)$$

(82)

$$\frac{d[G]}{dt} = [M] \left(\frac{k_C a_C k_3 [MG]}{k_C a_C + k_1 [TG] + k_2 [DG] + k_3 [MG]} \right) - [EM] \left(k_{-3} [G] \right)$$

(83)

$$\frac{d[M]}{dt} = -[M]\left(\frac{k_C a_C\left(k_1[TG]+k_2[DG]+k_3[MG]\right)}{k_C a_C + k_1[TG]+k_2[DG]+k_3[MG]}\right)\ldots\ldots\ldots$$

$$\ldots\ldots\ldots + [EM]\left(k_{-1}[DG]+k_{-2}[MG]+k_{-3}[G]\right) \tag{84}$$

If the mass transfer resistance is not present in the reaction $\left(k_C a_C >>> k_1[TG]+k_2[DG]+k_3[MG]\right)$, the set equations (79) to (84), assume the original form (equations 60 to 65). The mass transfer efficiency (MTE) can be defined as the equation (85)

$$MTE = \frac{k_C a_C}{k_C a_C + k_1[TG]+k_2[DG]+k_3[MG]} \tag{85}$$

Finally using the mass transfer definition inside the reactor description, the overall mathematical model is described by the equations (86 to 91).

$$V_Z \frac{dC_{TG}}{dZ} = [M]\left(-MTE\left(k_1[TG]\right)\right)-[FAME]\left(-k_{-1}[DG]\right) \tag{86}$$

$$V_Z \frac{dC_{DG}}{dZ} = [M]\left(MTE\left(k_1[TG]-k_2[DG]\right)\right)-[FAME]\left(k_{-1}[DG]-k_{-2}[MG]\right) \tag{87}$$

$$V_Z \frac{dC_{MG}}{dZ} = [M]\left(MTE\left(k_2[DG]-k_3[MG]\right)\right)-[FAME]\left(k_{-2}[MG]-k_{-3}[G]\right) \tag{88}$$

$$V_Z \frac{dC_{FAME}}{dZ} = [M]\left(MTE\left(k_1[TG]+k_2[DG]+k_3[MG]\right)\right)-[FAME]\left(k_{-1}[DG]+k_{-2}[MG]+k_{-3}[G]\right) \tag{89}$$

$$V_Z \frac{dC_G}{dZ} = [M]\left(MTE\left(k_3[MG]\right)\right)-[FAME]\left(k_{-3}[G]\right) \tag{90}$$

$$V_Z \frac{dC_M}{dZ} = [M]\left(-MTE\left(k_1[TG]+k_2[DG]+k_3[MG]\right)\right)+[FAME]\left(k_{-1}[DG]+k_{-2}[MG]+k_{-3}[G]\right) \tag{91}$$

Where:

$$k_i = A_i e^{\frac{E_i}{RT}}\left(\frac{C_{cat}}{k_{icat}+C_{cat}}\right) \tag{92}$$

The equation (92) include the Temperature and the catalyst concentration inside the reaction rate. Where k_i is the reaction rate of the component i, T (k) is the reaction temperature and R (Kcal/mol.K) is the gas constant, A^o is the standard reaction frequency factor, E_i (Kcal/mol) is the activation energies, k_{cat} is a value that quantifies the catalyst effect on the reaction and C_{cat} is the catalyst concentration.

9.4 Mathematical model of the membrane effect on the biodiesel production using LLFR

A schematic diagram of the LLFRM configuration including a differential element of volume is shown in Figure 3. The ester-rich phase wet the packing surface and the alcoholic phase down between the ester-rich phase and the membrane. The hydrodynamics of this flow is explained because the ester-rich phase wettability over the packing is bigger than the alcoholic phase wettability. From a differential element with reaction in figure 7.2 is possible to obtain the equation (93).

$$F_i^V - F_i^{V+\Delta V} - J_i^M \cdot \Delta A^M + r_i \cdot \Delta V = 0 \quad (93)$$

The reaction volume is the reactor volume (cylinder) without the volume occupied by the package and without the volume occupied by the membranes (Equation 94).

The membrane perimeter is constant with the length, so, the differential membrane area is presented by the equation (95). Using the equations (94) and (95) in the equation (93) is possible obtain the equation (96).

$$\Delta V = \left(\pi \left(\frac{D_{rxn}}{2} \right)^2 - n_{Mem} \pi \left(\frac{D_{Mem}}{2} \right)^2 - n_{Pack} \pi \left(\frac{D_{Pack}}{2} \right)^2 \right) \cdot \Delta Z \quad (94)$$

$$\Delta A^M = \left(n_{mem} \pi D_{Mem} \right) \cdot \Delta Z \quad (95)$$

$$\frac{F_i^V - F_i^{V+\Delta V}}{\Delta Z} - J_i^M \cdot \left(n_{mem} \pi D_{Mem} \right) + r_i \cdot \frac{\pi}{4} \left(D_{rxn}^2 - n_{Mem} D_{Mem}^2 - n_{Pack} D_{Pack}^2 \right) = 0 \quad (96)$$

The limit to zero of the equation (96) allows us to obtain the final differential equation system (equation 97).

$$\frac{dF_i^R}{dz} = r_i \cdot \frac{\pi}{4} \left(D_{rxn}^2 - n_{Mem} D_{Mem}^2 - n_{Pack} D_{Pack}^2 \right) - J_i^M \cdot \left(n_{mem} \pi D_{Mem} \right) \qquad i = 1,2,3...,6 \quad (97)$$

The equation (97) can be reorganized to the equation (99).

$$\frac{dF_i^R}{dz} = r_i \cdot \frac{\pi}{4 D_{rxn}^2} \left(1 - n_{Mem} \frac{D_{Mem}^2}{D_{rxn}^2} - n_{emp} \frac{D_{Pack}^2}{D_{rxn}^2} \right) - J_i^M \cdot \pi n_{Mem} D_{Mem} \qquad i = 1,2,3...,6 \quad (98)$$

$$\frac{dF_i^R}{dz} = r_i \cdot \frac{\pi D_{rxn}^2}{4} \left(1 - \Omega_{Mem} - \Omega_{Pack} \right) - J_i^M \cdot \pi n_{Mem} D_{Mem} \qquad i = 1,2,3...,6 \quad (99)$$

Where Ω_{Mem} is the fraction area occupied by the membranes (equation 100) and Ω_{Pack} is the fraction area occupied by the packing (equation 101).

$$\Omega_{Mem} = n_{Mem} \left(\frac{D_{Mem}}{D_{rxn}} \right)^2 \qquad (100)$$

$$\Omega_{Pack} = n_{Pack} \left(\frac{D_{Pack}}{D_{rxn}} \right)^2 \qquad (101)$$

From the equation (99) the transversal area occupied by the membrane and the packing must be lower than the available area in the reactor (equation 102).

$$\Omega_{Mem} + \Omega_{Pack} \leq 1 \qquad (102)$$

For calculating J_M and the permeate composition is necessary the use of the equations (103 to 105).

$$\frac{dF_i^M}{dz} = J_i^M \pi n_{mem} D_{Mem} \qquad i = 1,2,3...,6 \qquad (103)$$

$$J_M = \frac{\Delta P}{\mu_M^{mem} (R_m + k\phi J_M)} \qquad i = 1,2,3...,6 \qquad (104)$$

$$J_i^M = w_i^{OH} J^M \qquad i = 1,2,3...,6 \qquad (105)$$

To solve the equation system (99 to 105) is necessary use the kinetic with the mass transfer efficiency (equation 106 to 111).

$$r_{TG} = [M]\left(-MTE\left(k_1[TG]\right)\right) - [FAME]\left(-k_{-1}[DG]\right) \qquad (106)$$

$$r_{DG} = [M]\left(MTE\left(k_1[TG] - k_2[DG]\right)\right) - [FAME]\left(k_{-1}[DG] - k_{-2}[MG]\right) \qquad (107)$$

$$r_{MG} = [M]\left(MTE\left(k_2[DG] - k_3[MG]\right)\right) - [FAME]\left(k_{-2}[MG] - k_{-3}[G]\right) \qquad (108)$$

$$r_{FAME} = [M]\left(MTE\left(k_1[TG] + k_2[DG] + k_3[MG]\right)\right)......... \qquad (109)$$

$$...........- [FAME]\left(k_{-1}[DG] + k_{-2}[MG] + k_{-3}[G]\right)$$

$$r_G = [M]\left(MTE\left(k_3[MG]\right)\right) - [FAME]\left(k_{-3}[G]\right) \qquad (110)$$

$$r_M = [M]\left(-MTE\left(k_1[TG] + k_2[DG] + k_3[MG]\right)\right)......... \qquad (111)$$

$$........+ [FAME]\left(k_{-1}[DG] + k_{-2}[MG] + k_{-3}[G]\right)$$

9.5 Activity model

The activity coefficient of the UNIFAC model (γ_i^w) using mass fraction as concentration unity (OICHI; PRAUSNITZ, 1978) is given by:

$$\ln \gamma_i^w = \ln \gamma_i^C + \ln \gamma_i^R \tag{112}$$

$$\ln \gamma_i^C = 1 - \frac{\zeta M_i \phi_i'}{w_i} + \ln \frac{\zeta M_i \phi_i'}{w_i} - 5 q_i' M_i \left(1 - \frac{\phi_i'}{\theta_i'} - \ln \frac{\theta_i'}{\phi_i'}\right) \tag{113}$$

$$\ln \gamma_i^R = \sum_{k=1}^{G} v_k^{(i)} \left[\ln \Gamma_k - \ln \Gamma_k^{(i)}\right] \tag{114}$$

$$\ln \Gamma_k = M_k Q_k \left[1 - \ln\left(\sum_{j=1}^{k} \Theta_j' \tau_{jk}\right) - \sum_{j=1}^{k} \left(\frac{\Theta_j' \tau_{kj}}{\sum_{k=1}^{K} \Theta_k' \tau_{kj}}\right)\right] \tag{115}$$

$$\zeta = \sum_{j=1}^{K} \frac{w_j}{M_j} \tag{116} \qquad r_i' = \frac{1}{M_i} \sum_{k=1}^{G} v_k^{(i)} R_k \tag{117} \qquad q_i' = \frac{1}{M_i} \sum_{k=1}^{G} v_k^{(i)} Q_k \tag{118}$$

$$\theta_i' = \frac{q_i' w_i}{\sum_{j=1}^{K} q_j' w_j} \tag{119} \qquad \phi_i' = \frac{r_i' w_i}{\sum_{j=1}^{K} r_j' w_j} \tag{120} \qquad \Theta_j' = \frac{Q_j W_j}{\sum_{k=1}^{G} Q_k W_k} \tag{121}$$

$$W_i = \frac{\sum_{k=1}^{G} v_k^{(i)} w_i}{\sum_{i=1}^{i} \sum_{k=1}^{G} v_k^{(i)} w_i} \tag{122} \qquad \tau_{ij} = \exp \frac{-a_{ij}}{T} \tag{123}$$

10. References

ABELS, C.; CARSTENSEN, F.; WESSLING, M. "Membrane processes in biorefinery applications", **Journal of Membrane Science**, v. 444, pp. 285–317, 2013. Elsevier.

ALVES, M. J.; NASCIMENTO MENDONÇA, S.; PEREIRA GOMES, I.; et al. "Biodiesel purification using micro and ultrafiltration membranes", **Renewable Energy**, v. 58, pp. 15–20, 2013. Elsevier Ltd.

AMIN, I. N. H. M.; MOHAMMAD, A. W.; MARKOM, M.; PENG, L. C.; HILAL, N. "Flux decline study during ultrafiltration of glycerin-rich fatty acid solutions", **Journal of Membrane Science**, v. 351, n. 1–2, pp. 75–86, 2010. Elsevier B.V.

ANDREATTA, A. E.; CASÁS, L. M.; HEGEL, P.; BOTTINI, S. B.; BRIGNOLE, E. A. "Phase Equilibria in Ternary Mixtures of Methyl Oleate, Glycerol, and Methanol", **Industrial & Engineering Chemistry Research**, v. 47, n. 15, pp. 5157–5164, 2008. JOUR, American Chemical Society.

ARANSIOLA, E. F.; OJUMU, T. V.; OYEKOLA, O. O.; MADZIMBAMUTO, T. F.; IKHU-OMOREGBE, D. I. O. "A review of current technology for biodiesel production: State of the art", **Biomass and Bioenergy**, v. 61, pp. 276–297, 2014. Elsevier Ltd.

ARAUJO, P. J. P.; LEILA, P.; RAVAGNANI, T. M. K. "Application of ultrafiltration membranes in the separation of Ethylic route biodiesel", **Chemical Engineering Transactions**, v. 24, pp. 769–774, 2011.

ATADASHI, I. M.; AROUA, M. K.; ABDUL AZIZ, A. R.; SULAIMAN, N. M. N. "Membrane biodiesel production and refining technology: A critical review", **Renewable and Sustainable Energy Reviews**, v. 15, n. 9, pp. 5051–5062, 2011. Elsevier Ltd.

ATADASHI, I. M.; AROUA, M. K.; AZIZ, A. R. A.; SULAIMAN, N. M. N. "Refining technologies for the purification of crude biodiesel", **Applied Energy**, v. 88, n. 12, pp. 4239–4251, 2011. Elsevier Ltd.

ATADASHI, I. M.; AROUA, M. K.; AZIZ, A. R. A.; SULAIMAN, N. M. N. "High quality biodiesel obtained through membrane technology", **Journal of Membrane Science**, v. 421–422, pp. 154–164, 2012. Elsevier.

BAKER, R. W. R. W. **Membrane technology and applications**. 2004.

BALAT, M.; BALAT, H. "Progress in biodiesel processing", **Applied Energy**, v. 87, n. 6, pp. 1815–1835, 2010. Elsevier Ltd.

BAROUTIAN, S.; AROUA, M. K.; RAMAN, A. A. A.; SULAIMAN, N. M. N. "A packed bed membrane reactor for production of biodiesel using activated carbon supported catalyst", **Bioresource Technology**, v. 102, n. 2, pp. 1095–1102, 2011. Elsevier Ltd.

BARREAU, A; BRUNELLA, I.; DE HEMPTINNE, J.-C.; et al. "Measurements of Liquid−Liquid Equilibria for a Methanol + Glycerol + Methyl Oleate System and Prediction Using Group Contribution Statistical Associating Fluid Theory", **Ind. Eng. Chem. Res.**, v. 49, n. 12, pp. 5800–5807, 2010.

BARREDO-DAMAS, S.; ALCAINA-MIRANDA, M. I.; BES-PIÁ, A.; et al. "Ceramic membrane behavior in textile wastewater ultrafiltration", **Desalination**, v. 250, n. 2, pp. 623–628, 2010.

BASSO, R. C.; DE ALMEIDA MEIRELLES, A. J.; BATISTA, E. A. C. "Liquid-liquid equilibrium of pseudoternary systems containing glycerol+ethanol+ethylic biodiesel from crambe oil (Crambe abyssinica) at T/K=(298.2, 318.2, 338.2) and thermodynamic modeling", **Fluid Phase Equilibria**, v. 333, pp. 55–62, 2012. Elsevier B.V.

BASSO, R. C.; SILVA, C. A. S. DA; SOUSA, C. D. O.; MEIRELLES, A. J. D. A.; BATISTA, E. A. C. "LLE experimental data, thermodynamic modeling and sensitivity analysis in the ethyl biodiesel from macauba pulp oil settling step", **Bioresource Technology**, v. 131, pp. 468–475, 2013.

BATISTA, E.; MONNERAT, S.; KATO, K.; STRAGEVITCH, L.; MEIRELLES, A. J. A. "Liquid-liquid equilibrium for systems of canola oil, oleic acid, and short-chain alcohols", **Journal of Chemical and Engineering Data**, v. 44, n. 6, pp. 1360–1364, 1999.

BELLO, N.; NARVÁEZ, P. C.; CADAVID, J. G.; et al. "Characterization and evaluation of poly(ether sulfone) membranes in biodiesel production using liquid-liquid film reactors", **Chemical Engineering and Processing: Process Intensification**, 2016. Elsevier B.V.

BENETI, S. C.; LANZA, M.; MAZUTTI, M. A.; et al. "Experimental (liquid+liquid) equilibrium data for ternary and quaternary mixtures of fatty acid methyl and ethyl esters (FAME/FAEE) from soybean oil", **The Journal of Chemical Thermodynamics**, v. 68, pp. 60–70, 2014.

BERGMANN, J. C.; TUPINAMBÁ, D. D.; COSTA, O. Y. A.; et al. "Biodiesel production in Brazil and alternative biomass feedstocks", **Renewable and Sustainable Energy Reviews**, v. 21, pp. 411–420, 2013. JOUR, .

BIRD, R. B.; STEWART, W. E.; LIGHTFOOT, E. N. **Transport Phenomena**. 2002.

BORUGADDA, V. B.; GOUD, V. V. "Biodiesel production from renewable feedstocks: Status and opportunities", **Renewable and Sustainable Energy Reviews**, v. 16, n. 7, pp. 4763–4784, 2012. Elsevier.

BRADSHAW, G. B.; MEULY, W. C. "Preparation of detergents", US patent 2,360,844, 1944.

CADAVID, J. G.; GODOY-SILVA, R. D.; NARVAEZ, P. C.; CAMARGO, M.; FONTEIX, C. "Biodiesel production in a counter-current reactive extraction column: Modelling, parametric identification and optimisation", **Chemical Engineering Journal**, v. 228, pp.

717–723, 2013. Elsevier B.V.

CAO, P.; DUBÉ, M. A.; TREMBLAY, A. Y. "High-purity fatty acid methyl ester production from canola, soybean, palm, and yellow grease lipids by means of a membrane reactor", **Biomass and Bioenergy**, v. 32, n. 11, pp. 1028–1036, 2008a.

CAO, P.; DUBÉ, M. A.; TREMBLAY, A. Y. "Methanol recycling in the production of biodiesel in a membrane reactor", **Fuel**, v. 87, n. 6, pp. 825–833, 2008b.

CAO, P.; TREMBLAY, A. Y.; DUBÉ, M. A; MORSE, K. "Effect of Membrane Pore Size on the Performance of a Membrane Reactor for Biodiesel Production", **Industrial & Engineering Chemistry Research**, v. 46, n. 1, pp. 52–58, 2006.

CAO, P.; TREMBLAY, Y.; DUBE, M. A.; MORSE, K. "Effect of Membrane Pore Size on the Performance of a Membrane Reactor for Biodiesel Production", , pp. 52–58, 2007.

DO CARMO, F. R.; EVANGELISTA, N. S.; DE SANTIAGO-AGUIAR, R. S.; FERNANDES, F. A. N.; DE SANT'ANA, H. B. "Evaluation of optimal activity coefficient models for modeling and simulation of liquid–liquid equilibrium of biodiesel+glycerol+alcohol systems", **Fuel**, v. 125, pp. 57–65, 2014. Elsevier Ltd.

CASTANHEIRO, J. E.; RAMOS, A. M.; FONSECA, I. M.; VITAL, J. "Esterification of acetic acid by isoamylic alcohol over catalytic membranes of poly(vinyl alcohol) containing sulfonic acid groups", **Applied Catalysis A: General**, v. 311, n. 1–2, pp. 17–23, 2006.

CHENG, L. H.; CHENG, Y. F.; YEN, S. Y.; CHEN, J. "Ultrafiltration of triglyceride from biodiesel using the phase diagram of oil-FAME-MeOH", **Journal of Membrane Science**, v. 330, n. 1–2, pp. 156–165, 2009.

CHENG, L. H.; YEN, S. Y.; SU, L. S.; CHEN, J. "Study on membrane reactors for biodiesel production by phase behaviors of canola oil methanolysis in batch reactors", **Bioresource Technology**, v. 101, n. 17, pp. 6663–6668, 2010. Elsevier Ltd.

CHENG, L.-H.; YEN, S.-Y.; CHEN, Z.-S.; CHEN, J. "Modeling and simulation of biodiesel production using a membrane reactor integrated with a prereactor", **Chemical Engineering Science**, v. 69, n. 1, pp. 81–92, 2012. Elsevier.

CHIU, C.-W.; GOFF, M. J.; SUPPES, G. J. "Distribution of methanol and catalysts between biodiesel and glycerin phases", **AIChE Journal**, v. 51, n. 4, pp. 1274–1278, 2005. article, Wiley Subscription Services, Inc., A Wiley Company.

CHOI, H.; ZHANG, K.; DIONYSIOU, D. D.; OERTHER, D. B.; SORIAL, G. A. "Effect of permeate flux and tangential flow on membrane fouling for wastewater treatment", **Separation and Purification Technology**, v. 45, n. 1, pp. 68–78, 2005.

CHONG, M. F.; CHEN, J.; OH, P. P.; CHEN, Z.-S. "Modeling and simulation of the polymeric nanocapsule formation process", **AIChE Journal**, v. 7, n. PART 1, pp. 405–410, 2012.

COELHOSO, I. M.; CARDOSO, M. M.; VIEGAS, R. M. C.; CRESPO, J. P. S. G. "Transport mechanisms and modelling in liquid membrane contactors", **Separation and Purification Technology**, v. 19, n. 3, pp. 183–197, 2000.

DEROUSSEL, P.; KHAKHAR, D. V.; OTTINO, J. M. "Mixing of viscous immiscible liquids.

Part 2: Overemulsification-interpretation and use", **Chemical Engineering Science**, v. 56, n. 19, pp. 5531–5537, 2001.

DINDORE, V. Y.; BRILMAN, D. W. F.; VERSTEEG, G. F. "Modelling of cross-flow membrane contactors: Mass transfer with chemical reactions", **Journal of Membrane Science**, v. 255, n. 1–2, pp. 275–289, 2005.

DUBÉ, M. A.; TREMBLAY, A. Y.; LIU, J. "Biodiesel production using a membrane reactor", **Bioresource Technology**, v. 98, n. 3, pp. 639–647, 2007.

EL-ZANATI, E.; RITCHIE, S. M. C.; ABDALLAH, H. "Development of integrated catalytic membrane-based unit for biofuel production", **Pertanika Journal of Science and Technology**, v. 24, n. 1, pp. 89–99, 2016.

FALAHATI, H.; TREMBLAY, A. Y. "Flux dependent oil permeation in the ultrafiltration of highly concentrated and unstable oil-in-water emulsions", **Journal of Membrane Science**, v. 371, n. 1–2, pp. 239–247, 2011. Elsevier B.V.

FANGRUI, M.; HANNA, M. "Biodiesel production : a review 1", **Bioresource Technology**, v. 70, pp. 1–15, 1999.

DI FELICE, R.; DE FAVERI, D.; DE ANDREIS, P.; OTTONELLO, P. "Component Distribution between Light and Heavy Phases in Biodiesel Processes", **Industrial & Engineering Chemistry Research**, v. 47, n. 20, pp. 7862–7867, 2008. JOUR, American Chemical Society.

FILHO, D. C. M.; SALIM, V. M. M.; BORGES, C. P. "Chemical Engineering and Processing : Process Intensi fi cation Membrane contactor reactor for transesteri fi cation of triglycerides heterogeneously catalyzed", , v. 108, pp. 220–225, 2016.

FOLLEGATTI-ROMERO, L. A.; OLIVEIRA, M. B.; BATISTA, F. R. M.; et al. "Liquid-liquid equilibria for ternary systems containing ethyl esters, ethanol and glycerol at 323.15 and 353.15 K", **Fuel**, v. 94, pp. 386–394, 2012.

FRANC, B. B.; PINTO, F. M.; PESSOA, F. L. P.; et al. "Liquid−Liquid Equilibria for Castor Oil Biodiesel + Glycerol + Alcohol.pdf", **J. Chem. Eng. Data**, v. 54, pp. 2359–2364, 2009.

FRANÇA, B. B.; VILLARDI, H. G. D. A.; PESSOA, F. L. P.; ULLER, A. M. C. "Liquid-liquid equilibrium for compounds of soybean ethyl biodiesel production by transesterification", **Journal of Chemical and Engineering Data**, v. 58, n. 7, pp. 1927–1933, 2013.

FRASCARI, D.; ZUCCARO, M.; PINELLI, D.; PAGLIANTI, A. "A Pilot-Scale Study of Alkali-Catalyzed Sunflower Oil Transesterification with Static Mixing and with Mechanical Agitation", **Energy & Fuels**, v. 22, n. 3, pp. 1493–1501, 2008. article, .

FREEDMAN, B.; PRYDE, E. H.; MOUNTS, T. L. "Variables affecting the yields of fatty esters from transesterified vegetable oils", **Journal of the American Oil Chemists Society**, v. 61, n. 10, pp. 1638–1643, 1984. article, .

VAN GERPEN, J. "Biodiesel processing and production", **Fuel Processing Technology**, v. 86, n. 10, pp. 1097–1107, 2005.

GHADGE, S. V.; RAHEMAN, H. "Biodiesel production from mahua (Madhuca indica) oil

having high free fatty acids", **Biomass and Bioenergy**, v. 28, n. 6, pp. 601–605, 2005.

GLISIC, S.; SKALA, D. "The problems in design and detailed analyses of energy consumption for biodiesel synthesis at supercritical conditions", **Journal of Supercritical Fluids**, v. 49, n. 2, pp. 293–301, 2009.

GOMES, C. S. .; ARROYO, P. .; PEREIRA, N. . "Influence of oil quality on biodiesel purification by ultrafiltration", **Journal of Membrane Science**, v. 496, pp. 242–249, 2015.

GOMES, M. C. S.; ARROYO, P. A.; PEREIRA, N. C. "Biodiesel production from degummed soybean oil and glycerol removal using ceramic membrane", **Journal of Membrane Science**, v. 378, n. 1–2, pp. 453–461, 2011.

GOMES, M. C. S.; ARROYO, P. A.; PEREIRA, N. C. "Influence of acidified water addition on the biodiesel and glycerol separation through membrane technology", **Journal of Membrane Science**, v. 431, pp. 28–36, 2013.

GOMES, M. C. S.; PEREIRA, N. C.; BARROS, S. T. D. D. "Separation of biodiesel and glycerol using ceramic membranes", **Journal of Membrane Science**, v. 352, n. 1–2, pp. 271–276, 2010.

GONÇALVES, J. D.; AZNAR, M.; SANTOS, G. R. "Liquid–liquid equilibrium data for systems containing Brazil nut biodiesel+methanol+glycerin at 303.15K and 323.15K", **Fuel**, v. 133, pp. 292–298, 2014.

GONZÁLEZ, B.; CALVAR, N.; GÓMEZ, E.; DOMÍNGUEZ, Á. "Density, dynamic viscosity, and derived properties of binary mixtures of methanol or ethanol with water, ethyl acetate, and methyl acetate at T=(293.15, 298.15, and 303.15)K", **The Journal of Chemical Thermodynamics**, v. 39, n. 12, pp. 1578–1588, 2007.

GUERREIRO, L.; CASTANHEIRO, J. E.; FONSECA, I. M.; et al. "Transesterification of soybean oil over sulfonic acid functionalised polymeric membranes", **Catalysis Today**, v. 118, n. 1–2, pp. 166–171, 2006.

GUERREIRO, L.; PEREIRA, P. M.; FONSECA, I. M.; et al. "PVA embedded hydrotalcite membranes as basic catalysts for biodiesel synthesis by soybean oil methanolysis", **Catalysis Today**, v. 156, n. 3–4, pp. 191–197, 2010. Elsevier B.V.

H. S. FOGLER. **Elements of Chemical Reaction Engineering**. 4th Editio ed. 2006.

HAKIM, M.; NAJAFABADI, H. A.; PAZUKI, G.; VOSSOUGHI, M. "Novel Approach for Liquid − Liquid Phase Equilibrium of Biodiesel (Canola and Sunflower) + Glycerol + Methanol", **Industrial & Engineering Chemistry Research**, v. 53, pp. 855–864, 2014.

HARVEY, A. P.; MACKLEY, M. R.; SELIGER, T. "Process intensification of biodiesel production using a continuous oscillatory flow reactor", **Journal of Chemical Technology & Biotechnology**, v. 78, n. 2–3, pp. 338–341, 2003.

HE, B. "A NOVEL CONTINUOUS-FLOW REACTOR USING REACTIVE DISTILLATION FOR BIODIESEL PRODUCTION", **Production**, , n. December, 2006.

HE, H. Y.; GUO, X.; ZHU, S. L. "Comparison of membrane extraction with traditional extraction methods for biodiesel production", **JAOCS, Journal of the American Oil Chemists' Society**, v. 83, n. 5, pp. 457–460, 2006.

HOU, X.; QI, Y.; QIAO, X.; et al. "Lewis acid-catalyzed transesterification and esterification of high free fatty acid oil in subcritical methanol", **Korean Journal of Chemical Engineering**, v. 24, n. 2, pp. 311–313, 2007.

HUANG, H.; RAMASWAMY, S.; TSCHIRNER, U.; RAMARAO, B. "A review of separation technologies in current and future biorefineries", **Separation and Purification Technology**, v. 62, n. 1, pp. 1–21, 2008.

INOUE, T.; NAGASE, T.; HASEGAWA, Y.; et al. "Stoichiometric ester condensation reaction processes by pervaporative water removal via acid-tolerant zeolite membranes", **Industrial and Engineering Chemistry Research**, v. 46, n. 11, pp. 3743–3750, 2007.

JULIANA R.F. SILVA A, MARCIO A. MAZUTTI B, FERNANDO A.P. VOLL C, L. C.-F. C; MARCOS L. CORAZZA D, MARCELO LANZA E, WAGNER L. PRIAMO F, J. V. O. "Thermophysical properties of biodiesel and related systems: (Liquid + liquid) equilibrium data for Jatropha curcas biodiesel", **Journal of Chemical Thermodynamics**, v. 58, pp. 467–475, 2013.

JURAC, Z.; ZLATAR, V. "Optimization of raw material mixtures in the production of biodiesel from vegetable and used frying oils regarding quality requirements in terms of cold flow properties", **Fuel Processing Technology**, v. 106, pp. 108–113, 2013. Elsevier B.V.

KARMAKAR, A.; KARMAKAR, S.; MUKHERJEE, S. "Properties of various plants and animals feedstocks for biodiesel production", **Bioresource Technology**, v. 101, n. 19, pp. 7201–7210, 2010. Elsevier Ltd.

VAN KASTEREN, J. M. N.; NISWORO, A. P. "A process model to estimate the cost of industrial scale biodiesel production from waste cooking oil by supercritical transesterification", **Resources, Conservation and Recycling**, v. 50, n. 4, pp. 442–458, 2007.

KISS, A. A.; BILDEA, C. S. "A review of biodiesel production by integrated reactive separation technologies", **Journal of Chemical Technology & Biotechnology**, v. 87, n. 7, pp. 861–879, 2012.

KOBAYASHI, J.; MORI, Y.; KOBAYASHI, S. "Multiphase Organic Synthesis in Microchannel Reactors", **Chemistry – An Asian Journal**, v. 1, n. 1–2, pp. 22–35, 2006. article, WILEY-VCH Verlag.

KOVALSKY, P.; BUSHELL, G.; WAITE, T. D. "Prediction of transmembrane pressure build-up in constant flux microfiltration of compressible materials in the absence and presence of shear", **Journal of Membrane Science**, v. 344, n. 1–2, pp. 204–210, 2009.

KRAAI, G. N.; SCHUUR, B.; VAN ZWOL, F.; VAN DE BOVENKAMP, H. H.; HEERES, H. J. "Novel highly integrated biodiesel production technology in a centrifugal contactor separator device", **Chemical Engineering Journal**, v. 154, n. 1–3, pp. 384–389, 2009.

KUMAR, P.; DATTA, S.; NANDI, S.; AL, F. "Effect of mass transfer kinetics for maximum production of biodiesel from Jatropha Curcas oil : A mathematical approach q", , v. 134, pp. 39–44, 2014.

KUSDIANA, D.; SAKA, S. "Effects of water on biodiesel fuel production by supercritical methanol treatment", **Bioresource Technology**, v. 91, n. 3, pp. 289–295, 2004.

LEE, M.-J.; LO, Y.-C.; LIN, H.-M. "Liquid–liquid equilibria for mixtures containing water, methanol, fatty acid methyl esters, and glycerol", **Fluid Phase Equilibria**, v. 299, n. 2, pp. 180–190, 2010.

LEVENSPIEL, O. **Ingeniería de las reacciones quimicas**. Mexico, 1986.

LI, Z.; FIROOZABADI, A. "Initialization of phase fractions in Rachford-Rice equations for robust and efficient three-phase split calculation", **Fluid Phase Equilibria**, v. 332, pp. 21–27, 2012. Elsevier B.V.

LIKOZAR, B.; POHAR, A.; LEVEC, J. "Transesterification of oil to biodiesel in a continuous tubular reactor with static mixers: Modelling reaction kinetics, mass transfer, scale-up and optimization considering fatty acid composition", **Fuel Processing Technology**, v. 142, pp. 326–336, 2016.

DE LIMA DA SILVA, N.; SANTANDER, C. M. G.; BATISTELLA, C. B.; FILHO, R. M.; MACIEL, M. R. W. "Biodiesel production from integration between reaction and separation system: Reactive distillation process", **Applied Biochemistry and Biotechnology**, v. 161, n. 1–8, pp. 245–254, 2010.

LIU, X.; PIAO, X.; WANG, Y.; ZHU, S. "Liquid – Liquid Equilibrium for Systems of (Fatty Acid Ethyl Esters + Ethanol + Soybean Oil and Fatty Acid Ethyl Esters + Ethanol + Glycerol)", , , n. July 2007, pp. 359–362, 2008.

LOTERO, E.; LIU, Y.; LOPEZ, D. E.; et al. "Synthesis of Biodiesel via Acid Catalysis", **Industrial & Engineering Chemistry Research**, v. 44, n. 14, pp. 5353–5363, 2005. JOUR, American Chemical Society.

MAAIRA, J.; SANTANA, A.; RECASENS, F.; ANGELES LARRAYOZ, M. "Biodiesel production using supercritical methanol/carbon dioxide mixtures in a continuous reactor", **Fuel**, v. 90, n. 6, pp. 2280–2288, 2011.

MACHADO, A. B.; ARDILA, Y. C.; DE OLIVEIRA, L. H.; et al. "Liquid À Liquid Equilibrium Study in Ternary Castor Oil Biodiesel þ Ethanol þ Glycerol and Quaternary Castor Oil Biodiesel þ Ethanol þ Glycerol þ NaOH Systems at (298 . 2 and 333 . 2) K", **Journal of Chemical and Engineering Data**, v. 56, n. 5, pp. 2196–2201, 2011.

MACHADO, A. B.; ARDILA, Y. C.; DE OLIVEIRA, L. H.; AZNAR, M.; WOLF MACIEL, M. R. "Liquid-liquid equilibria in ternary and quaternary systems present in biodiesel production from soybean oil at (298.2 and 333.2) K", **Journal of Chemical and Engineering Data**, v. 57, n. 5, pp. 1417–1422, 2012.

MACHADO, D. R.; HASSON, D.; SEMIAT, R. "Effect of solvent properties on permeate flow through nanofiltration membranes. Part I: investigation of parameters affecting solvent flux", **Journal of Membrane Science**, v. 163, n. 1, pp. 93–102, 1999. JOUR, .

MACHADO, D. R.; HASSON, D.; SEMIAT, R. "Effect of solvent properties on permeate flow through nanofiltration membranes: Part II. Transport model", **Journal of Membrane Science**, v. 166, n. 1, pp. 63–69, 2000. JOUR, .

MAGHAMI, M.; YOUSEFI SEYF, J.; SADRAMELI, S. M.; HAGHTALAB, A. "Liquid-liquid

phase equilibrium in ternary mixture of waste fish oil biodiesel-methanol-glycerol: Experimental data and thermodynamic modeling", **Fluid Phase Equilibria**, v. 409, pp. 124–130, 2016.

MAGNUSSEN, T. "UNIFAC parameter table for prediction of liquid-liquid equilibriums", **Industrial & Engineering …**, v. 20, n. 2, pp. 331–339, 1981.

MAZUTTI, M. A.; VOLL, F. A. P.; CARDOZO-FILHO, L.; et al. "Thermophysical properties of biodiesel and related systems: (Liquid+liquid) equilibrium data for soybean biodiesel", **The Journal of Chemical Thermodynamics**, v. 58, n. 2013, pp. 83–94, 2013.

MESQUITA, F. M. R.; BESSA, A. M. M.; DE LIMA, D. D.; DE SANT'ANA, H. B.; DE SANTIAGO-AGUIAR, R. S. "Liquid-liquid equilibria of systems containing cottonseed biodiesel+glycerol+ethanol at 293.15, 313.15 and 333.15K", **Fluid Phase Equilibria**, v. 318, pp. 51–55, 2012. Elsevier B.V.

MESQUITA, F. M. R.; EVANGELISTA, N. S.; DE SANT'ANA, H. B.; DE SANTIAGO-AGUIAR, R. S. "Liquid-liquid equilibrium for the glycerol + alcohol + coconut biodiesel system at different temperatures and atmospheric pressure", **Journal of Chemical and Engineering Data**, v. 57, n. 12, pp. 3557–3562, 2012.

MESQUITA, F. M. R.; FEITOSA, F. X.; SOMBRA, N. E.; DE SANTIAGO-AGUIAR, R. S.; DE SANT'ANA, H. B. "Liquid-liquid equilibrium for ternary mixtures of biodiesel (soybean or sunflower) + glycerol + ethanol at different temperatures", **Journal of Chemical and Engineering Data**, v. 56, n. 11, pp. 4061–4067, 2011.

MUÑOZ, R.; MUÑOZ, R.; REYES, I.; et al. "Biodiesel Microfiltration Dynamics During Transesterification of Rapeseed Oil Biodiesel Microfiltration Dynamics During Transesterification of Rapeseed Oil", , , n. October, 2014.

NARVÁEZ, P. C.; NORIEGA, M. A.; CADAVID, J. G. "Kinetics of palm oil ethanolysis", **Energy**, v. 83, pp. 337–342, 2015.

NARVÁEZ, P. C.; RINCÓN, S. M.; SÁNCHEZ, F. J. "Kinetics of palm oil methanolysis", **JAOCS, Journal of the American Oil Chemists' Society**, v. 84, n. 10, pp. 971–977, 2007.

NARVÁEZ, P. C.; SÁNCHEZ, F.; GODOY S, R. D. "Continuous Methanolysis of Palm Oil Using a Liquid – Liquid Film Reactor", **American Oil Chemestry Society**, v. 86, pp. 343–352, 2009.

NARVÁEZ, P. C.; SÁNCHEZ, F. J.; GODOY-SILVA, R. D. "Continuous methanolysis of palm oil using a liquid-liquid film reactor", **JAOCS, Journal of the American Oil Chemists' Society**, v. 86, n. 4, pp. 343–352, 2009.

NARVAEZ P.C, RINCON S.M, C. L. . AND S. F. . "Determination of some physical and transport properties of palm oil and of its methyl esters", **Latin American Applied Research**, v. 38, pp. 1–6, 2008.

NEGI, D. S.; SOBOTKA, F.; KIMMEL, T.; WOZNY, G.; SCHOMÄCKER, R. "Liquid−Liquid Phase Equilibrium in Glycerol−Methanol−Methyl Oleate and Glycerol−Monoolein−Methyl Oleate Ternary Systems", **Industrial & Engineering Chemistry Research**, v. 45, n. 10,

pp. 3693–3696, 2006. JOUR, American Chemical Society.

NORIEGA, M. A. A.; NARVÁEZ, P. C. C.; HEINZ, C. "Kinetics of Jatropha oil methanolysis", **Fuel**, v. 134, pp. 244–249, 2014. Elsevier Ltd.

NORIEGA, M. A. A.; NARVÁEZ, P. C. C.; IMBACHI, A. D. D.; CADAVID, J. G. G.; HABERT, A. C. C. "Liquid-liquid equilibrium for biodiesel-glycerol-methanol or ethanol systems using UNIFAC correlated parameters", **Energy**, v. 111, pp. 841–849, 2016.

NOUREDDINI, H.; ZHU, D. "Kinetics of transesterification of soybean oil", **Journal of the American Oil Chemists' Society**, 1997.

OH, P. P.; CHONG, M. F.; LAU, H. L. N.; CHOO, Y. M.; CHEN, J. "Modeling of a Membrane Reactor System for Crude Palm Oil Transesterification . Part I : Chemical and Phase Equilibrium", **AIChE Journal**, v. 61, n. 6, pp. 1968–1978, 2015.

OICHI, T.; PRAUSNITZ, J. M. "Solvent Activities in Polymer Solutions Using a Group-Contribution Method", **Industrial & Engineering Chemistry Process Design & Development**, v. 17, n. 3, pp. 333–339, 1978.

OLIVEIRA, M. B.; BARBEDO, S.; SOLETTI, J. I.; et al. "Liquid-liquid equilibria for the canola oil biodiesel + ethanol + glycerol system", **Fuel**, v. 90, n. 8, pp. 2738–2745, 2011.

OLIVEIRA, M. B.; QUEIMADA, A J.; COUTINHO, J. A P. "Modeling of Biodiesel Multicomponent Systems with the Cubic-Plus-Association (CPA) Equation of State", **Industrial & Engineering Chemistry Research**, v. 49, pp. 1419–1427, 2010.

OLIVEIRA, M. B.; TELES, A. R. R.; QUEIMADA, A. J.; COUTINHO, J. A P. "Phase equilibria of glycerol containing systems and their description with the Cubic-Plus-Association (CPA) Equation of State", **Fluid Phase Equilibria**, v. 280, n. 1–2, pp. 22–29, 2009.

OPENSHAW, K. "A review of Jatropha curcas: An oil plant of unfulfilled promise", **Biomass and Bioenergy**, v. 19, n. 1, pp. 1–15, 2000.

OTHMAN, R.; MOHAMMAD, A. W.; ISMAIL, M.; SALIMON, J. "Application of polymeric solvent resistant nanofiltration membranes for biodiesel production", **Journal of Membrane Science**, v. 348, n. 1–2, pp. 287–297, 2010.

OW, U. S. E. P. A. "Method 1664 , Revision A : N-Hexane Extractable Material (HEM ; Oil and Grease) and Silica Gel Treated N-Hexane Extractable Material (SGT - HEM ; Non-polar Material) by Extraction and Gravimetry", **U.S. Epa**, , n. February, 1999.

QIU, Z.; ZHAO, L.; WEATHERLEY, L. "Process intensification technologies in continuous biodiesel production", **Chemical Engineering and Processing: Process Intensification**, v. 49, n. 4, pp. 323–330, 2010. Elsevier B.V.

ROCHA, E. G. D. A.; FOLLEGATTI-ROMERO, L. A. "Liquid – liquid equilibria for ternary systems containing ethylic palm oil biodiesel + ethanol + glycerol / water : Experimental data at", , , n. February, 2014.

ROSTAMI, M.; RAEISSI, S.; MAHMOODI, M.; NOWROOZI, M. "Liquid–Liquid Equilibria in Biodiesel Production", **Journal of the American Oil Chemists' Society**, pp. 147–154, 2012.

SALEH, J. "A Membrane Separation Process for Biodiesel Purification", , pp. 242, 2011.

SALEH, J.; DUBÉ, M. A.; TREMBLAY, A. Y. "Effect of soap, methanol, and water on glycerol particle size in biodiesel purification", **Energy and Fuels**, v. 24, n. 11, pp. 6179–6186, 2010.

SALEH, J.; DUBÉ, M. A.; TREMBLAY, A. Y. "Separation of glycerol from FAME using ceramic membranes", **Fuel Processing Technology**, v. 92, n. 7, pp. 1305–1310, 2011. JOUR, Elsevier B.V.

SARIN, R.; SHARMA, M.; SINHARAY, S.; MALHOTRA, R. K. "Jatropha-Palm biodiesel blends: An optimum mix for Asia", **Fuel**, v. 86, n. 10–11, pp. 1365–1371, 2007.

SARKAR, B.; SRIDHAR, S.; SARAVANAN, K.; KALE, V. "Preparation of fatty acid methyl ester through temperature gradient driven pervaporation process", **Chemical Engineering Journal**, v. 162, n. 2, pp. 609–615, 2010. Elsevier B.V.

SEGUR, J. "Physical properties of glycerol and its solutions", **Glycerol**, pp. 1–27, 1953.

SEGUR, J. B.; OBERSTAR, H. E. "Viscosity of Glycerol and Its Aqueous Solutions", **Industrial & Engineering Chemistry**, v. 43, n. 9, pp. 2117–2120, 1951.

SHAH, T. N.; RITCHIE, S. M. C. "Esterification catalysis using functionalized membranes", **Applied Catalysis A: General**, v. 296, n. 1, pp. 12–20, 2005.

SHI, W.; HE, B.; CAO, Y.; et al. "Continuous esterification to produce biodiesel by SPES/PES/NWF composite catalytic membrane in flow-through membrane reactor: Experimental and kinetic studies", **Bioresource Technology**, v. 129, pp. 100–107, 2013.

SHI, W.; HE, B.; DING, J.; et al. "Preparation and characterization of the organic-inorganic hybrid membrane for biodiesel production", **Bioresource Technology**, v. 101, n. 5, pp. 1501–1505, 2010. Elsevier Ltd.

SHI, W.; HE, B.; LI, J. "Esterification of acidified oil with methanol by SPES/PES catalytic membrane", **Bioresource Technology**, v. 102, n. 9, pp. 5389–5393, 2011. Elsevier Ltd.

SHI, W.; LI, H.; ZHOU, R.; QIN, X.; et al. "Preparation and characterization of phosphotungstic acid/PVA nanofiber composite catalytic membranes via electrospinning for biodiesel production", **Fuel**, v. 180, pp. 759–766, 2016.

SHI, W.; LI, H.; ZHOU, R.; ZHANG, H.; DU, Q. "Biodiesel production from soybean oil by quaternized polysulfone alkali-catalyzed membrane", **Bioresource Technology**, v. 210, pp. 43–48, 2016.

SHUIT, S. H.; ONG, Y. T.; LEE, K. T.; SUBHASH, B.; TAN, S. H. "Membrane technology as a promising alternative in biodiesel production: A review", **Biotechnology Advances**, v. 30, n. 6, pp. 1364–1380, 2012. Elsevier Inc.

SØRENSEN, J. M.; MAGNUSSEN, T.; RASMUSSEN, P.; FREDENSLUND, A. "Liquid—liquid equilibrium data: Their retrieval, correlation and prediction Part II: Correlation", **Fluid Phase Equilibria**, v. 3, n. 1, pp. 47–82, 1979.

STAMENKOVIC, O. S.; LAZIC, M. L.; TODOROVIC, Z. B.; VELJKOVIC, V. B.; SKALA, D.

U. "The effect of agitation intensity on alkali-catalyzed methanolysis of sunflower oil", **Bioresource Technology**, v. 98, n. 14, pp. 2688–2699, 2007.

SUBRAMANIAN, R.; RAGHAVARAO, K. S. M. S.; NAKAJIMA, M.; et al. "Application of dense membrane theory for differential permeation of vegetable oil constituents", **Journal of Food Engineering**, v. 60, n. 3, pp. 249–256, 2003.

SUN, J.; JU, J.; JI, L.; ZHANG, L.; XU, N. "Synthesis of Biodiesel in Capillary Microreactors", **Industrial & Engineering Chemistry Research**, v. 47, n. 5, pp. 1398–1403, 2008. JOUR, American Chemical Society.

THERM, J. C.; MAZUTTI, M. A; VOLL, F. A P.; et al. "Thermophysical properties of biodiesel and related systems : (Liquid + liquid) equilibrium data for castor oil biodiesel", , v. 62, pp. 17–26, 2013.

THOMPSON, J. C.; HE, B. B. "Biodiesel Production Using Static Mixers", **Transactions Of The Asabe**, v. 50, n. 1, pp. 161–166, 2007.

TORRES, J. .; RODRIGUEZ, N. .; TOLEDO, J.; et al. "Ultra fi ltration polymeric membranes for the puri fi cation of biodiesel from ethanol", **Journal of Cleaner Production**, v. 141, pp. 641–647, 2017.

VASUDEVAN, P. T.; BRIGGS, M. "Biodiesel production--current state of the art and challenges.", **Journal of industrial microbiology & biotechnology**, v. 35, n. 5, pp. 421–430, 2008.

VENERAL, J. G.; JUNIOR, D. L. R.; MAZUTTI, M. A.; et al. "Thermophysical properties of biodiesel and related systems: Low-pressure vapour-liquid equilibrium of methyl/ethyl Jatropha curcas biodiesel", **Journal of Chemical Thermodynamics**, v. 60, pp. 46–51, 2013. Elsevier Ltd.

VIENNET, R.; FONTEIX, C.; MARC, I. "Multicriteria optimization using a genetic algorithm for determining a Pareto set", **International Journal of Systems Science**, v. 27, n. 2, pp. 255–260, 1996. JOUR, Taylor & Francis.

WALTER, E.; PRONZATO, L. "Identification of parametric models", **Communications and Control Engineering**, 1997.

WANG, Y.; WANG, X.; LIU, Y.; et al. "Refining of biodiesel by ceramic membrane separation", **Fuel Processing Technology**, v. 90, n. 3, pp. 422–427, 2009. Elsevier B.V.

WEN, Z.; YU, X.; TU, S. T.; YAN, J.; DAHLQUIST, E. "Intensification of biodiesel synthesis using zigzag micro-channel reactors", **Bioresource Technology**, v. 100, n. 12, pp. 3054–3060, 2009. Elsevier Ltd.

WILKE, C. R.; CHANG, P. "Correlation of diffusion coefficients in dilute solutions", **AIChE Journal**, v. 1, n. 2, pp. 264–270, 1955.

WU, S.; BOUCHARD, C.; KALIAGUINE, S. "Zeolite Containing Catalytic Membranes As Interphase Contactors", **Res. Chem. Intermed.**, v. 24, n. 3, pp. 273–289, 1998.

XU, W.; GAO, L.; WANG, S.; XIAO, G. "Biodiesel production in a membrane reactor using MCM-41 supported solid acid catalyst", **Bioresource technology**, v. 159, pp. 286–91, 2014. Elsevier Ltd.

XU, W.; GAO, L.; XIAO, G. "Biodiesel production optimization using monolithic catalyst in a fixed-bed membrane reactor", **Fuel**, v. 159, pp. 484–490, 2015.

XU, W.; JIANG, F.; GAO, L. J.; XIAO, G. M. "KF/Al2O3/Ceramic Membrane Catalyst for Biodiesel Production", **Advanced Materials Research**, v. 634–638, pp. 783–786, 2013. JOUR, Trans Tech Publications.

YU, D.; TIAN, L.; WU, H.; et al. "Ultrasonic irradiation with vibration for biodiesel production from soybean oil by Novozym 435", **Process Biochemistry**, v. 45, n. 4, pp. 519–525, 2010. Elsevier Ltd.

ZHANG, H.; DING, J.; QIU, Y.; ZHAO, Z. "Kinetics of esterification of acidified oil with different alcohols by a cation ion-exchange resin/polyethersulfone hybrid catalytic membrane", **Bioresource Technology**, v. 112, pp. 28–33, 2012. Elsevier Ltd.

ZHENG, Y.; QUAN, J.; NING, X.; et al. "Lipase-catalyzed transesterification of soybean oil for biodiesel production in tert-amyl alcohol", **World Journal of Microbiology and Biotechnology**, v. 25, n. 1, pp. 41–46, 2009.

ZHOU, H.; LU, H.; LIANG, B. "Solubility of multicomponent systems in the biodiesel production by transesterification of Jatropha curcas L. oil with methanol", **Journal of Chemical and Engineering Data**, v. 51, n. 3, pp. 1130–1135, 2006.

ZHU, M.; HE, B.; SHI, W.; et al. "Preparation and characterization of PSSA/PVA catalytic membrane for biodiesel production", **Fuel**, v. 89, n. 9, pp. 2299–2304, 2010. Elsevier Ltd.